Integration of nutritional status with germline proliferation:

characterizing the roles of NHR-88 and NHR-49 in the *C. elegans* gonad

Alison Brooks

A dissertation
submitted in partial fulfillment of the
requirements for the degree of

Doctor of Philosophy

University of Washington

2011

Sue Biggins, Chair

Weiqing Li

Dana Miller

Program Authorized to Offer Degree:

Molecular and Cellular Biology

University of Washington

Abstract

Integration of nutritional status with germline proliferation:
characterizing the roles of NHR-88 and NHR-49 in the *C. elegans* gonad

Alison Brooks

Chair of Supervisory Committee:
Affiliate Professor, Sue Biggins
Department of Biochemistry

As organisms cycle between feeding and fasting, they must balance nutritional input with energy expenditures such as reproduction, growth, and repair. To achieve the proper equilibrium, these processes must be tightly regulated, requiring that nutritional status be communicated to all tissues. Lipid-responsive transcription factors called nuclear receptors are key to this transmission of information. Despite a growing knowledge of nuclear receptors, one significant question that remains is how this class of proteins integrates an environmental signal into an organismal response. I have chosen to address this question using the nematode *C. elegans*, in which the nuclear receptor NHR-49 plays a central role. Complementing previous work demonstrating a requirement of NHR-49 for metabolic homeostasis in fed and fasted worms, I have characterized additional facets of the NHR-49-dependent fasting response, including regulation of cell cycle and autophagy-related genes. My findings have also uncovered an extreme sensitivity to NHR-49 protein levels, as demonstrated by toxicity of multiple *nhr-49* rescue constructs. Since the presence of genomic regions including the 3'UTR ameliorates this toxicity, I propose that miRNAs may be involved in titration of NHR-49 levels. To elucidate this involvement, I focused my studies on the two miRNAs predicted to target *nhr-49*: mir-243 and

mir-797. Although I was unable to define the requirement for these miRNAs in fed animals, this research lead me to the establishment of a role for both mir-243 and mir-797 in recovery from the NHR-49-regulated fasting response, adult reproductive diapause (ARD). Additionally, my work implicated another nuclear receptor, NHR-88, in ARD entry and recovery. I also found that a mutation in *nhr-88* synthetically interacts with two other alleles: *cyp-35a5(ok1985)* and the as-yet unidentified *fhc10*. Together these genes regulate the size of the mitotically proliferating population in the germline, fecundity, fat metabolism, and lifespan, possibly in response to a dihomo-gamma-linolenic acid-derived ligand. This newly defined network provides a model for studying nuclear receptor-driven transmission of environmental signals throughout the organism. Finally, identification of three factors with selective ARD phenotypes make this diapause a more viable tool for studying conserved processes such as stem cell maintenance and protective autophagy during starvation.

Table of Contents

List of Abbreviations

3’ UnTranslated Region (3’UTR)

Activation Function (AF)

Adult Reproductive Diapause (ARD)

DeoxyriboNucleic Acid (DNA)

Differential Interference Contrast Microscopy (DIC)

Dihomo-Gamma-Linolenic Acid (DGLA)

DNA-Binding Domain (DBD)

Ethyl MethaneSulfonate (EMS)

Green Fluorescent Protein (GFP)

Hepatocyte Nuclear Factor 4α (HNF4α)

ImmunoPrecipitation (IP)

Ligand-Binding Domain/Pocket (LBD/P)

MicroRNA (miRNA)

Mitotic Region (MR)

Mos-mediated Single Copy Insertion (MosSCI)

Nuclear Receptor (NR)

Nuclear Hormone Receptor (NHR)

Phospholipid (PL)

Peroxisome Proliferator-Activated Receptor (PPAR)

PolyUnsaturated Fatty Acid (PUFA)

Quantitative Real-Time Polymerase Chain Reaction (qRT-PCR)

RNA Interference (RNAi)

Single Nucleotide Polymorphism (SNP)

Standard Deviation (SD)

Standard Error of the Mean (SEM)

Transition Zone (TZ)

TriAcylGlyceride (TAG)

List of Figures

Page

List of Tables

Page

Acknowledgements

I would like to acknowledge Dr. Marc Van Gilst for allowing me the scientific freedom to explore the questions that I found most interesting and the rest of the Van Gilst lab for scientific input and support throughout the years. Other labs, especially the Priess and Miller labs, have been a wealth of technical assistance and experimental advice – thank you. I would also like to thank my committee members, Sue Biggins, Linda Breeden, Bruce Edgar, Steven Hahn, Weiqing Li, and Dana Miller, for feedback and direction. I would particularly like to thank Dana for her careful reading of my dissertation and Sue for her positivity, encouragement, and guidance during the final months of my graduate career. Lastly, I would like to thank my friends and family, especially my parents, my sister, and my fiancé, for their unwavering love and support.

Dedication

To my parents,
for instilling in me a passion for learning
and then making my education possible.

Chapter I: Nuclear receptors coordinate organismal response to the environment

To provide energy for activities such as growth, repair, movement, and progeny production, an organism must extract nourishment from its environmental surroundings. These nutrients come largely in the form of carbohydrates and lipids which can be metabolized to generate ATP for immediate use, biosynthetic precursor molecules required for cellular processes, and energy depots in the form of fat stores. Based on its current nutritional status, an organism must tune its metabolism to balance these energy inputs with the amount of energy being consumed.

Nuclear receptors (NRs), a conserved class of proteins involved in metabolic regulation throughout metazoans, play a critical role in maintenance of this metabolic homeostasis (Sladek, 2011). Effects on specific sets of target genes are exquisitely regulated through interactions with promoter elements, coactivators and corepressors, dimerization partners, and ligands. In many cases, this target set changes depending on the condition of the organism, demonstrating an *in vivo* form of selective modulation. Furthermore, mutations in these receptors have been linked to a host of human diseases, from cancer to metabolic syndromes to reproductive disorders. Expansion of the NR family and the subsequent specialization of its members within the genetically tractable *Caenorhabditis* lineage provides a more manageable system in which to investigate how these proteins allow adaptation of the organism to its environment.

Structure-function relationship of nuclear receptors

The NR family is defined by both functional and structural commonalities. Firstly, all NRs act as transcription factors, usually by binding to DNA as either homo- or heterodimers (Figure 1.1) (Sladek, 2011). Secondly, NRs are thought to respond to signals from hydrophobic ligands, though there remain a large number of orphan receptors for which this ligand is unidentified (Sladek, 2011). Structural similarities include a ligand-binding domain (LBD) consisting of 11 to 12 helices designed to accommodate these hydrophobic molecules and a DNA-binding domain (DBD) comprising two zinc finger motifs (Bain et al., 2007). Target gene specificity stems from the P-box, a six-residue sequence that is involved in recognition of DNA response elements and is partially dependent on two conserved arginine residues that make direct and water-mediated contacts with the DNA (Lu et al., 2008). Most nuclear receptors also

contain two activation function (AF) domains – a variable AF1 at the N-terminal tail, which is believed to be ligand-independent, and the ligand-dependent AF2 located within the LBD (Hadzopoulou-Cladaras et al., 1997). The dimerization interface spans the DBD and the LBD (Aggelidou et al., 2006; Bain et al., 2007).

Nuclear receptor regulation of metabolism

While members of the nuclear receptor family regulate a wide variety of physiological processes, the majority of these are either developmental or metabolic in nature. For example, the mammalian hepatocyte nuclear factor 4α (HNF4α) is required for liver and colon development, plays a critical role in insulin production in pancreatic β-cells, and is important in the regulation of glucose and lipid metabolism in both the fed and fasted states (Garrison et al., 2006; Naiki et al., 2002; Parviz et al., 2003; Ryffel, 2001). Recently, the number of predicted HNF4α targets has been reported to be close to 10,000 based on *in silico* prediction using results from protein binding microarrays printed with known and predicted HNF4α-binding oligonucleotides (Bolotin et al., 2010). Of these, 240 were confirmed as novel regulatory targets using a combination of literature searches, chromatin IP experiments, and microarray of cells in which HNF4α had been knocked down by RNAi; in addition to confirming "conventional," metabolic targets such as apolipoproteins and lipases, this approach also implicated HNF4α in apoptosis and cell cycle control (Bolotin et al., 2010). The importance of HNF4α in lipid metabolism is further substantiated by phenotypes associated with knockouts or point mutants. While defects in gastrulation cause knockout mice to die *in utero* around day 10, conditional knockouts in the adult liver lead to increased hepatic lipid and decreased circulating cholesterol and triglycerides (Chen et al., 1994; Hayhurst et al., 2001). A number of naturally-occurring, heterozygous point mutants identified in maturity onset diabetes of the young (MODY) cases have been linked to both deficient insulin secretion and reduced serum triglycerides and apolipoproteins, reminiscent of the liver-specific knock-out mouse phenotypes (Shih et al., 2000). In addition to the early requirement for HNF4α in embryogenesis, this NR is required to maintain kidney and liver cells in a differentiated state, as evidenced by its role as a tumor suppressor in renal cell carcinoma and hepatocellular carcinoma (Kalkuhl et al., 1996; Sel et al., 1996). For example, loss of HNF4α expression has been reported to induce a loss of epithelial morphology accompanied by a switch from an expression profile representing mature

hepatocytes to one characteristic of undifferentiated hepatoblasts in fast-growth mouse hepatocellular carcinoma models (Lazarevich et al., 2004). Forced re-expression of HNF4α reversed both the transcriptional and morphological changes (Lazarevich et al., 2004).

The peroxisome proliferator-activated receptor (PPARs) family provides additional examples of nuclear receptors central to mammalian metabolism. All three isoforms work to coordinate nutrient response as a heterodimer with retinoid X receptor (RXR): PPARγ regulates genes involved in glucose metabolism in adipose tissue, PPARδ, which is expressed in most human tissues, regulates lipid transport and β-oxidation, while PPARα regulates lipid metabolism genes, primarily within the liver (Feige et al., 2006). PPARα is also critical for the metabolic changes that allow adaptation to fasting. Oil red O staining of 24-hour fasted PPARα null mice demonstrated accumulation of lipids within the liver, likely due to impaired upregulation of β-oxidation pathways and the inability to properly mobilize fat stores (Kersten et al., 1999). As with HNF4α, the PPARs also act as developmental regulators: PPARγ drives adipocyte differentiation and all three have been directly implicated in gametogenesis and fertility (Feige et al., 2006; Huang, 2008).

Factors affecting nuclear receptor activity

Nuclear receptors can influence expression of different groups of target genes depending on factors such as nutritional status or developmental timing (Gronemeyer et al., 2004). The primary mechanism for this is differential ligand binding, which induces a conformational change in the AF2 coactivator interface, thus enabling binding of proteins such as SRC-1 and the MED1 subunit of the Mediator complex to promote transcription of targets (Savkur and Burris, 2004). However, the presence of ligand may not always be sufficient to cause coactivator binding; a crystal structure of HNF4α LBD dimer showed only one partner bound to coactivator peptide, even though both partners contained free fatty acids in the binding pocket (Duda et al., 2004).

Despite the importance of the ligand in nuclear receptor function, about half of the human NRs remained "orphaned" without endogenous ligands (Sladek, 2011). Both HNF4α and PPARα were classified as orphan receptors until just a few years ago. Even though both had been shown to bind fatty acids within the ligand-binding pocket, these lipids were dismissed as candidates for true endogenous ligands (Dhe-Paganon et al., 2002; Forman et al., 1997). In the case of HNF4α,

ligand-binding domains purified from bacteria contained a number of 10 to 18-carbon fatty acids, the most predominant of which were palmitic acid (C16:0) and palmitoleic acid (C16:1) (Dhe-Paganon et al., 2002; Wisely et al., 2002). The irreversible binding of these fatty acids precluded their use as signaling molecules used to tailor metabolic response to nutritional status (Wisely et al., 2002). However, lipids including palmitic acid, were able to activate the HNF4α homolog in a *Drosophila* ligand sensor system (Palanker et al., 2009). In 2009, the Sladek lab discovered reversible, fasting-dependent binding of linoleic acid (LA, C18:2n6) within the HNF4α ligand-binding pocket (Yuan et al., 2009). LA was probably not identified in previous experiments looking at fats bound in the HNF4α ligand-binding pocket because it is present in bacteria only in trace amounts (Perez and Van Gilst, 2008); differences in the lipid profiles of bacteria and mammalian cells are a major caveat in interpreting ligand binding data based on bacterially-expressed human proteins. Although LA did not induce transcriptional changes of select HNF4α targets in a cell culture-based luciferase reporter assay, microarrays of HNF4α-expressing cells demonstrated that LA decreases expression of most of the HNF4α targets assayed (Yuan et al., 2009). Given that LA is bound to HNF4α exclusively in the fed state, where it has been shown that a major function of HNF4α is to oppose gene activation by PPARα via competition for promoter binding sites (Martinez-Jimenez et al., 2010), the inability of LA to induce HNF4α transactivation could be because its major function is to prevent PPARα binding . PPARα, which has long been a target of drugs such as fibrates, also remained orphaned until 2009. 1-palmitoyl-2-oleoyl-sn-glycerol-3-phosphocholine was isolated with immunoprecipitated hepatic PPARα and subsequently shown to alter PPARα-dependent gene expression in both cell culture and mice (Chakravarthy et al., 2009).

Both HNF4α and PPARα bind fatty acid ligands to regulate transcription of lipid metabolism. In the case of HNF4α, the ligand must be derived from the diet, as mammals are incapable of synthesizing LA. This linoleic acid auxotrophy raises the possibility that HNF4α may be acting as a nutrient sensor, using LA as a proxy for food intake (Sladek, 2011). A common trend among lipid sensors such as these NRs is a feed-forward loop aimed at maintaining lipid homeostasis (Chawla et al., 2001). HNF4α and PPARα, as well as cholesterol sensing NRs, activate a suite of genes to ensure proper delivery of their lipophilic ligands to the nucleus (such as ATP-binding cassette transporters and lipid-binding proteins) and subsequent clearance of those ligands (Chawla et al., 2001). Ligand removal is a task performed largely by

the cytochrome P450 family of enzymes, whose members are responsible for metabolism of both endogenous and xenobiotic compounds. This self-regulatory feedback loop ensures a robust but transitory response, allowing NRs to continually monitor and react to changing nutritional status.

Nuclear receptor function can be also modulated by post-transcriptional or post-translational mechanisms that are nutritionally regulated but not ligand-dependent. For example, phosphorylation of HNF4α by protein kinase A affects its ability to bind DNA in the fasted state (Viollet et al., 1997). There are also reports of miRNAs targeting nuclear receptors. These small, non-coding RNAs post-transcriptionally regulate gene expression by binding to sites within the 3'UTR of their targets, most frequently by physically preventing translation or destabilizing the mRNA (Almeida et al., 2011). HNF4α is predicted to affect miRNA expression (Yang and Wang, 2011), while HNF4α protein levels are reportedly regulated by two different miRNAs (Takagi et al., 2010). Since it has been shown that expression of miRNAs can change based on diet and fasting, miRNA targeting of NRs may provide another degree of nutrient-dependent regulation (Hoekstra et al., 2011).

Nuclear receptors in Caenorhabditis elegans

The genome of the nematode *Caenorhabditis elegans* encodes 284 nuclear hormone receptors (NHRs), including 269 HNF4-like supplementary nuclear receptors resulting from a massive expansion in the history of the lineage and 15 receptors with clear homologs in mammals (Bertrand et al., 2004). These conserved NRs, including DAF-12, the homolog to the Vitamin D receptor in mammals, and NHR-23, which is homologous to the mammalian RORα, have been implicated almost exclusively in developmental roles, including molting and the formation of the stress-resistant dauer (Gissendanner et al., 2004).

The roles of the supplementary nuclear receptors are much more diverse, most likely resulting from a distribution of ancestral HNF4 functions and subsequent specialization. Thus, within the supplementary NRs, a subset of proteins tends to be more involved in development, while the remaining receptors play a role that is primarily metabolic. For example, NHR-31, which is 49% similar to HNF4α, is essential for proper outgrowth of the *C. elegans* excretory cell, a requirement that mimics the ability of HNF4 to regulate proliferation of kidney cells (Grigo et al., 2008; Hahn-Windgassen and Van Gilst, 2009). Conversely, NHR-49, sharing 52%

similarity with HNF4α, is required for proper metabolic function (Van Gilst et al., 2005a; Van Gilst et al., 2005b).

Using C. elegans *NHR-49 as a model for nuclear receptor control of metabolism*

In a screen to identify functions of *C. elegans* supplementary nuclear receptors, RNAi was used to deplete a number of the genes most similar to mammalian HNF4α and the resulting knockdown strains were assayed for developmental and lifespan phenotypes (Van Gilst et al., 2005a). Of the genes tested, only two – NHR-31 and NHR-49 – demonstrated any phenotype. While RNAi against NHR-31 led to the excretory cell defect described above, depletion of NHR-49 shortened lifespan (Van Gilst et al., 2005a). Additional characterization showed that NHR-49 was required for expression of target genes similar to those affected by disruption of mammalian HNF4α and PPARα, including genes involved in fatty acid β-oxidation and desaturation, as well as lipid and glucose transport. In addition to sharing homologous regulators, the metabolic processes in mammals and nematodes are highly conserved; *C. elegans* homologs have been found for key mammalian enzymes acting in pathways including glycolysis, gluconeogenesis, fatty acid synthesis, lipid desaturation, and β-oxidation (Van Gilst et al., 2005a). The overlap in target genes of the mammalian lipid sensors HNF4α and PPARα and the nematode receptor NHR-49, all of which coordinate lipid and carbohydrate metabolism via very similar metabolic pathways, makes NHR-49 an excellent model system in which to study the mechanisms of this regulation.

A fundamental tool in the study of any *C. elegans* gene is a deletion mutant. While RNAi depletion often phenocopies a deletion allele, it rarely results in complete elimination of target protein and is subject to off-target effects. Additionally, not all experiments are RNAi-compatible. For example, combining fasting or starvation protocols with RNAi would require soaking a population of worms in a double-stranded RNA solution to maintain gene depletion throughout the treatment, which can last up to 30 days. However, preliminary data show that the starvation-induced diapause described in this dissertation is not as robust in axenic media, making deletion mutants a better option (personal communication with Giana Angelo). Animals containing the predicted null *nhr-49(nr2041)* deletion allele are short-lived, starvation sensitive, and show a misregulation of lipid and glucose metabolism genes in both the fed and fasted states (Van Gilst et al., 2005a). Additionally, an *nhr-49* knockout worm has lipid-related defects such

as high fat storage and elevated levels of saturated lipids (Van Gilst et al., 2005a). However, there is no embryonic lethality associated with mutations in NHR-49, suggesting that the developmental role of HNF4α was either taken by another NHR after the family expanded in nematodes or that the developmental requirement for these receptors is not an ancestral characteristic (Chen et al., 1994). Gene expression analysis by qRT-PCR shows that NHR-49 is required for activation of β-oxidation and fatty acid desaturation, in addition to repression of lipid remodeling and sphingolipid metabolism (Pathare, submitted). Selective modulation of these transcriptionally-coupled target sets is achieved in part through association with different heterodimer partners. In this way, NHR-49 is more like the mammalian RXR, which heterodimerizes with multiple partners, than PPARα, which binds only RXR, or HNF4α, which acts only as a homodimer. To date, NHR-49 is the only *C. elegans* NR that has been shown to act with multiple dimer partners (Pathare, submitted).

Nuclear receptor control of the C. elegans *fasting response*

Initial characterization of *nhr-49* mutants identified a starvation sensitivity phenotype, stemming in part from NHR-49 control of fasting response genes. During short-term fasts (less than 12 hours), worms alter expression of β-oxidation, lipid transport, and saturation genes to mobilize fat stores; NHR-49 is required for expression changes of 8 out of 18 fasting-response genes assayed (Van Gilst et al., 2005b). In the case of prolonged food deprivation, *C. elegans* enter an arrested state dependent on the point of food removal (Figure 1.2). If starvation occurs early during the first or final larval stages, animals will arrest as L1s or L4s, respectively (Angelo and Van Gilst, 2009; Johnson et al., 1984). However, if food is removed later during L1 or L4, individuals will start on the pathway to dauer or enter adult reproductive diapause (ARD), both of which maintain longevity much longer than that reported for L1 or L4 arrests (Angelo and Van Gilst, 2009; Cassada and Russell, 1975).

Entry into the dauer diapause is regulated by environmental conditions including crowding, temperature, and food availability. Integration of food signal into the dauer decision goes through the nuclear receptor DAF-12, the only nematode NHR that has been paired with a ligand (Motola et al., 2006). In nutrient-rich conditions, cholesterol-derived dafachronic acids bind within the DAF-12 ligand-binding pocket, causing conformational changes that displace the corepressor DIN-1 (Bethke et al., 2009). In its transcriptionally active state, DAF-12 promotes

progression through L3 and the reproductive life history. However, when food is not present, the corepressor stays bound and the worms arrest. Recent experiments have identified a feedback loop in place to ensure a switch-like decision at this branch point. In a favorable environment, DAF-12 activates expression of genes required for L3 developmental and the let-7 family of miRNAs, which repress L2-specific programs (Bethke et al., 2009). The let-7 miRNAs also prevent transcription of DAF-12, thus guaranteeing commitment to the L3 fate (Hammell et al., 2009).

The regulation of the adult reproductive diapause (ARD) is less well defined. If withdrawn from food during the receptive window in L4, individuals will go through the final molt and then arrest as adults (Angelo and Van Gilst, 2009). While starved adults die within a few days as fertilized embryos hatch internally ("bagging"), animals in ARD can survive starvation periods recorded up to 80 days (Angelo and Van Gilst, 2009). Hallmarks of this phenotype include arrested or very slowly developing embryos and cessation of fertilization events (preventing death by bagging), remodeling of the germline and somatic tissues (mobilizing energy stores to ensure survival of required tissues), and maintenance of longevity (Angelo and Van Gilst, 2009). As with dauer, population density is an additional influence on ARD entry (Angelo and Van Gilst, 2009). To date, the only genetic factor known to regulate this diapause is NHR-49. Instead of arresting in ARD, *nhr-49* mutants frequently die by bagging. Those that have inviable embryos are able to escape this fate and enter a state of slow starvation that shares some characteristics with the diapause without protecting longevity or fecundity (Angelo and Van Gilst, 2009); personal communication with Giana Angelo). Both *nhr-49* and wild-type animals show plasticity of the germline during starvation and refeeding, but the mutants do not exhibit somatic remodeling of the muscle, intestine, or hypodermis as seen in an N2 worm (Angelo and Van Gilst, 2009). As *nhr-49* mutants can form dauers and *daf-12* mutant animals are able enter ARD, it has been determined that NHR-49 is not required in the dauer diapause and DAF-12 is dispensable for entry into ARD (personal communication with Giana Angelo). Thus *nhr-49* mutants provide a novel tool to study nuclear receptor control of fasting-dependent physiological changes. Although the ARD phenotype is unique to worms, the protective adaptations occurring on the level of tissues and cells are likely to be conserved in mammals.

Metabolism and the germline

As outlined above, a common feature of *C. elegans* starvation responses is the delay of reproductive activities. *C. elegans* is a naturally androdioecious species, existing largely as a population of self-fertilizing hermaphrodites with a low frequency of males (Stewart and Phillips, 2002). Within an adult hermaphrodite, there are two U-shaped gonad arms, each containing approximately 1000 germ "cells" that are actually open to a common cytoplasm. Ligands produced by the somatic distal tip cell maintain the distal-most germ cells in mitosis, but concentrations of proliferation factors decrease as cells move proximally, leading to an increase of pro-meiotic factors and eventual differentiation (Crittenden et al., 2003). Sperm are produced when cells first start differentiating late in the L3 stage and ending at the L4 molt; the germline of a wild-type adult worm generates only oocytes (Kimble and Crittenden, 2007). Oogenesis is a major factor in the high metabolic cost of reproduction, as oocytes are packed full of lipid-rich yolk. In *C. elegans*, yolk lipoproteins originate in the intestine, where they are processed, exported into the body cavity, and taken up by the germline for packaging into developing oocytes (Kimble and Sharrock, 1983). Even before they provide for the developing embryo, the lipids are critical in the fertilization process, where they act as precursors for sperm recruitment signals (Kubagawa et al., 2006).

Since reproduction has such a high metabolic demand, a fasted animal frequently does not produce progeny until nutrient availability improves, either due to the simple lack of incoming energy or as a result of a concerted redistribution of energy away from reproductive processes. It is this concept that has led to the antagonistic pleiotropy theory, which postulates an inverse correlation between fecundity and longevity stemming from dedication of resources to one process over the other (Jenkins et al., 2004). Dietary restricted animals provide an excellent example in support of this model; brood size is reduced in mice, flies, and nematodes with limited caloric intake, while lifespan is increased (Partridge et al., 2005). Similarly, germline-less nematodes and fruit flies, which necessarily have a brood size of zero, are also long-lived, providing that the somatic gonad remains intact (Flatt et al., 2008; Hsin and Kenyon, 1999). However, a trade-off does not always exist, as evidenced by long-lived *daf-2* alleles that have variable effects on progeny production and the increase in lifespan caused by knockdown of *daf-2* in adults that is not accompanied by a reduction in brood size (Dillin et al., 2002; Gems et al., 1998). These counterexamples suggest that regulation of somatic repair may be balanced with

something more subtle than number of progeny. Instead, a trade-off may exist between lifespan and a specific aspect of reproduction that is necessary but not sufficient to result in a change in brood size. Because progeny production in *C. elegans* requires the coordination of myriad processes, such as gametogenesis, the switch from sperm to oocyte production, sperm activation and recruitment, fertilization, and egg-laying, alterations in this hypothetical property may not always lead to fluctuations in brood size.

Although there is still debate regarding the existence of a trade-off between brood size and lifespan, there are multiple examples of communication between the tissues governing these energy expenditures. Lipid metabolism is key to crosstalk between the germline and soma, thus allowing coordination of nutrient allocation to these tissues. Recently, three separate labs have implicated two lipases, an acyl-coA reductase, and a desaturase gene in the extension of lifespan in animals lacking a germline (Goudeau et al., 2011; McCormick et al., 2011; Wang et al., 2008). What role this lipid-driven interaction plays in balancing metabolic demands between somatic repair and progeny production or integration of nutritional status into brood size determination remains to be seen.

Description of dissertation

In mammals, HNF4α and PPARα are ideally poised to act as nutrient sensors, as they regulate a suite of genes important for lipid and glucose metabolism in response to binding of metabolic intermediates. The primary goals of my dissertation research have been to investigate how nuclear receptors such as these communicate nutritional status to the organism and elucidate the adaptive changes induced by these transcription factors in response to changes in nutrient availability. I address these questions using NHR-49 and NHR-88, two *C. elegans* proteins that I propose as regulators of the feeding/fasting response in this organism. These NRs are central to *C. elegans* nutrient-responsive networks that I expanded and defined as part of my dissertation research, and which can serve as more tractable models for the mammalian system. The first, the NHR-49-dependent adult reproductive diapause, provides a model for cellular adaptation to starvation. Although it is clear that the physiological changes associated with ARD are protective, the extent of these adaptations remains unknown. Furthermore, NHR-49 is the only gene known to regulate entry, maintenance, or exit from the diapause. The second *C. elegans* system I took advantage of was one of communication between tissues, specifically the germline

and soma. Others have postulated a trade-off between lifespan and brood size as a result of this communication, but the existence of counter-examples implies that the factors in balance are not simply fecundity and longevity. My work uses a regulatory network surrounding NHR-88 to address not only an alternative identity of the lifespan-balancing phenotype, but also how this homeostasis integrates nutritional status information, potentially via recognition of a lipid ligand by this orphan receptor.

In chapter two, I describe the complexities of NHR-49 regulation and the importance for titration of this protein in a healthy worm. *nhr-49* deletion mutants have the same lifespan as transgenic lines overexpressing the gene in a mutant background, suggesting that *nhr-49* expression must be tightly regulated. Transcriptional analysis of these overexpression lines revealed misregulation of a number of NHR-49 targets, though none that clearly explain the toxicity of the construct. I found that inclusion of introns and the 3'UTR reduces toxicity of the overexpression plasmid and permits partial rescue of *nhr-49(nr2041)* lifespan. The requirement of the 3'UTR led me to investigate two *nhr-49*-targeting miRNAs: mir-243 and mir-797. Although I have not definitely shown a role for either miRNA is regulation of NHR-49, I did discover that they are involved in recovery from the adult reproductive diapause. The mutant phenotypes I describe are the first reported for the *mir-243* and *mir-797* deletion alleles, and distinctive in that they require deletion of only a single miRNA species. Even if these miRNAs are not acting through regulation of NHR-49, they are still valuable tools in studying the fasting response. Furthermore, the involvement of miRNAs in ARD reveals a common theme in diapause states, as the nuclear receptor DAF-12 and the let-7 family of miRNAs form a feedback loop to regulate dauer (Bethke et al., 2009; Hammell et al., 2009). Mammalian nuclear receptors also regulate and are regulated by miRNAs (Takagi et al., 2010; Yang and Wang, 2011) suggesting that the involvement of these small, non-coding mRNAs in fasting might be conserved.

The third chapter summarizes work implicating a new nuclear receptor, NHR-88, in the integration of nutritional status with reproduction. While possessing negligible mutant phenotypes on its own, fecundity, fat metabolism, germline organization, and longevity are all affected when *nhr-88* is combined with mutations in two other genes. One of these is *cyp-35a5*, a cytochrome P450 acting in xenobiotic metabolism and lipid homeostasis (Aarnio et al., 2011; Menzel et al., 2005). The other is an unidentified gene discovered as a background mutation in

the *cyp-35a5* deletion strain. Together these genes regulate brood size, the mitotic population in the germline, lipid composition, and lifespan. Analysis of these factors demonstrated a strong inverse correlation between the number of mitotic germ cells and lifespan, consistent with examples of germline-soma crosstalk reported by others (Goudeau et al., 2011; McCormick et al., 2011; Wang et al., 2008). As NHR-88 is required for this relationship, I hypothesize that it is critical in communicating information about germ cell status to the somatic tissues. I additionally demonstrate a role for NHR-88 in lipid-induced sterility, possibly providing clues as to the endogenous ligand of this orphan nuclear receptor.

The final chapter deals with expanding the definition of the *C. elegans* ARD fasting response and determining the roles of NHR-49 and NHR-88 in it. Analysis of microarrays comparing fed and fasted populations uncovered 12 categories of genes that are differentially regulated depending on nutrient availability, many of which are dependent on NHR-49. Expression data also shows that *nhr-88* is activated in an NHR-49-dependent manner when animals are fasted for 8 hours. Finally, I demonstrated a requirement for NHR-88 in the adult reproductive diapause, providing yet another tool with which to study cellular adaptations to fasting outside of the pleiotropic *nhr-49* genetic background.

In summary, my work has implicated NHR-49 in aspects of the fasting response beyond the metabolic requirements previously defined. I have also described the role of another nuclear receptor, NHR-88, in coordinating somatic and germline processes in the fed state and in the adult reproductive diapause in response to starvation. Finally, I identified two miRNAs that are necessary for proper recovery from ARD. Taken together, these data lay the groundwork for description of a regulatory network spanning the germline and soma that integrates metabolites, nuclear receptors, and miRNAs to adapt *C. elegans* to variable food availability. Structural and functional homology between mammalian and nematode receptors, as well as common metabolic pathways, suggest that there may also be similarities in the nutrient response mechanisms across evolution.

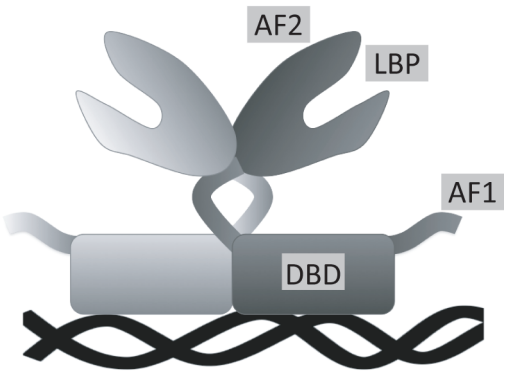

Figure 1.1. Schematic representation of a nuclear receptor heterodimer. The dimerization interface spans DNA-binding and ligand-binding domains of both receptors. Protein domains are labeled in the receptor on the left. DBD: DNA-binding domain; LBP: ligand-binding pocket; AF: activation function.

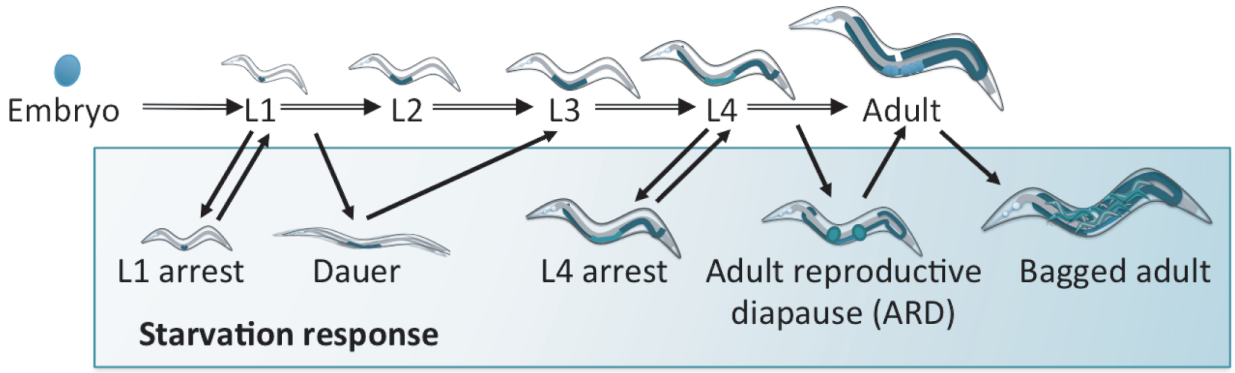

Figure 1.2. Nutrient-dependent life history decisions in *C. elegans*. In favorable environments, *C. elegans* embryos hatch and proceed through four larval stages to adult in about 3 days. However, if food is removed the animal will enter a characteristic arrest, dependent upon the timing of starvation. L1 and L4 larvae arrest as such, and upon refeeding they re-enter the developmental pathway at the same stage they exited. Dauer and ARD are long-lived diapauses that animals enter to and exit from at different stages. A starved adult survives only a few days before fertilized embryos hatch internally, killing the adult in a process known as "bagging".

Chapter II: Sensitivity to NHR-49 protein level reveals role for miRNAs in adult reproductive diapause

The level at which certain proteins are maintained in a cell is often important, as evidenced by the multiple strategies organisms have evolved to regulate transcription, translation, and degradation. miRNAs act at the translational level, binding to mRNAs to alter efficiency of translation and thus protein level. To date, these small molecules have been implicated in processes including both normal development and cancer. I have discovered a possible role for miRNAs in regulating *nhr-49*, a *C. elegans* nutrient receptor that is required for entry into the adult reproductive diapause (ARD). The inability to rescue longevity with transgenic *nhr-49* suggested that worms are quite sensitive to NHR-49 levels, as both deletion mutants and overexpression lines are short-lived. However, adding back the endogenous 3'UTR moderates the effect of overexpression, allowing partial rescue of the lifespan phenotype to occur and implicating miRNAs in the process. The miRNAs predicted to regulate *nhr-49* are especially important in mediating rescue from ARD, where they likely exert their influence both on *nhr-49* and other targets. In addition to providing another example of miRNA tuning in development, these miRNAs are the first mutants identified that are defective only in the recovery phase of ARD, allowing future dissection of the genes involved in this process.

Introduction

Nuclear receptors (NRs) are lipid-responsive transcription factors present throughout metazoans. Due to their lipophilic binding pockets, they are ideally suited to act as lipid sensors; as a class, they are involved in processes ranging from growth and development to environmental sensing to diseases such as cancer and diabetes (Sladek, 2011). While most species possess a limited number of these proteins and achieve specificity via dimerization and other protein interactions, there has been a massive expansion and specialization of NRs in the *Caenorhabditis* lineage (Taubert et al., 2011). Interestingly, this expansion is limited to a single branch; of the 284 NRs present in the model organism *C. elegans*, 269 are believed to be derived from an ancestor of HNF4α (Taubert et al., 2011). One of these nuclear receptors is NHR-49, a transcription factor that differentially regulates genes involved in lipid and glucose metabolism in the fed and fasted states (Van Gilst et al., 2005a; Van Gilst et al., 2005b). *nhr-49* deletion

mutants are short-lived and have a reduced brood, both of which have been attributed in part to increased levels of saturated fat caused by misregulation of desaturases (Pathare, submitted; Van Gilst et al., 2005a).

In addition to its role in coordinating mobilization of fat stores during fasting, NHR-49 is also required for entry into an alternative, starvation-dependent *C. elegans* life stage termed adult reproductive diapause, or ARD (Angelo and Van Gilst, 2009). This diapause, which occurs with complete removal from food during the final larval stage, is characterized by two factors. The first is cessation of ovulation or fertilization events (Angelo and Van Gilst, 2009). The second, extreme plasticity of both the germline and soma, contributes to the maintenance of lifespan and fertility during the starvation period (Angelo and Van Gilst, 2009). *nhr-49* mutants are defective in the entry phase of this diapause, failing to properly arrest fertilization and embryonic development; the majority of an *nhr-49* population die as a "bag of worms" as a result of internal hatching (Angelo and Van Gilst, 2009). However, if embryos are inviable, these mutants can escape bagging and enter a diapause-like state. Examination of these slowly starving mutants has also demonstrated a role for NHR-49 in maintenance of and recovery from ARD (Angelo and Van Gilst, 2009).

Recently, nuclear receptors (including HNF4α) have been implicated in the regulation of microRNAs (miRNAs) (Yang and Wang, 2011). These small, non-coding RNAs were first cloned in *C. elegans* close to two decades ago, but have since been discovered in plants, viruses, insects, and mammals (Kim and Nam, 2006). Their most common function is to post-transcriptionally silence targets by binding to the 3'UTR of mRNAs to cause transcript degradation or disrupt translation, although there is some evidence that they serve to activate translation under special conditions, such as serum starvation (Almeida et al., 2011). Although some *C. elegans* miRNAs, such as the originally identified lin-4 and let-7, have been well characterized, the majority of miRNA deletions have subtle phenotypes in worms, either as single mutants or when deleted in combination with other family members (Alvarez-Saavedra and Horvitz, 2010; Miska et al., 2007). Mutants that do show phenotypes demonstrate miRNA involvement in developmental timing, as seen for both lin-4 and let-7 (Almeida et al., 2011). For example, the let-7 miRNA family participates in a feedback loop with *C. elegans* nuclear receptor DAF-12 to ensure a switch-like decision between normal development and the dauer starvation response (Hammell et al., 2009). My work has elucidated a potential role for miRNAs

in the regulation of NHR-49. I have also identified NHR-49-dependent and –independent starvation-related phenotypes for two single miRNA mutants that may provide insight into regulation of the physiological changes associated with entry into and exit from adult reproductive diapause.

Results

NHR-49 protein levels must be tightly regulated

One of my initial aims was to interrogate the relationship between structure and function in NHR-49. As described in Appendix I, I created a series of FLAG-tagged mutant cDNA constructs with the goal of introducing them transgenically into *nhr-49* mutants and then assaying for rescue of various phenotypes (Figure 2.1). I chose lifespan as the primary phenotype to assay for rescue, as *nhr-49* mutants are significantly shorter-lived than their wild-type N2 counterparts, with a mean lifespan of around 10 days versus approximately 18 days for N2 (see Table 2.1). Although rescue of longevity might not be correlated with every phenotype, lifespan experiments are easy to do on multiple lines in parallel and some NHR-49 regulatory targets have been implicated in longevity (Pathare, submitted). I found that the wild-type cDNA sequence was incapable of rescuing the mutant lifespan (Figure 2.2A). Furthermore, outcrossing of this line to the N2 strain demonstrated that the array actually decreased lifespan by about 20% when introduced as an integrated extrachromosomal array in a wild-type background (Figure 2.2A). Germline silencing of high copy arrays has been reported to occasionally spread throughout the organism, shutting off transcription of both transgenic and genomic copies of the target sequence in an RNAi-like fashion (Dernburg et al., 2000); however, Western blotting against FLAG-NHR-49 demonstrated that tagged protein was being expressed in the worms, suggesting that this mechanism was not responsible for the decreased lifespan (Figure 2.1B).

My first hypothesis was that the rescue plasmid did not contain necessary regulatory regions to allow for proper expression of NHR-49 or that the FLAG tag was disrupting expression or folding of the long isoform (Figure 2.1A). I reasoned that if missing sequence was the reason for lack of rescue, then introduction of the cosmid containing the genomic *nhr*-49 locus, along with 27 kilobases upstream and 1.6 kilobases downstream, should allow for successful complementation of the *nhr-49* lifespan phenotype. However, introduction of this cosmid as an extrachromosomal array failed to improve lifespan of the *nhr-49* deletion mutant;

lifespan was again reduced, from 10.0 ± 2.8 days to 8.6 ± 1.8 days (Figure 2.2B), but no other phenotypes were tested. The similar toxicities of the cosmid and the cDNA construct suggested that the failure of the parent plasmid to rescue was not due to missing genomic sequence. I next tested the hypothesis that the truncated protein predicted to result from the *nhr-49(nr2041)* deletion might have dominant negative activity that prevented proper function of the full-length protein produced off of the extrachromosomal array. This was considered a valid possibility because *in silico* translation of the *nhr-49(nr2041)* product corresponds to the DNA-binding domain, which could potentially bind to DNA to regulate target genes constitutively. Worms heterozygous for the *nhr-49(nr2041)* deletion had a wild-type lifespan, indicating that there is no dominant negative activity of the mutant protein (Figure 2.2C). These data, which argued against missing genomic elements or dominant negative interactions of the deletion product, caused us to focus on issues of localization or copy number.

While injecting constructs to yield high copy extrachromosomal arrays can frequently rescue mutant phenotypes, one potential obstacle is germline silencing of the repetitive array (Kelly et al., 1997). As our lab had previously shown that NHR-49 was required for starvation-dependent germline remodeling during starvation, I postulated that there might be a need for NHR-49 within the gonad in the fed state (Angelo and Van Gilst, 2009). In an attempt to introduce NHR-49 throughout the organism at physiological levels, I switched to either microparticle bombardment, which randomly inserts a low-copy array into the genome (Praitis et al., 2001) or MosSCI, which uses transposon technology to target a single-copy insertion to a specific locus (Frokjaer-Jensen et al., 2008). However, even after multiple bombardment experiments and injecting hundreds of worms for MosSCI, I was unable to generate stable integrant lines by either method. This latter failure is likely due to technical problems, as neither I nor a technician were able to generate a line with the empty targeting vector; although I attempted to introduce several different constructs by bombardment, I did not perform an empty vector control for this protocol. The closest I came was a heterozygous line containing an unstable MosSCI targeting array. This line had a lifespan of 11.0 ± 0.7 days compared to 8.6 ± 0.5 days for the *nhr-49* mutant control (Figure 2.2D). However, even though the injection line carried the *nhr-49(nr2041)* allele, the genetic background also contained the genomic *unc-119(ed3)* mutation and transposon insertion. While I cannot definitively say whether the array actually rescued the lifespan phenotype, it seems unlikely that full rescue of the *nhr-49* mutant

phenotype was achieved. Taken together, these lifespan data show that *C. elegans* are very sensitive to absolute levels of NHR-49 protein. Deletion mutants are short-lived and overexpressing the NR decreases lifespan even further. Successful bombardment or MosSCI experiments may provide a means to introduce an *nhr-49* transgene without toxicity by reducing copy number and avoiding germline silencing.

Misregulation of NHR-49 target genes by overexpression of the nhr-49 *transgene is inconsistent with toxicity*

Because NHR-49 regulates sets of genes that are known to be involved in lifespan, I was interested in exploring whether the toxicity associated with overexpression of NHR-49 was due to misregulation of these genes (Pathare, submitted; Van Gilst et al., 2005a). I performed qRT-PCR on synchronized L4 populations of lines containing the integrated cDNA rescue construct (*fhc01*) in both N2 and *nhr-49* mutant backgrounds. I looked for changes in expression of known NHR-49 targets, including genes involved in β-oxidation, sphingolipid metabolism, and fatty acid desaturation (Pathare, submitted). As expected, the overall trend is that the addition of exogenous NHR-49 and deletion of *nhr-49* have opposite effects on transcription (Figure 2.3). For example, desaturases are highly down-regulated in an *nhr-49* background, while the overexpression vector has minimal effect in the N2 background and increases their levels in the mutant background (Figure 2.3A). If anything, I would anticipate a positive influence from the increased expression of these genes, as our lab has demonstrated a strong correlation between increased desaturation and lifespan (Pathare, submitted). Furthermore, expression of NHR-49-activated β-oxidation genes is reduced in the mutant but increased in the transgenic lines (Figure 2.3). Conversely, preliminary data also suggests that NHR-49 overexpression has the same effect on sphingolipid and lipid-remodeling genes as that reported for deletion of *nhr-49* (Pathare, submitted), although the effect is muted (Figure 2.3B). However, misregulation of these genes is not thought to affect the *nhr-49* mutant lifespan (Pathare, submitted).

Interestingly, another of my projects demonstrated a positive correlation between increased β-oxidation and lifespan in *C. elegans*. I completed a screen in which I mutagenized an *acs-2::GFP* strain, which functions as a reporter for the β-oxidation module of the NHR-49-mediated fasting response. It has been shown that NHR-49 dramatically increases expression of *acs-2* when food is removed (Figure 2.4A)(Van Gilst et al., 2005a); I was interested in isolating

EMS-generated mutants that inappropriately increased β-oxidation in the fed state (Figure 2.4B). Of 13 unoutcrossed mutant lines, 7 were significantly longer-lived than the *acs-2::GFP* parent strain (Figure 2.4C). Sequencing through the *nhr-49* locus revealed that only one of these strains contained a mutation in the region; this allele was designated *nhr-49(fhc1804)*. Due to technical difficulties involving gradual silencing of the *acs-2::GFP* transgene, the other mutants were not mapped. The *fhc1804* point mutation causes an alanine to threonine mutation that is predicted to fall at the mouth of the ligand-binding pocket, where it could alter ligand accessibility or exchange (Figure 2.5A). It is worth noting that this same mutation came out of another screen looking for constitutive ARD phenotypes conducted by summer student Julie Grimm. As expected for a mutant with increased β-oxidation, biochemical fat storage assays measured a decrease in fat storage in the original *nhr-49(fhc1804)* mutant (Figure 2.5B). To evaluate the effect of this mutation on the expression of NHR-49 target genes, I performed qRT-PCR on synchronized L4s in *nhr-49(fhc1804)* mutants in both *acs-2::GFP* and N2 backgrounds. The point mutation had opposite effects on the β-oxidation gene set in these two backgrounds; in most cases, genes that were increased by the point mutant in the *acs-2::GFP* line were decreased in an N2 background and vice versa (Figure 2.5C). Additionally, two different outcrossed *nhr-49(fhc1804)* lines also had different expression profiles (Figure 2.5C). The lack of a common trend among the *fhc1804*-containing lines, along with the difficulty I experienced in generating these homozygous mutant lines, suggests that significant metabolic adjustments must be made to accommodate the point mutant; presence of the translational *acs-2::GFP* transgene may either mask these changes or may itself be protective. Nevertheless, data collected from this screen indicates that increased expression of β-oxidation genes might increase lifespan instead of having a detrimental effect.

NHR-49 predicted target of post-transcriptional regulation

One key difference between the constitutive activity in the EMS mutant and the overexpression of *nhr-49* in the transgenic lines is that *nhr-49(fhc1804)* is at the genomic locus, ensuring proper copy number, regulation, and localization. Even though I performed a series of experiments testing the role for each of these factors in NHR-49-driven toxicity, I failed to achieve all three at once. As miRNAs have been shown to be key regulators of other *C. elegans*

nuclear receptors (Hammell et al., 2009), I decided to investigate the potential for miRNA regulation of NHR-49.

Using the miRanda miRNA target prediction algorithm available on MicroCosm, I identified two miRNAs predicted to target the 3'UTR of *nhr-49*: mir-243 and mir-797. To be physiologically relevant, the miRNAs must be expressed in the same spatiotemporal environment as the *nhr-49* mRNAs on which they need to act. Others have found that a transcriptional reporter of mir-243 is expressed in the intestine, a head neuron, and the spermathecal-uterine valve starting at mid-embryo; the *mir-797* promoter drove expression in the pharynx, distal tip cell, and rectal gland at different times from late embryo through L4 (summarized in Figure 2.6A) (Martinez et al., 2008). Previous attempts to make an *nhr-49* transcriptional fusion failed due to toxicity of the construct (Marc Van Gilst, unpublished data), so I instead relied on immunohistochemistry with anti-FLAG antibodies. I found FLAG-tagged NHR-49 present in nuclei throughout the germline and intestine, starting early in embryogenesis (Figure 2.6B). Because I was fixing extruded gonads and intestines, I was unable to examine other tissues for NHR-49 localization. A transcriptional reporter with the *nhr-49* promoter driving expression of GFP linked to the *nhr-49* 3'UTR confirmed the intestinal expression and also showed expression in the seam cells and some neurons (Figure 2.6C). However, this reporter construct was introduced as a high copy array, so the absence of GFP in the germline could be due either to silencing of the array or because the *nhr-49* promoter does not drive expression in that tissue.

The finding of two miRNAs, predicted to both target *nhr-4*9 and to overlap in expression pattern, strengthened the hypothesis that post-transcriptional regulation might play an important role managing NHR-49 levels or localization. The requirement for protein titration by these miRNAs would help to further explain the toxicity of the rescue constructs lacking the predicted binding sites. As this putative miRNA-driven regulation of *nhr-49* would require the presence of the 3'UTR for miRNA recognition, I made a final construct containing the same promoter as before, driving expression of the *nhr-49* genomic locus, complete with the 3'UTR. Introduction of this plasmid, even as a high copy, non-integrated array, increased *nhr-49* mutant lifespan from 8.9 ± 0.6 days to 13.4 ± 1.4 days (Figure 2.8).

Since I hypothesized that miRNAs might be playing a role in regulation of NHR-49, I was curious as to how the miRNAs themselves might be regulated. I found that neither fasting

nor disruption of *nhr-49* by either RNAi or deletion had an effect on the localization of transcriptional reporters of mir-243 and mir-797 (Figure 2.7). I also tested the role of NHR-64, a nuclear receptor whose knockdown was shown to produce the reverse phenotype from that seen when *nhr-49* RNAi was combined with desaturase defects (Liang et al., 2010). I reasoned that these opposing phenotypes might result from repression of *nhr-49* via NHR-64 regulation of miRNAs. However, RNAi against *nhr-64* had no effect on GFP localization in the reporter strains (Figure 2.7). While elucidating the regulatory mechanisms of *mir-243* and *mir-797* is a goal for future work, requirement of the NHR-49 3'UTR for phenotypic improvement is a suggestive that these or other, as yet unidentified miRNAs, are critical for regulation of NHR-49 protein levels.

miRNA mutant defects most severe in recovery from adult reproductive diapause

To begin to get a sense for processes in which these miRNAs play a role, I began preliminary characterization of available mutants. MT15454 contains a deletion covering *mir-243*, while MT16309 is missing both *mir-797* and the neighboring *mir-247*; as neither line had been outcrossed, they may have harbored background mutations resulting from the mutagenesis. I also created a double mutant lacking both *nhr-49*-targeting miRNAs by crossing these two lines together. Deletion of *mir-243* decreases lifespan slightly in both the N2 and *mir-247&mir-797* background, but neither deletion has any significant effect on brood size (Figure 2.A and B). While the slight reduction in progeny production of the double mutant might suggest some redundancy in regulation of *nhr-49* or other targets by mir-243 and mir-797, it could also be an effect of background mutations in the unoutcrossed strains. Finally, I assayed the effect of these miRNA deletions on the saturated fat ratio. Since this value is abnormally high in *nhr-49* mutants due to misregulation of desaturase genes (Pathare, submitted), I expected deregulation of *nhr-49* to also alter this ratio. However, the deletions had no effect, either singly or in combination, arguing that mir-243 and mir-797 do not affect this aspect of NHR-49 activity (Figure 2.9C).

In addition to its metabolic targets, NHR-49 regulates genes required for entry into and recovery from the starvation-induced adult reproductive diapause (ARD). I found that when removed from food in the receptive window, *mir-243*, *mir-247&mir-797*, and the double mutant were all able to arrest (although there seemed to be a disproportionate number that arrested as L4

instead of continuing into ARD, based on whether germline retraction occurred during the maintenance phase) and showed some evidence of characteristic tissue remodeling (Figure 2.10A). However, these worms were unable to maintain fertility during the starvation period. Upon recovery I noticed severe physiological defects, including cellularization of germ-like cells, distal tip cell (DTC) migration defects, possible seam cell defects, and yolk accumulation (Figure 2.10B-D). Further investigation revealed seam cell defects to be specific to *mir-247&mir-797* and presence of cellularized bodies and mistargeted DTCs to be unique to *mir-243* (personal communication with Emily Fawcett). Excessive yolk was seen in recovered animals from both single and the double mutant. As will likely be the case with many *C. elegans* miRNAs for which no phenotype has been reported, the roles of mir-243 and mir-797 appear to be limited to a very specific demand: in this case, recovery from ARD.

Discussion

In an attempt to perform structure-function analysis on the nuclear receptor NHR-49, I discovered that its expression levels must be exquisitely regulated. I have implicated the 3'UTR in this process and propose that *nhr-49*-targeting miRNAs, specifically mir-243 and mir-797, might also be important. In addition to a possible role in the regulation of NHR-49, these miRNAs are key players in recovery from the starvation-induced adult reproductive diapause.

NHR-49 levels must be tightly controlled to maintain normal lifespan

Introduction of a gene of interest as a high copy array is a common means of achieving phenotypic rescue in *C. elegans*. Adding back NHR-49 in the form of an integrated cDNA plasmid driven by the *nhr-49* promoter failed to improve lifespan of the *nhr-49(nr2041)* mutant and was actually toxic in the N2 background (Figure 2.2A). The lifespan curves of the *nhr-49* mutant with and without the transgene are nearly overlapping, demonstrating that both deletion and overexpression of *nhr-49* have the same detrimental effect on the organism. However, using the genomic locus and the 3'UTR increased lifespan of the mutant by 50% (Figure 2.8). It is possible that better rescue could be achieved by combining low-copy integration methods with this new 3'UTR-containing construct. The requirement for the 3'UTR implicates regulation by miRNAs, of which there are two predicted to target *nhr-49*. This post-transcriptional regulation likely acts to titrate protein levels or limit tissues in which NHR-49 is expressed.

While at first this rescue seems to contradict the inability for K10C3 to improve lifespan of *nhr-49(nr2041)* worms (Figure 2.2B), the cosmid contains close to 30 kilobases of sequence surrounding the *nhr-49* locus that may be contributing to toxicity of the cosmid. The requirement for the 3'UTR may also help to explain why low-copy integration by bombardment or MosSCI failed. The rescue constructs used in these protocols had no 3'UTR, so if miRNA-mediated tissue specificity is important, then introducing into the genome a ubiquitous version of *nhr-49* that is resistant to this regulation could prove lethal. However, introducing this same version on an extrachromosomal array allows for the formation of chimeric worms, in which the array is lost or silenced in tissues where it may be toxic. The requirement for tissue-specific regulation could also explain why the increased expression of β-oxidation genes and decreased expression of desaturases were not beneficial to lifespan of the transgenic lines (Figure 2.3A); even though these directional changes in the gene modules are predicted to improve longevity, it is possible that there is a specific tissue where these changes must occur.

Previous work has shown NHR-49 to be central to many aspects of *C. elegans* metabolism (Pathare, submitted; Van Gilst et al., 2005a; Van Gilst et al., 2005b); it follows that the organism would tightly regulate such a key player. I found this to be the case and believe regulation occurs via non-coding sequences, likely by miRNAs. Now that the need for these other sequences has been established, it would be interesting to evaluate rescue constructs containing either the cDNA and the 3'UTR or the genomic sequence through the stop codon only, to parse the effects of introns versus the 3'UTR. If these experiments implicate the 3'UTR, its importance could be further validated by selectively mutating residues in the cDNA-UTR construct that are believed to play a role in miRNA recognition. Finally, complete rescue may be achieved by low-copy integration of the constructs that partially improve lifespan at high copy number.

Newly identified phenotypes for mir-243 and mir-797

miRNA target prediction led us to investigate two miRNAs: mir-243 and mir-797. As with the majority of *C. elegans* miRNAs, neither the single nor the double mutants had significant fed phenotypes. Thus, even though the 3'UTR is required for exogenous *nhr-49* to improve lifespan of the *nhr-49* deletion mutant, deleting the miRNAs that are predicted to target this 3'UTR has no real consequence in the fed state. This apparent discrepancy may arise from

the existence of other, unidentified miRNAs involved in regulation of NHR-49, complication of the miRNA deletion phenotype by misregulation of multiple targets in combination with NHR-49, or a regulatory role for the 3'UTR outside of miRNAs.

As NHR-49 is also required in the fasted state, I assayed the miRNA mutants for their ability to enter, maintain, and recover from the adult reproductive diapause. Unlike in an unstressed state, *mir-243* and *mir-247&mir-797* animals showed significant defects in recovery from ARD. *mir-243* mutants accumulate what appear via DIC microscopy to be undifferentiated spermatocytes and exhibit gonadal migration defects, while recovered *mir-247&mir-797* animals show a seam cell defect; both genotypes amass excess yolk (Figure 2.10B-D). These are the first phenotypes reported for these miRNA mutants. Additionally, the identification of these miRNAs as critical to healthy exit from ARD will allow for better understanding of the processes involved in recovery.

NHR-49 is one of the few targets in common between the two miRNAs and the yolk recovery phenotype seen in the miRNA mutants is also shared by the *nhr-49* deletion strain. I therefore speculate that this specific phenotype is due to misregulation of the nuclear receptor upon return to food. It is curious that *nhr-49* mutants, which have no NHR-49 protein, closely resemble miRNA mutant recovered ARD animals, which would theoretically have increased *nhr-49* expression given the traditional association of miRNAs with translational repression. This dichotomy suggests that the miRNAs may actually be behaving as activators as they do in quiescent mammalian cells under serum starvation conditions (Vasudevan et al., 2007). Monitoring NHR-49 protein levels as ARD progresses would address this hypothesis.

On the other hand, the phenotypes specific to the single deletion mutants are likely to be caused by misregulation of targets other than NHR-49 (Tables 2.2 and 2.3). For example, mir-797 is also predicted to target another nuclear receptor, NHR-88, which is expressed in the hypodermis surrounding the seam cells of adult animals (Table 2.2, Figure 3.2A). While its function there is currently unknown, misregulation may cause the vacuolization that seen in that tissue upon recovery of the *mir-247&mir-797* mutants.

There are also good candidates for genes whose misregulation may cause the recovery phenotypes of *mir-243* mutants. These animals show abnormal tracking of the DTC as the germline refills, which may be attributable to any of the predicted targets with reported migration phenotypes, such as the Golgi complex member *cogc-4* or the actin isoform *act-4* (Table 2.3).

Accumulation of cells reminiscent of undifferentiated spermatocytes, both within and outside of the gonad, may be caused by misregulation of genes involved in gametogenesis; mir-243 is predicted to target a number of genes that have been annotated as spermatogenesis-enriched, as well as the gene *lin-9* (Table 2.3). Mutation in *lin-9* leads to ectopic sperm within the body cavity, providing another example of a miRNA mutant having the same phenotype as interruption of a target gene (Beitel et al., 2000); as with the *nhr-49* and miRNA deletion yolk recovery phenotypes, this may suggest an activation role for mir-243 upon recovery. Another possibility is that improper migration of the distal tip results in the mitotic stem cell population being positioned in the incorrect niche, such that these cells are receiving signals to differentiate into sperm instead of oocytes.

Interestingly, both the ectopic sperm phenotype in the *mir-243* mutants and the seam cell defect seen in the *mir-247&mir-797* background point towards problems with cell differentiation. Entry into ARD implies a successful molt from the final larval stage to adulthood; this transition is normally characterized by final differentiation and fusion of seam cells (Altun, 2009) and an irreversible switch from spermatogenesis to oogenesis within the germline (Kuwabara and Perry, 2001), among other physiological changes. However, I see what appear to be unfused seam cells in *mir-247&mir-797* and undifferentiated spermatocytes in *mir-243*, suggesting that these mutants may cause heterochronic defects that affect specific tissues. This hypothesis is consistent with the many other heterochronic defects associated with miRNAs (Resnick et al., 2010). Additionally, differences in developmental timing between different tissues may also explain why many *mir-243;mir-247&mir-797* animals starved during the receptive window arrested as L4s instead of developing into arrested adults; if tissues used for determining age for ARD entry are developing more quickly than other tissues, the worms would be starved before the optimal window. Further work is required to definitively identify the abnormalities seen in *mir-243* and *mir-247&mir-797* recovered animals as yolk, spermatocytes, and seam cells; this could be done by crossing the mutants to transgenic lines carrying GFP reporters marking these specific tissues.

Experimental Procedures

Strains and maintenance

The wild-type N2 (Bristol) strain, *unc-119(ed3)III*, *mir-243(n4759)IV, mir-247&mir-797(n4505)X*, VT1474 *unc-119(ed3)III;maIs177[unc-119(+) + Pmir-243::GFP]*, VT1673 *unc-119(ed3)III*; *maIs256[unc-119(+) + Pmir-247-797::GFP]*, EG4322 *ttTi5605II;unc-119(ed9)III*, and EG5003 *unc-119(ed3)III;cxTi10882IV* were provided by the Caenorhabditis Genome Center, which is funded by the NIH National Center for Research Resources (NCRR). *nhr-49(nr2041)I* was a gift from Carl Johnson at Axys Pharmaceuticals and was outcrossed to N2. *nhr-49(fhc1804)I* was recovered in an EMS mutagenesis screen in a fasting reporter background containing *acs-2::GFP*. Millions of genomes were mutagenized using standard protocols (Brenner, 1974) and screened in both the F1 and F2 generations for GFP expression on well-fed plates. Worm maintenance was carried out at 20˚C using standard methods.

Cloning and plasmids

All plasmids were constructed using standard molecular techniques. Rescue constructs, with the exception of *fhc06*, contained 2100 base pairs of the *nhr-49* promoter driving expression of the *nhr-49* cDNA tagged with 2-4 copies of the FLAG epitope sequence. *fhc01* was subcloned into the L3691 backbone, while *fhc04* is in the MosSCI targeting vector pCFJ151 (Addgene, Cambridge, MA). The *fhc06* construct, also in the L3691 subcloning vector, contained the same promoter region upstream of the entire *nhr-49* genomic locus, with 2 FLAG tag sequences inserted just after the start site. The *nhr-49* transcriptional reporter contained the same promoter sequence as above upstream of GFP and the *nhr-49* 3'UTR in the L3691 backbone. The K10C3 cosmid was acquired from the Sanger Institute.

Transgenic rescue of nhr-49(nr2041)

Transgenic lines containing high-copy extrachromosomal arrays were generated by co-injecting the rescue construct with a *myo-3::GFP* marker following standard procedures (Mello et al., 1991). In the case of the *fhcEx01* array, integrated lines were generated from injection lines via irradiation with 4000 rads and selection for the *myo-3::GFP* reporter, as described (Mello and Fire, 1995). Attempts to create low-copy integrated arrays used either microparticle

bombardment or chromosome II-directed Mos-mediated single copy gene insertion followed published protocols (Frokjaer-Jensen et al., 2008; Praitis et al., 2001).

Visualization of FLAG-NHR-49

For Western blotting, protein samples were made by picking approximately 25 adult worms into nematode solubilization buffer (0.3% ethanolamine, 2mM EDTA, 1mM PMSF, 5mM DTT, 1X protease inhibitor). Samples were microwaved and boiled to denature the proteins and then the lysate was passed through a 26-gauge needle. Samples were loaded onto a NuPAGE 10% Bis-Tris gel (Invitrogen, Grand Island, NY) and run using the XCell *SureLock* Mini-Cell (Invitrogen, Grand Island, NY) for 90 minutes at 200 volts at 4˚C. Transfer to a 0.45µm nitrocellulose membrane (Bio-Rad, Hercules, CA) was done at 35 volts for 1 hour in the XCell II Blot Module (Invitrogen, Grand Island, NY) at 4˚C. Blots were blocked and then cut based on visible ladder so that higher molecular weight proteins could be probed for the FLAG epitope using a commercially available anti-FLAG rabbit polyclonal antibody from Sigma-Aldrich (St. Louis, MO) and the lower molecular weight proteins could be probed with anti-actin mouse mAb from Calbiochem/EMD Biosciences (San Diego, CA) for a loading control. Incubation in a 1:1000 dilution of primary antibodies occurred overnight at 4˚C. The FLAG (top) half of the blot was probed with a 1:3000 dilution of donkey anti-rabbit IgG HRP-linked whole antibody (Amersham, Piscataway, NJ) and the actin (bottom) half was probed with 1:10,000 goat anti-mouse total Ig peroxidase conjugate (Calbiochem/EMD Biosciences, San Diego, CA) for 1 hour at room temperature. Detection of HRP was done using the Pierce ECL Western blotting substrate (Rockford, IL).

For immunohistochemistry, gonads from mixed-stage adult worms were prepared using a formaldehyde freeze/crack protocol. Primary incubation with 1:250 anti-FLAG rabbit polyclonal antibody from Sigma-Aldrich (St. Louis, MO) occurred overnight at 4˚C and secondary incubation occurred for 1 hour at room temperature with 1:1000 Cy3-conjugated AffiniPure donkey anti-rabbit from Jackson ImmuoResearch (West Grove, PA). Images were acquired using a Zeiss AxioImager Z1 microscope equipped with an AxioCam 5 MRm camera and Axiovision 4.8 software (Gottingen, Germany).

Lifespan assays

Lifespans were determined by counting the number of days individual worms survived after the L4 molt. Experiments were conducted at 20˚C on *Escherichia coli* strain HT115 transformed with empty vector unless otherwise noted. HT115 was used instead of OP50 because RNAi experiments were conducted in parallel. Live animals were moved to fresh plates daily during the reproductive period, after which they were moved every two to three days. Worms were considered dead when they no longer responded to gently prodding. Bagged animals were censored. Lifespan curves and statistical data, including *P*-values from a one-way ANOVA followed by either a Bonferroni post-test (Figure 2.2, 2.8, 2.9) or a Dunnett multiple comparison test (Figure 2.4), were produced and analyzed using GraphPad Prism 5 (GraphPad Software, San Diego, CA).

Brood size assays

L4 animals were picked to individual OP50 plates on day 0. Adults were moved to new plates daily as long as they were laying embryos. Progeny plates were maintained at 20˚C until worms were L3-L4, at which point the number of larvae were counted and recorded. Individuals that bagged while other worms in the group were still laying were censored. Statistical analyses, including *P*-values from a one-way ANOVA followed by a Bonferroni multiple comparison test of relevant strains, used GraphPad Prism 5 (GraphPad Software, San Diego, CA).

RNA extraction and qRT-PCR

Larvae were synchronized by hatching embryos collected by bleaching a gravid population on unseeded nematode growth media (NGM) plates. 20-24 hours later, the synchronized population was plated to high growth (HG) plates seeded with *Escherichia coli* strain OP50 and grown to mid-L4 at room temperature, at which point they were collected in M9, washed 5 times to remove excess bacteria, and then frozen in an ethanol-dry ice bath. Samples were stored at -80˚C until ready for processing.

RNA extraction was done using the QIAGEN RNeasy Plus Mini kit (Germantown, MD). The protocol used was that for purifying total RNA from animal cells. Tissues/cells were disrupted by sonication and homogenized using a QIAshredder column (QIAGEN, Germantown, MD). cDNA synthesis was conducted using M-MuLV reverse transcriptase (20,000 units, New

England BioLabs, Ipswich, MA), 1X of the provided reverse transcriptase buffer, 1mM dNTPs (Invitrogen, Carlsbad, CA), and RNaseOUT recombinant ribonuclease inhibitor (2000 units, Invitrogen, Carlsbad, CA) templated with 5µg RNA and 30µg random primers (Invitrogen, Carlsbad, CA) in a 100µl reaction incubated at 42˚C for 1 hour.

30µl PCR reactions consisting of 0.3µM primers, $1/500^{th}$ of the above cDNA reaction, 125µM dNTPs (Invitrogen, Carlsbad, CA), 1.5mM $MgCl_2$, 1X reaction buffer, and 0.75 units of Taq DNA polymerase (Invitrogen, Carlsbad, CA) were prepared in 96-well plates. Reactions were run using a Bio-Rad iCycler equipped with a MyiQ Single Color Real-Time PCR Detection System (Hercules, CA) to automatically monitor formation of double-stranded DNA product using SYBR-Green (Molecular Probes, Eugene, Oregon). Data shown ± SEM are ΔΔCt values, while *P*-values are based on t-tests of ΔCt values normalized to *nhr-23* expression. qRT-PCR primers were designed by Pranali Pathare and Tessie Ng using Primer 3 software (Rozen and Skaletsky, 2000).

Lipid purification and analysis

To collect worms for lipid analysis, approximately 30,000 L1s synchronized by an overnight hatch on unseeded NGM plates were plated to NGM plates seeded with *Escherichia coli* strain OP50 and grown at room temperature. Once the population reached mid-L4, the worms were collected and washed 5 times with M9. Once excess buffer was aspirated from the worm pellet, the sample was frozen in a ethanol-dry ice bath and transferred to -80˚C. For fat storage measurements, phospholipid (PL) and triacylglyceride (TAG) fractions were purified as described (Perez and Van Gilst, 2008). The resultant fatty acid methyl esters were analyzed by gas chromatography/mass spectrometry (GC/MS) (Agilent 5975GC, 6920MS). To quantify TAG and PL yields, total PL and TAG were compared to the internally added standards (1,2-Dihepatdecanoyl-*sn*-Glycero-3-Phosphocholine, Avanti Polar Lipids, Alabaster, AL and tritridecanoin, Nu-Chek Prep, Elysian, MN). Data were presented as a TAG:PL ratio, which was determined by measuring the sum of all fatty acids found in TAGs versus the sum of all fatty acids found in PLs (Ashrafi et al., 2003).

Protein structure prediction

Structural effects of the *fhc1804* mutation on the NHR-49 ligand binding domain were predicted

using the Automated Mode interface of SWISS-MODEL (Arnold et al., 2006; Guex and Peitsch, 1997; Kiefer et al., 2009; Peitsch, 1995; Schwede et al., 2003). Visualization and protein models were generated by Charles Brooks using VMD (Humphrey et al., 1996).

miRNA target prediction

miRNA target prediction was done using the MicroCosm interface available from miRBase (Griffiths-Jones, 2004; Griffiths-Jones et al., 2006; Griffiths-Jones et al., 2008; Kozomara and Griffiths-Jones, 2011). Annotation of target gene functions was based on phenotypes, expression data, and gene ontology information available on WormBase.

Adult reproductive diapause

To induce adult reproductive diapause, synchronized L4s were starved at mid-L4 as described (Angelo and Van Gilst, 2009). Starvations were maintained on sterilely poured NGM plates at 20˚C. Individual animals were picked to NGM plates seeded with *Escherichia coli* strain OP50 for recovery.

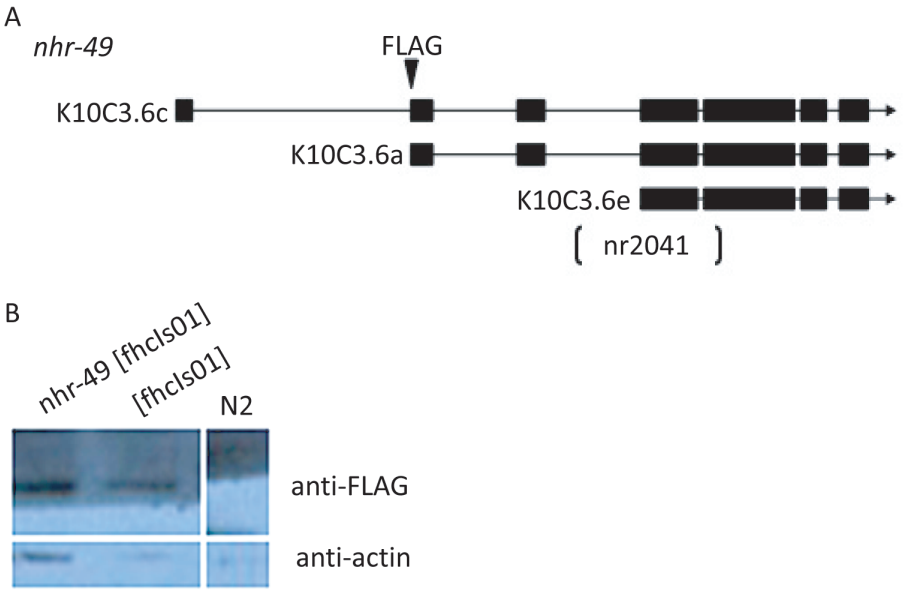

Figure 2.1. Creation of transgenic *nhr-49* overexpression lines. (A) *nhr-49* locus, showing spliceoforms, position of *nr2041* deletion, and location of FLAG insertion for plasmid construction. (B) Western blot verifying presence of FLAG-NHR-49 protein in overexpression lines.

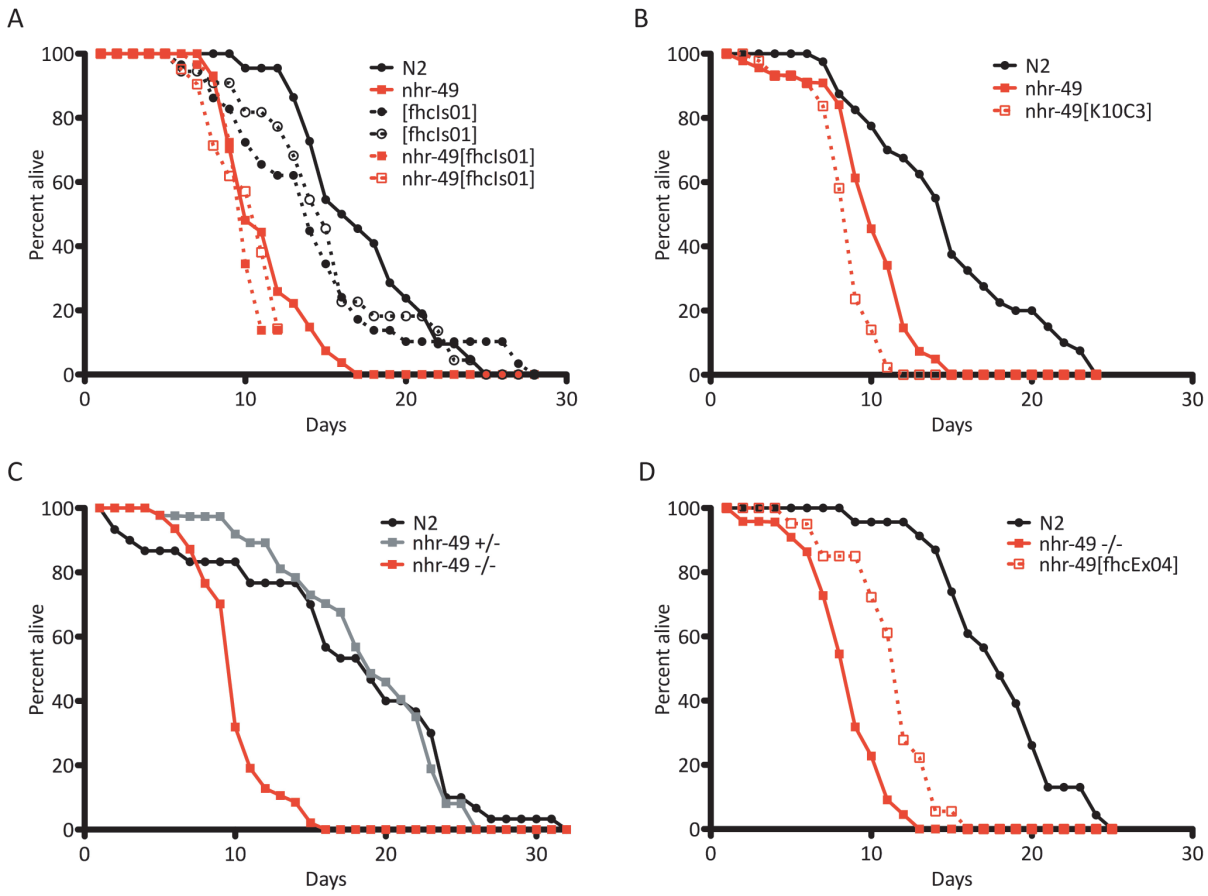

Figure 2.2. Deletion or overexpression of *nhr-49* reduces lifespan. (A) Representative lifespan curves of N2, *nhr-49(nr2041)*, and transgenic lines overexpressing *nhr-49* in both the N2 and *nhr-49(nr2041)* backgrounds. Two lines of each genotype were assayed to account for lifespan decreases due to point of integration. Mean lifespans ± SD are: N2: 18.6 ± 5.4; *nhr-49(nr2041)*: 11.6 ± 2.3****; *fhcIs01[FLAG-nhr-49$_{cDNA}$]*: 14.5 ± 5.6***, 15.2 ± 4.8*; *nhr-49(nr2041); fhcIs01[FLAG-nhr-49$_{cDNA}$]*: 9.7 ± 2.1$^{\dagger ns}$, 9.8 ± 1.0$^{\dagger ns}$. (B) Lifespan of a transgenic line overexpressing the K10C3 cosmid in an *nhr-49* background. Mean lifespans ± SD are: N2: 14.9 ± 5.0; *nhr-49(nr2041)*: 10.0 ± 2.8****; *nhr-49(nr2041);fhcEx02[K10C3]*: 8.6 ± 1.8$^{\dagger ns}$. (C) Lifespan curves of N2, *nhr-49(nr2041)/+* heterozygotes, and *nhr-49(nr2041)*. Mean lifespans ± SD are: N2: 18.0 ± 7.6; *nhr-49(nr2041)/+*: 18.9 ± 2.0^{ns}; *nhr-49(nr2041)*: 10.7 ± 5.2****. (D) Lifespan of transgenic worms containing extrachromosomal arrays of the MosSCI rescue plasmid in an *nhr-49* mutant background. Mean lifespans ± SD are: N2: 18.1 ± 3.8; *nhr-49(nr2041)*: 8.6 ± 2.4****; *nhr-49(nr2041)I;ttTi5605II;unc-119(ed9)III;fhcEx04[unc-119(+) + FLAG-nhr-49$_{cDNA}$]*: 11.1 ± 3.0$^{\dagger **}$. All experiments were repeated once and included at least 16 individual worms per genotype (see Table 2.1 for details). Controls shown with transgenic lines were assayed in parallel to account for experimental variations in N2 and *nhr-49* mutant lifespans. Significance values shown are based on comparison to N2 unless marked with †, in which case comparison is to *nhr-49(nr2041)*. $^{*}P < 0.05$, $^{***}P < 0.001$, $^{****}P < 0.0001$, ^{ns}not significant.

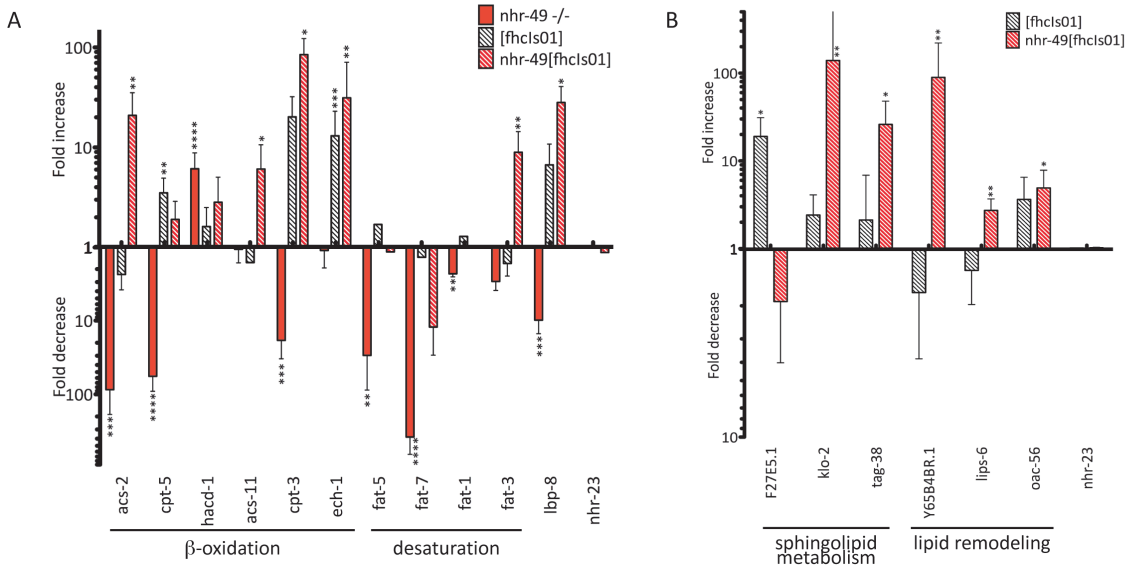

Figure 2.3. Overexpression of NHR-49 variably affects target gene expression. (A) β-oxidation and desaturase gene expression changes, as measured by qRT-PCR for *nhr-49(nr2041), fhcIs01[FLAG-nhr-49$_{cDNA}$]*, and *nhr-49(nr2041);fhcIs01[FLAG-nhr-49$_{cDNA}$]* grown to L4. (B) qRT-PCR data showing sphingolipid metabolism and lipid remodeling gene expression changes in *fhcIs01[FLAG-nhr-49$_{cDNA}$]*, and *nhr-49(nr2041);fhcIs01[FLAG-nhr-49$_{cDNA}$]* grown to L4. These gene classes are increased in an *nhr-49(nr2041)* mutant (Pathare, submitted). Gene classifications are shown under gene names. Differences shown are means from one experiment performed in duplicate, ± SEM when compared to an N2 population. $^{*}P < 0.05$, $^{**}P < 0.01$, $^{***}P < 0.001$, $^{****}P < 0.0001$.

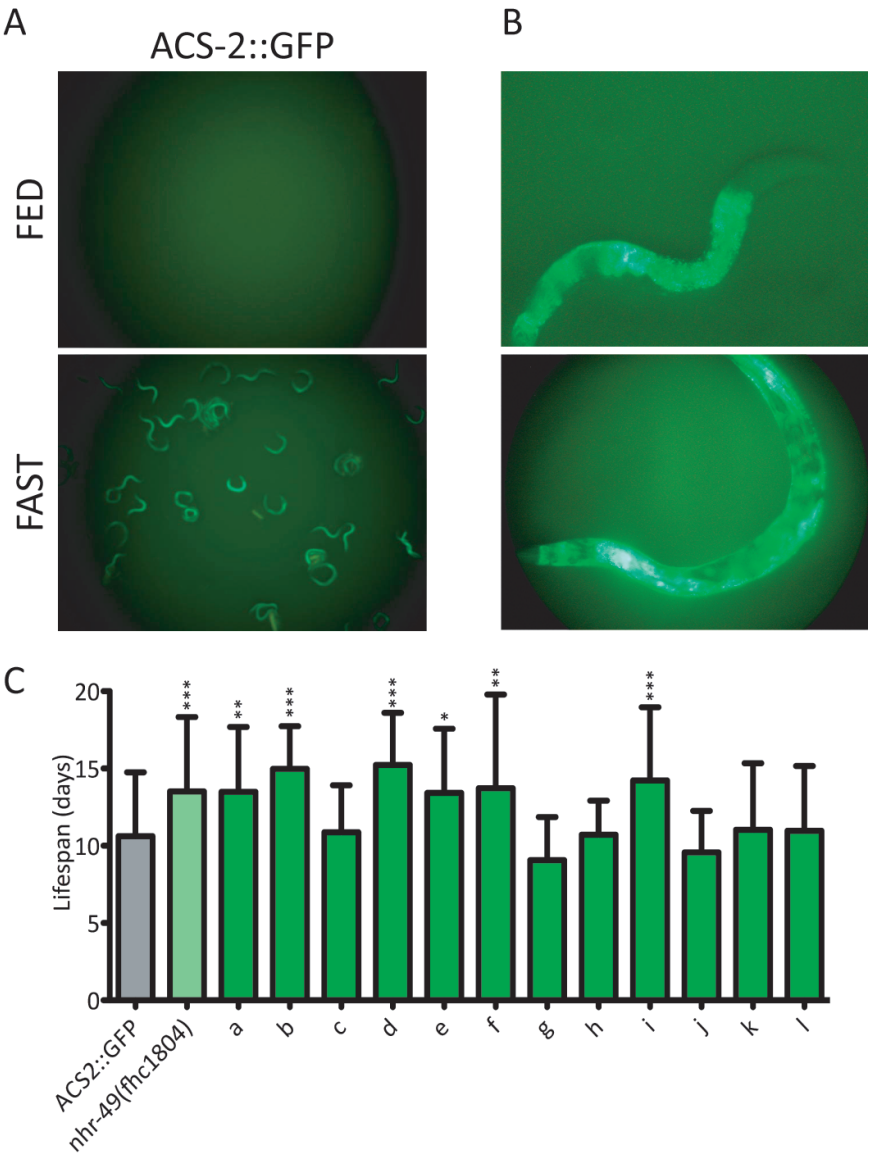

Figure 2.4. Increased β-oxidation correlated to increased lifespan. (A) Fed and fasted plates of transgenic lines carrying the *acs-2::GFP* reporter (Images acquired by Giana Angelo). (B) Sample images of fed worms from two constitutive GFP lines from the screen. (C) Mean lifespans ± SD for 13 EMS-generated mutants exhibiting constitutive activation of the β-oxidation gene, *acs-2*. *acs-2::GFP* lifespan was measured in 3 separate experiments (141 individual animals), *nhr-49(fhc1804)* lifespan was measured in 2 separate experiments (86 individuals) and the other mutant lifespans were measured once (n>22 individuals). Mutant longevity is compared to the *acs-2::GFP* parent strain. $^{*}P < 0.05$, $^{**}P < 0.01$, $^{***}P < 0.001$.

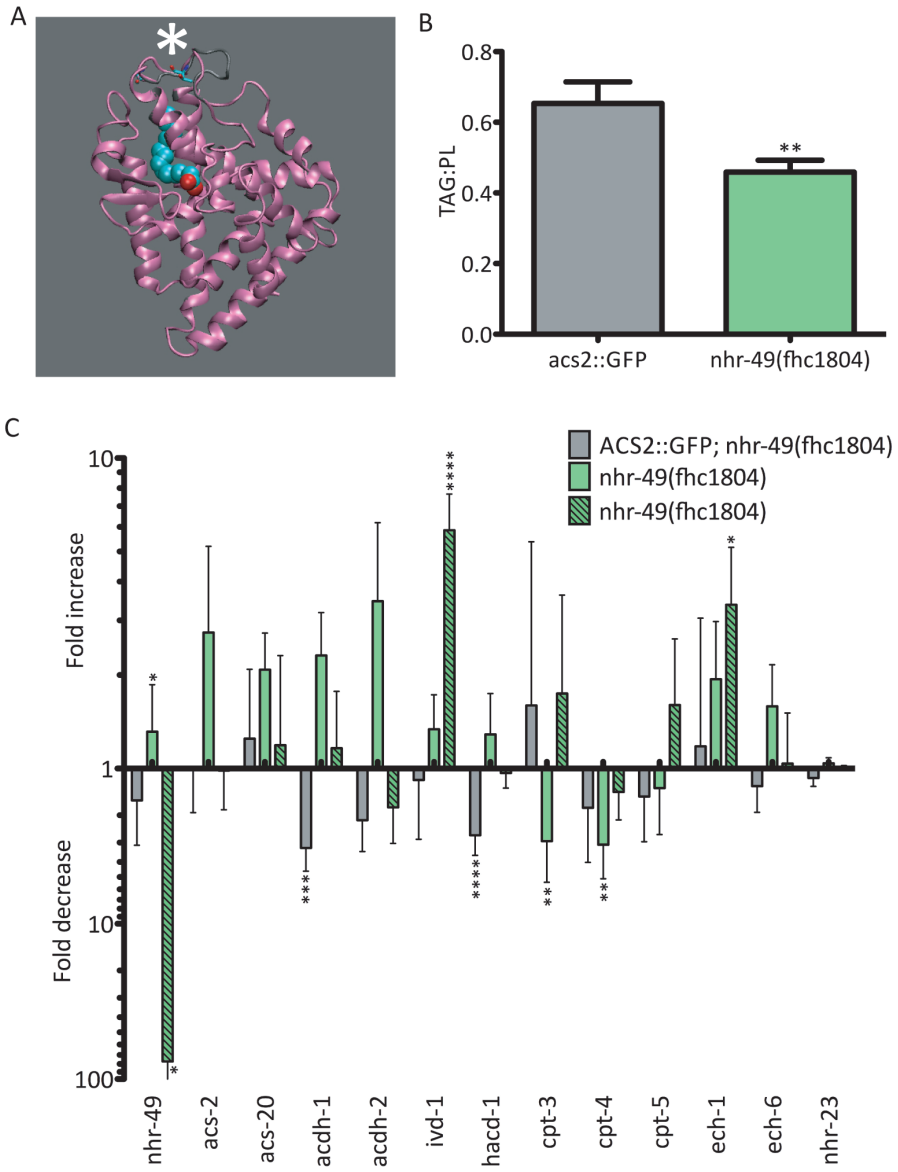

Figure 2.5. Ligand-binding domain mutant of NHR-49 alters β-oxidation. (A) Predicted protein structure of native (purple) and mutant (grey) NHR-49 ligand-binding domain. Asterisk denotes region of the protein structure that is predicted to change (image generated by Charles Brooks). (B) Ratio of triglyceride to phospholipid as a measure of fat storage in the constitutively active NHR-49 mutant and the *acs-2::GFP* parent strain. Mean from at least 12 experiments is shown ± SEM. (C) qRT-PCR expression data for a panel of NHR-49 β-oxidation target genes in original and outcrossed constitutive NHR-49 mutants, compared to the appropriate parent strain. Differences shown are means of at least two experiments performed in duplicate ± SEM. $^{*}P < 0.05$, $^{**}P < 0.01$, $^{***}P < 0.001$, $^{****}P < 0.0001$.

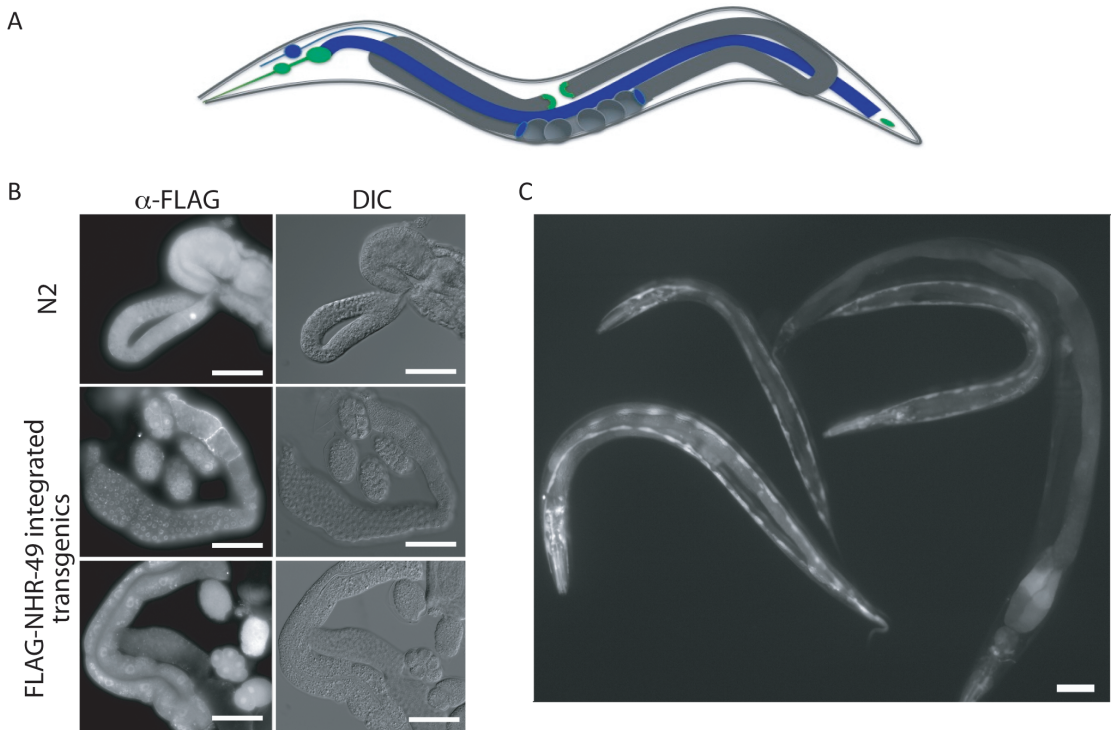

Figure 2.6. miRNA expression overlaps with NHR-49 localization. (A) Summary of reporter construct expression patterns of *mir-243* (blue) and *mir-247&mir-797* (green). *Pmir-243* drove expression in a head neuron, the intestine, and the spermathecal-uterine valve, while *Pmir-797* drove expression in the pharynx, distal tip cell, and renal gland (Martinez et al., 2008). (B) FLAG-NHR-49 protein localizes to the germline and intestinal nuclei in a low-copy, integrated strain. The signal seen in the N2 control is non-specific background. (C) Expression of *Pnhr-49*::GFP reporter in seam cells, head neurons, pharynx, and intestine. Scale bar = 50μm for all images.

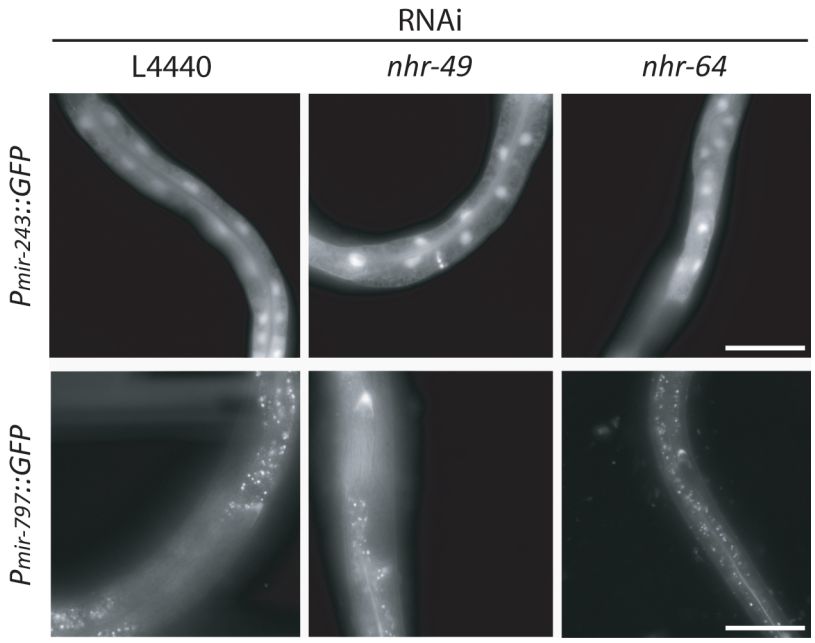

Figure 2.7. miRNA expression is not affected by depletion of *nhr-49* or *nhr-64*. Live images of *Pmir-243::GFP* and *Pmir-797::GFP* on L4440 empty vector, *nhr-49* RNAi, and *nhr-64* RNAi. Expression of the reporter looks the same despite the different RNAi constructs. *Pmir-243::GFP* panels focus on intestinal expression of the worm, while *Pmir-797* panels focus on the distal tip cell. GFP expression in other tissues was also unaffected. Scale bar = 50μm and all images were acquired at the same magnification.

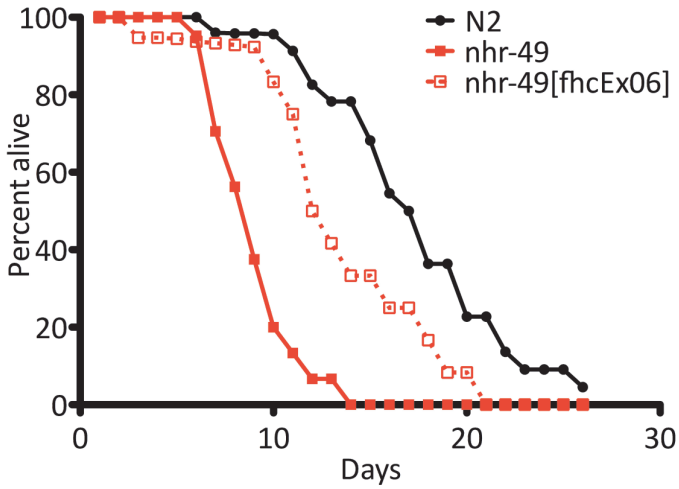

Figure 2.8. Inclusion of genomic regions allows for rescue of *nhr-49* mutant lifespan. Lifespan of transgenic worms containing extrachromosomal *fhc06* in an *nhr-49* mutant background. Means from one experiment with at least 12 individual lifespans ± SD are: N2: 17.5 ± 4.9; *nhr-49(nr2041)*: 8.9 ± 2.2****; *nhr-49(nr2041);fhcEx06[FLAG-nhr-49$_{geno}$]*: 13.4 ± 4.8$^{\dagger **}$. Worms were grown on OP50. †compared to *nhr-49(nr2041)* control, $^{*}p < 0.05$, $^{****}p < 0.0001$.

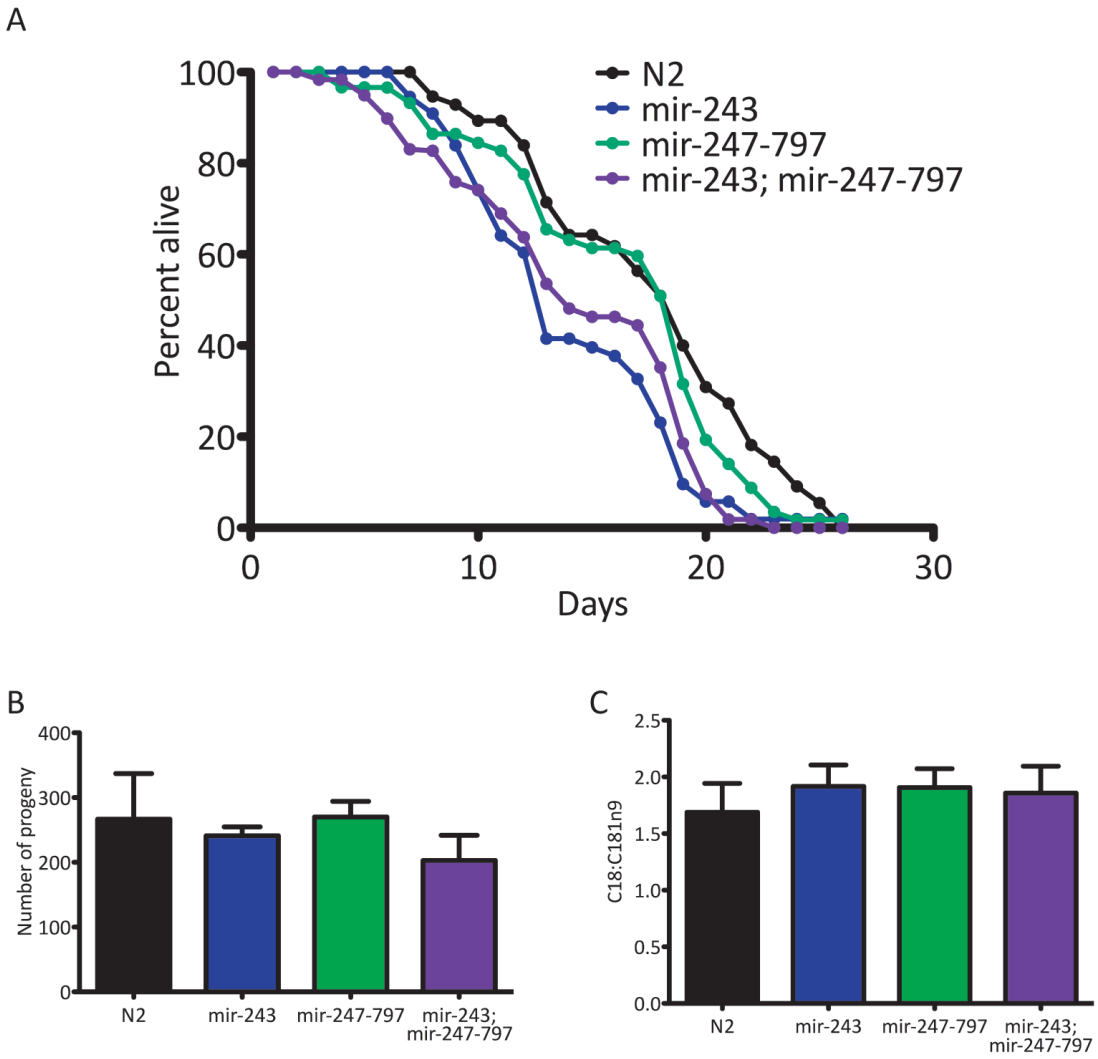

Figure 2.9. miRNA deletion mutants have minimal fed phenotypes. (A) Lifespans of miRNA mutants. Mean lifespans were calculated from at least 44 individual lifespans from one experiment. Means ± SD are: N2: 17.9 ± 5.0; *mir-243*: 14.67 ± 4.5**; *mir-247&mir-797*: 18.0 ± 4.3; *mir-243;mir-247&mir-797*: 16.1 ± 4.1. (B) Total number of progeny produced by miRNA mutants. Brood sizes are means of at least 4 individuals measured in one experiment. Worms were grown on OP50 at 20˚C for both brood and lifespan experiments. (C) Desaturation ratio of miRNA mutants. Means from at least 8 experiments are shown ± SEM. $^{**}p < 0.01$

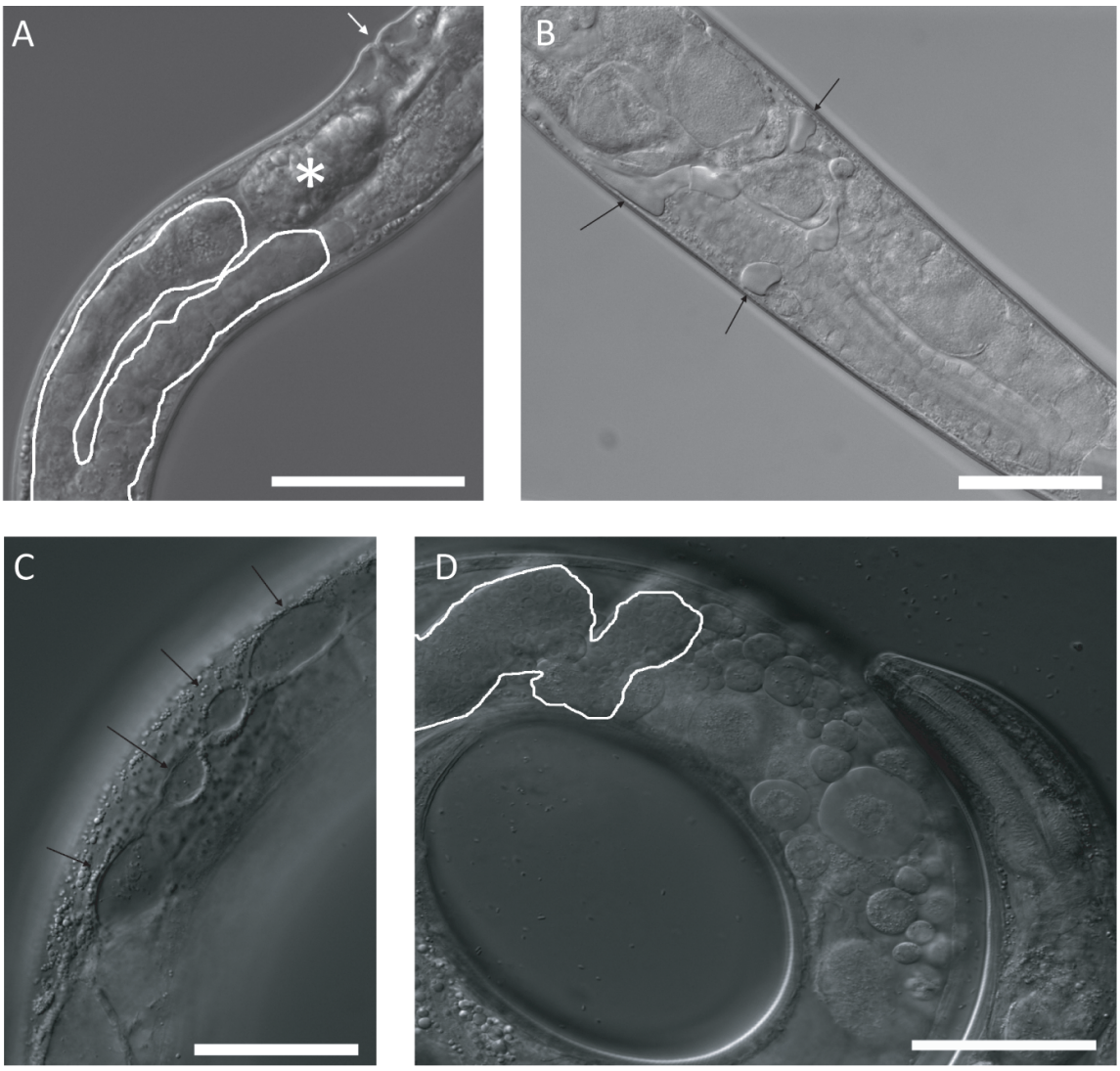

Figure 2.10. miRNA mutants have distinct ARD recovery phenotypes. (A) 11-day starved *mir-243;mir-247&mir-797* ARD animal. The germline is outlined, the held embryo is marked by an asterisk, and the vulva is denoted by an arrow. (B) 8-day starved *mir-243;mir-247&mir-797* animal, 3 days post-recovery. Excess yolk is marked by black arrows. (C) 16-day starved *mir-797* ARD, 5 days post-recovery. Focal plane is at the hypodermis of the animal. Arrows mark vacuoles in seam cell pattern. (D) 7-day-starved *mir-243* mutant ARD animal, 5 days post-recovery. Gonad is outlined in white, demonstrating migration defect. Note also the cellularization and possible ectopic sperm. Scale bar = 50μm for all images. Images in (A) and (C) acquired by Emily Fawcett.

Table 2.1. Lifespan data from rescue experiments.

		Mean lifespan ± SD	*n*
04.22.08	N2	14.9 ± 5.0	40
	nhr-49(nr2041)	10.0 ± 2.8****	41
	nhr-49(nr2041);fhcEx02[K10C3]	8.6 ± 1.8$^{\dagger ns}$	43
06.04.08	N2	18.0 ± 7.6	29
	nhr-49(nr2041)	10.7 ± 2.0****	41
	nhr-49(nr2041)/+	18.9 ± 5.2^{ns}	37
09.27.08	N2	18.6 ± 5.4	24
	nhr-49(nr2041)	11.6 ± 2.3****	47
	fhcIs01[FLAG-nhr-49$_{cDNA}$]	14.5 ± 5.6***	29
	fhcIs01[FLAG-nhr-49$_{cDNA}$]	15.2 ± 4.8*	22
	nhr-49(nr2041); fhcIs01[FLAG-nhr-49$_{cDNA}$]	9.7 ± 2.1$^{\dagger ns}$	16
	nhr-49(nr2041); fhcIs01[FLAG-nhr-49$_{cDNA}$]	9.8 ± 1.0$^{\dagger ns}$	25
08.21.09	N2	18.1 ± 3.8	23
	nhr-49(nr2041)	8.6 ± 2.4****	22
	nhr-49(nr2041)I;ttTi5605 II;unc-119(ed9) III; fhcEx04[unc-119(+) + FLAG-nhr-49$_{cDNA}$]	11.1 ± 3.0$^{\dagger *}$	19
01.30.10‡	N2	17.5 ± 4.9	22
	nhr-49(nr2041)	8.9 ± 2.2***	15
	nhr-49(nr2041); fhcEx06[FLAG-nhr-49$_{geno}$]	13.4 ± 4.8$^{\dagger *}$	12

		Mean lifespan ± SEM
all experiments	N2	17.4 ± 0.7
	nhr-49(nr2041)	10.0 ± 0.6****

$^{*}p < 0.05$, $^{**}p < 0.01$, $^{***}p < 0.001$, $^{****}p < 0.0001$, ^{ns}not significant.
Significance values shown are based on comparison to N2 unless marked with †, in which case comparison is to *nhr-49(nr2041)*.

Table 2.2. Selected targets of mir-797.

Sequence ID	Gene name	Description
K10C3.6	nhr-49	Nuclear hormone receptor expressed in seam cells
K08A2.5	nhr-88	Nuclear hormone receptor expressed in hypodermis
K06A1.4	nhr-22	Nuclear hormone receptor expressed in seam cells
F18A1.2	lin-26	Zinc-finger protein required for differentiation of some ectodermal cell types; expressed in the hypodermis
W09C2.1	elt-1	GATA transcription factor essential to fate of most epidermal cells

Table 2.3. Selected targets of mir-243.

Sequence ID	Gene name	Description
K10C3.6	nhr-49	Nuclear hormone receptor expressed in seam cells
C32D5.2	sma-6	Kinase implicated in oocyte and germline maintenance
ZK484.8	nspd-1	Spermatogenesis-enriched protein of unknown function
Y51H7C.6	cogc-4	Conserved oligomer Golgi complex member required for normal distal tip cell migration
F56A3.4	spd-5	Coiled-coil domain protein involved in sperm-related meiosis
T03F1.5	gsp-4	Predicted phosphatase present at high levels in differentiating and mature sperm
ZK637.7	lin-9	Novel protein implicated in somatic gonad formation and reproduction; mutants have sperm present in the body cavity
M03F4.2	act-4	Actin isoform present in somatic gonad tissues; mutants have migration defects
F46A9.5	skr-1	Member of the ubiquitin ligase complex required for the mitosis/meiosis switch

Chapter III: NHR-88, CYP-35A5, and *fhc10(+)* interact to determine fertility, fecundity, and longevity in *C. elegans*

Many changes must occur for an animal to adjust to variable nutritional status. On an organismal level, allotment of energy and metabolic precursors must be tuned to maximize fitness. On a cellular level, these changes are effected in part by nutrient-responsive transcription factors altering expression of metabolic genes. In *Caenorhabditis elegans,* the nuclear receptor NHR-49 is one such transcription factor. Preliminary microarray data suggested that NHR-49 might activate NHR-88 as part of its role as a central metabolic regulator. Although GFP reporter expression, lifespan, brood size, and fat profile data revealed NHR-88 to be acting independently of NHR-49, I identified two genes which do interact with *nhr-88*: the cytochrome P450 *cyp-35a5* and *fhc10*, an unknown allele which I isolated from the *cyp-35a5(ok1985)* mutant background. Even though I found no phenotypes while characterizing the *nhr-88* mutant in the fed state, I discovered that NHR-88 cooperates with CYP-35A5 and *fhc10(+)* to affect brood size, gonadal morphology, lifespan, and fat composition in the worm. NHR-88 is also partially required for sterility induced by the lipid dihomo-gamma-linolenic acid (DGLA). The involvement of NHR-88 in these processes is consistent with a model in which the nuclear receptor is responding to a DGLA-derived ligand, which is in turn modulated by CYP-35A5 and *fhc10(+)*.

Introduction

As an organism experiences variation in food availability, it responds by adjusting the allocation of nutrients to energy-intensive processes including growth, longevity, and progeny production. The nuclear receptor class of transcription factors provides excellent candidates for proteins regulating this response, as its members are characterized by lipophilic ligand-binding pockets through which they can sense alterations in fatty acid metabolites and effect a transcriptional adaptation. NHR-49, an orphan receptor in *Caenorhabditis elegans* with homology to mammalian receptors including HNF4α and PPARα, has a well-characterized role in maintaining metabolic homeostasis (Van Gilst et al., 2005a). This nuclear receptor differentially regulates glucose and lipid metabolism genes, including genes involved in β-oxidation, sphingolipid metabolism, and fatty acid desaturation (Pathare, submitted; Van Gilst et al., 2005a). As a result, *nhr-49* mutants are high fat and have increased saturated fat, which leads

to shortened lifespan and reduced brood (Pathare, submitted). This study focuses on NHR-88, another, less studied *C. elegans* nuclear receptor that is reported to also have increased fat storage (comment from Dr. K. Ashrafi to the National Bioresource Project of Japan). Preliminary microarray data suggests that it is downstream of NHR-49, while experiments done by the Ashrafi lab place it upstream of the cytochrome P450 gene *cyp-35a5* (Jones, 2009).

Polyunsaturated fatty acids (PUFAs) are critical for processes such as signaling, membrane structure, development, and fertility in organisms ranging from nematodes to humans (Watts and Browse, 2002). However, unlike mammals, which require certain essential fatty acids in their diets, worms are PUFA prototrophs, as the *C. elegans* genome contains a full complement of PUFA biosynthesis genes (Watts and Browse, 2002). These desaturases, which introduce double bonds, and elongases, which increase chain length, are present mainly within the intestine (Brock et al., 2006). This tissue is the primary site of both PUFA biosynthesis and storage, taking the place of the mammalian liver and adipose tissue (Ashrafi et al., 2003; Brock et al., 2006). The fat content of a worm population can easily be assayed by esterification followed by analysis on a gas chromatograph/mass spectrometer to give a fatty acid profile (Watts and Browse, 2002). This profile reflects changing nutritional status caused by variable food sources or fasting; changes in the abundance of specific lipids are especially pronounced in the mono- and polyunsaturated fatty acids, making them excellent precursors for feeding or fasting signals (Brooks et al., 2009; Van Gilst et al., 2005b). Recently, PUFA-derived signaling molecules called N-acylethanolamines (NAEs) have been implicated in integration of nutritional status with phenotypic outputs in *C. elegans* (Lucanic et al., 2011). Levels of these compounds increase in starved L1s following 6 hours of feeding and decrease upon dietary restriction (DR); furthermore, addition of exogenous NAEs can completely reverse the lifespan increase caused by DR, suggesting that they may act as the fed signal (Lucanic et al., 2011). In mammals, the endocannabinoid system also affects energy homeostasis, by binding both the canonical cannabinoid receptors and members of the PPAR family of nuclear receptors (Di Marzo and Matias, 2005; O'Sullivan, 2007).

Another class of molecules linked to both NAE metabolism and nuclear receptors is the cytochrome P450s. These oxygenases have been shown to act on endocannabinoids to form bioactive epoxides (Snider et al., 2010), which in turn have been shown to activate nuclear receptors, including PPARα (Ng et al., 2007). There are 77 cytochrome P450 genes in

C. elegans, with reported roles in fat storage, xenobiotic metabolism, and development (Aarnio et al., 2011; Gerisch and Antebi, 2004; Menzel et al., 2005). For example, DAF-9 synthesizes steroidal ligands for the nuclear receptor DAF-12 to induce a reproductive life history over the long-lived, stress-resistant dauer state (Jia et al., 2002).

Reproduction in *C. elegans* occurs primarily through self-fertilization of hermaphrodites, although males do arise at a low frequency. The hermaphrodite gonad consists of two reflexed arms, each consisting of a syncytium of "cells" arrayed distally to proximally. Cells closest to the distal tip cell, a somatic cell that caps the germline, are maintained in mitosis by a number of pro-proliferative factors (Crittenden et al., 2003). As cells move proximally, the concentration of pro-mitotic factors decreases while pro-meiotic factors increase, driving cells to begin differentiating (Crittenden et al., 2003). The boundary where this occurs is referred to as the transition zone and can be identified by a characteristic crescent shape of DAPI-stained nuclei. The region from the distal tip to the transition zone is referred to as the mitotic region (MR). The first 300 germ cells differentiate into sperm, after which all future germ cells differentiate as oocytes (Singson, 2001). Because *C. elegans* hermaphrodites produce all of their sperm during L4 before switching to oogenesis early in adulthood, selfed broods are sperm-limited (Ward and Carrel, 1979). The theory of antagonistic pleiotropy holds that there must be a tradeoff between brood size and lifespan, as an organism cannot dedicate its finite resources to optimizing both processes (Jenkins et al., 2004). While this model has been challenged, most recently by data demonstrating genetic separation of lifespan and fitness in experimentally evolved *C. elegans* lines (Anderson et al., 2011), it remains true that many longevity-increasing mutations have a negative effect on fecundity (Jenkins et al., 2004).

My characterization of the *C. elegans* nuclear receptor NHR-88 has implicated this transcription factor, along with the cytochrome P450 CYP-35A5 and the as-yet unidentified *fhc10(+)* allele, in maintaining balance between somatic and reproductive outputs. Together, these genes affect lifespan, brood size, the mitotic germ cell population, and fat metabolism. Furthermore, they show altered sensitivity to PUFA-induced sterility, suggesting that these lipid species may be involved in the coordination of efforts towards the equilibrium of nutrient distribution.

Results

NHR-88: a downstream regulator of NHR-49 targets?

I first became interested in NHR-88 when preliminary microarray data showed *nhr-88* to be 5-fold reduced in an *nhr-49* mutant background. However, follow-up qRT-PCR found that there was an insignificant increase in *nhr-88* transcript in an *nhr-49* mutant compared to the N2 control, suggesting that, if anything, NHR-49 may actually be a repressor of *nhr-88* expression (Figure 3.1A). These data suggested that a subset of NHR-49 target genes might be regulated through NHR-88. To test this hypothesis, a technician and I performed qRT-PCR analysis comparing N2, *nhr-49*, and *nhr-88* worms using an NHR-49 target gene primer panel. While expression of a number of these genes changed in the *nhr-88* background in a direction consistent with NHR-49 repression of *nhr-88*, the differences were orders of magnitude smaller than those seen in *nhr-49* worms (Figure 3.1B). I interpreted these minimal effects as tissue specificity, overlapping targets, or background.

To further explore the potential interaction between NHR-49 and NHR-88, I created a transgenic strain of *C. elegans* expressing an extrachromosomal array containing 1500 base pairs of the NHR-88 promoter upstream of GFP. Due to the reported intestinal phenotypes of *nhr-88* depletion (comment from Dr. K. Ashrafi to the National Bioresource Project of Japan), I was surprised that this transcriptional reporter shows no detectable expression in the intestine at any developmental stage (Figure 3.2A). I instead observed expression in a number of head and tail neurons, starting just before hatching and continuing through adulthood (Figure 3.2A). To narrow down the identity of these neurons, I soaked a mixed-stage population of transgenic worms in the lipophilic probe DiI, which stains sensory neurons (Shaham, 2006). The DiI filling pattern did not overlap with the expression pattern of the reporter construct, suggesting that NHR-88 is not expressed in sensory neurons (Figure 3.3). The reporter construct also drove expression in the hypodermis and vulva in adult animals and within the hypodermis of dauers (Figure 3.2A). I cannot exclude the possibility that NHR-88 may be acting within the germline; germline silencing of extrachromosomal arrays makes it impossible to rule out this localization with current expression plasmids. Restricted localization of NHR-88 could explain why I see such minor transcriptional changes, both for *nhr-88* in *nhr-49* worms and for NHR-49 targets in the *nhr-88* strain; however, there were no obvious changes in localization or intensity of the *nhr-88* reporter in an *nhr-49* background (Figure 3.2B).

To confirm that there was no physiologically relevant interaction between *nhr-49* and *nhr*-88 in the fed state, a technician and I performed standard phenotypic assays to look for a possible epistatic relationship between the two mutants. The *nhr-88(tm1033)* strain contains a 769-base pair deletion, which is predicted to be a nonsense mutation that truncates all isoforms before the DNA-binding residues, likely making it a null allele; I made the double mutant by crossing this strain into one containing the *nhr-49(nr2041)* allele. I found that the *nhr-88* mutant was aphenotypic and unable to suppress *nhr-49* defects for every phenotype examined. For example, lifespan analysis showed no difference between the mean lifespans of N2 and *nhr-88(tm1033)* animals (15.4 ± 4.2 days and 14.9 ± 4.9 days, respectively); the *nhr-88* deletion had a minimal effect on the shortened lifespan of *nhr-49(nr2041)* mutants (increasing it from 7.6 ± 1.5 days to 8.3 ± 1.9 days) (Figure 3.4A). Similarly, the *nhr-88* mutation has no significant effect on brood size, either on its own or in the *nhr-49* background (Figure 3.4B). I also found the *nhr-88* deletion to have no effect on timing of progeny production or bagging frequency of selfed hermaphrodites, as might be expected if the role of NHR-88 in the vulval neurons was to control egg-laying (Figure 3.4C-D). Finally, I explored the role of NHR-88 in fat storage and lipid profile. As the *nhr-88* deletion caused no significant changes in the expression of NHR-49-regulated desaturases or β-oxidation genes, I expected to see little evidence of altered metabolism in the mutants. Indeed, desaturation ratio and lipid profile were the same in *nhr-88* and N2 worms (Figure 3.4E-F). Additionally, the *nhr-49;nhr-88* double mutant showed no improvement over the *nhr-49* single mutant's increased C18:0 to C18:1n9 ratio, in either the triglyceride or the phospholipid fractions (Figure 3.4E and data not shown). Thus, all data indicate that NHR-88 acts independently from NHR-49 in the fed state.

Identification of fhc10

I extended my studies to include CYP-35A5, a cytochrome P450 that was shown by the Ashrafi lab to be downstream of NHR-88 (Jones, 2009). To investigate the relationship between NHR-88 and this P450, I acquired the deletion strain RB1613 containing the *cyp-35a5(ok1985)* allele, which deletes 807-base pairs from the C-terminus of the protein. The protein product is predicted to terminate translation before the heme-binding domain, which should abrogate its oxygenase activity. Preliminary phenotypic analyses defining the epistatic relationship of the

two mutations proved promising (see next section), so I outcrossed the *cyp-35a5* allele. The resultant line had no phenotypes in common with the original, unoutcrossed strain.

As the RB1613 line had maintained its lifespan, brood size, and fat phenotypes over this period of time, I concluded that they were the result of a background mutation caused by the mutagenesis process rather than normal variation within a single mutant strain. I outcrossed the line once again, this time selecting mutants based on phenotype instead of the presence of the *cyp-35a5* deletion. Homozygous mutants from the first cross were selected based on an extreme 25˚C brood defect that was lost in subsequent generations, possibly as a result of the outcrossing or adaptation to the increased temperature. Brood, lifespan, fat, and germline phenotypes were separated from the *cyp-35a5(ok1985)* allele by the second outcross. Further outcrossing followed the secondary allele, designated *fhc10*, based on slight uncoordination (Figure 3.5). This Unc phenotype continued to segregate with the *nhr-88*-interacting phenotypes. Although I did not collect any segregation data, I infer based on the observations described above that the original RB1613 strain is a *cyp-35a5;fhc10* double mutant, and will refer to it as such.

I chose a two-step approach to cloning *fhc10*. I first mated *fhc10* hermaphrodites with CB4856 (Hawaiian) males. The presence of mapped single nucleotide polymorphisms (SNPs) between these two strains allows for mapping of other mutations (Davis et al., 2005). Comparison of SNPs in phenotypically wildtype and mutant pools of F2 animals placed the *fhc10* allele on the X chromosome (Figure 3.6). I am currently in the process of preparing this strain for whole-genome sequencing.

fhc10 *and* cyp-35a5 *interact with* nhr-88 *to affect fecundity*

One of the first synthetic interactions that I discovered between *nhr*-88 and the *cyp-35a5;fhc10* double mutant related to fecundity. The 20˚C brood size of the unoutcrossed *cyp-35a5;fhc10* line trends low, producing on average 203.9 ± 7.6 progeny compared to 235.7 ± 59.17 for the control. Combining all three mutations in an *nhr-88;cyp-35a5;fhc10* triple mutant increased brood size almost 30% over that of N2, again at 20˚C (Figure 3.7). Interestingly, this additive effect is seen only in the triple mutant; the *nhr-88;fhc10* and *nhr-88;cyp-35a5* double mutants have the same broods as the *fhc10* and *cyp-35a5* single mutants (Figure 3.7, Table 3.1). While neither single mutant changes fecundity significantly compared to N2, the *fhc10* brood

trends low, while the *cyp-35a5* brood trends high; increasing the number of animals assayed for these mutants will likely improve the significance values (Figure 3.7).

I also performed broods at high temperature, as it has been established that selfed fecundity decreases at increased temperature due to sperm defects including reduced activation (Harvey and Viney, 2007). Surprisingly, brood sizes for both the *cyp-35a5;fhc10* double mutant and the triple mutant dropped dramatically at 25˚C. While high temperature decreased N2 and *nhr-88* progeny production by approximately 50%, total brood size for the *cyp-35a5; fhc10* and *nhr-88;cyp-35a5;fhc10* strains fell to less than 20% of their size at 20˚C (Table 3.1). Temperature effects on fecundity of *fhc10* and *cyp-35a5* single mutants were similar to those on N2 broods (Table 3.1), suggesting that *fhc10(+)* and CYP-35A5 may be acting redundantly to maintain sperm integrity at high temperatures. Furthermore, the interaction of these genes with NHR-88 is also implicated in the maintenance of fertility at 25˚C; the temperature-dependent brood size decrease of the triple mutant cannot be rescued by addition of wild-type sperm by mating, indicating reproductive defects beyond sperm quality (Table 3.1).

fhc10, cyp-35a5, *and* nhr-88 *affect mitotic cells within the gonad*

I next examined the gonadal morphology of the mutants to determine whether there were any obvious changes to account for the differences in brood size. DAPI staining of extruded gonads showed *cyp-35a5;fhc10* double mutants to have an extreme phenotype that included fewer and larger germ cells, primarily within the mitotic region, while the other mutants had normal-sized germ cells (Figure 3.8). Closer inspection of the mitotic region (MR) showed a significant shortening in both the *cyp-35a5;fhc10* double mutant and the *fhc10* strain, suggesting that the *fhc10* allele may be the causative factor for this phenotype (Table 3.2). The inclusion of the *nhr-88* deletion in either of these strains lengthened the MR, leading to partial rescue for the triple mutant and complete rescue for *nhr-88;fhc10* (Table 3.2). Despite these combinatorial effects, gonads from *nhr-88* and *cyp-35a5* single mutants showed MR lengths comparable to wildtype, demonstrating that they do not affect the MR themselves, but instead modify the effects of *fhc10* (Table 3.2).

fhc10(+) is *required for a normal lifespan*

I found several strains to be marginally long-lived; *cyp-35a5;fhc10*, *nhr-88;cyp-35a5;fhc10*, *fhc10*, and *nhr-88;fhc10* mutants all had greater mean and maximum lifespans than N2 with HT115 bacteria as a food source (Table 3.3). As this increase is only seen in lines containing the *fhc10* mutation, *fhc10(+)* likely plays a more significant role in lifespan determination than does CYP-35A5. While the *fhc10* allele lengthens lifespan, the *nhr-88* deletion shortens it. There is a small but significant decrease in the *nhr-88* single mutant lifespan and the *nhr-88;cyp-35a5* double mutant; the *nhr-88* mutation also shortens *fhc10* and *cyp-35a5;fhc10* lifespans, though not significantly (Table 3.3).

Altered PUFA profiles in lines carrying the fhc10 *allele*

As part of the phenotypic analysis of the *cyp-35a5* and *fhc10* mutants, I also looked for changes in the fatty acid species present in the worms. While there was minimal change across most of the lipids analyzed (Table 3.4), the *cyp-35a5;fhc10* double and *fhc10* single mutants had increased C20 PUFAs (Figure 3.9C). Interestingly, it seems that NHR-88 may be required for this increase, as the triple mutant has lower abundance of these long-chain fats (Figure 3.9C). The change in fat profile upon deletion of *nhr-88* suggested that NHR-88 might be regulating expression of PUFA biosynthesis genes; however, qRT-PCR of these genes showed no change in expression levels in *nhr-88* mutants compared to N2 animals, suggesting that the *fhc10* allele may also need to be present for misregulation of PUFA biosynthesis to occur (Figure 3.9B).

nhr-88 *mutant shows reduced sensitivity to PUFA-induced sterility*

The increase in C20:3n6 (dihomo-gamma-linolenic acid, DGLA) in combination with the reduction in germ cells in the *cyp-35a5;fhc10* mutant mirrored the DGLA-induced sterility published by Watts and Browse (Watts and Browse, 2006). They reported that supplementation with C18:3n6 (GLA) or C20:3n6 (DGLA) induces sterility via degeneration of the germline, correlated with the concentration of DGLA present in the worm lipids (Watts and Browse, 2006). To test the sensitivity of my mutants to DGLA, I plated embryos on plates containing 0.1% tergitol and between 0mM and 0.8mM DGLA, let them develop into adults, and then scored for the presence of *in utero* embryos 2 days later. I found *nhr-88* mutants to be partially resistant to DGLA-induced sterility, while preliminary data show the *cyp-35a5;fhc10* and *nhr-88;cyp-*

35a5;fhc10 strains to be more sensitive to DGLA than wildtype (Figure 3.10A, B and Table 3.5). Presence of *fhc10* seems to have no effect on this phenomenon (Figure 3.10A, B and Table 3.5). I included *fat-3(wa22)*, which was reported to be resistant by Watts and Browse, as a positive control (Watts and Browse, 2006); the inability of this mutant to synthesize endogenous DGLA leads to greater resistance than that seen in *nhr-88* mutants. Analysis of the lipid species present in worms grown on DGLA confirms that exogenous lipid is being incorporated into the both N2 and *nhr-88* worms to a similar degree, eliminating the possibility that the *nhr-88* resistance phenotype is actually due to failure to take up DGLA (Figure 3.10C). Although the extreme variability among experiments means that *nhr-88* resistance is not statistically significant at any one concentration, *nhr-88* consistently requires higher DGLA concentrations to reach a given percent sterility compared to N2 controls within the same experiment. These data suggest that NHR-88 is at least partially required for DGLA-induced sterility.

Based on the mitotic region phenotypes seen with the *fhc10* allele, I looked for subtle changes in the germline at lower concentrations of DGLA in addition to scoring for sterility at high concentrations. To do this, I grew worms on plates containing 0.1% tergitol and 0.2mM DGLA from egg to 24 hours past L4 and then examined DAPI-stained, extruded gonads. While there was no obvious difference in overall size of the treated versus untreated gonads and I was looking at concentrations low enough to preserve a functional germline, I did find that DGLA causes a shortening of the mitotic region in wild-type animals. In a representative experiment, N2 animals grown on tergitol alone had an average MR length of 17.8 ± 3.0 cell diameters from the distal tip to the first row of the transition zone, while in animals grown on 0.2mM DGLA plates, the MR was reduced to 12.7 ± 2.3 cell diameters (Figure 3.11). These data suggest that minor increases in DGLA change the equilibrium point of the proliferation/differentiation switch in favor of differentiation, thereby causing a distal shift in the location of the transition zone. As with the sterility phenotype, it seems that NHR-88 may be partially responsible for the DGLA-induced shortening of the mitotic region, as the reduction in MR between 0mM and 0.2mM is not significant in preliminary analysis of an *nhr-88* mutant.

Discussion

Although I began my investigations of NHR-88 because I believed it to be downstream of NHR-49, I have concluded that NHR-49 does not regulate NHR-88 in the fed state. In the

process of defining the interaction between the two nuclear receptors, I discovered that the *nhr-88* single mutant has minimal effect on brood size, lifespan, or fat metabolism. However, I also identified two other alleles, *cyp-35a5(ok1985)* and *fhc10*, which have synthetic interactions with *nhr-88* and each other to regulate fecundity, longevity, PUFA content, and gonadal morphology. Finally, I demonstrated that the *nhr-88* mutant is resistant to DGLA-induced sterility, suggesting a possible role for NHR-88 in the recognition of this lipid.

NHR-49 does not regulate nhr-88 *in the fed state*

I first identified NHR-88 as a potential downstream target of NHR-49 by microarray, which suggested that NHR-49 activated *nhr-88*. The initial microarray data is complicated by the fact that notation of the *nhr-88* locus has changed over time: the microarray spot was initially identified as K08A2.7b, but this clone has since merged with *nhr-88* (K08A2.5). Sequence alignment shows that the microarray spot corresponds to an *nhr-88* intron, suggesting that the microarray is not actually measuring changes in abundance of the mature *nhr-88* mRNA. The invalidity of these microarray data is supported by qRT-PCR experiments demonstrating no significant change in *nhr-88* mRNA level in an *nhr-49* background (Figure 3.1A). I also looked for phenotypic epistasis between the two mutants and found minimal genetic interaction between the *nhr-49(nr2041)* and *nhr-88(tm1033)* alleles. Furthermore, deleting *nhr-49* had no effect on expression pattern of an *nhr-88* transcriptional reporter (reporter intensity was not quantitated). While it is possible that I assayed phenotypes for which *nhr-49* and *nhr-88* do not interact, it is more likely that the apparent regulation of NHR-88 by NHR-49 by microarray is an artifact.

Increased fecundity of nhr-88;cyp-35a5;fhc10 *mutant could be due to altered rate of spermatogenesis*

As discussed in the introduction, self-fertilized broods of *C. elegans* hermaphrodites are sperm-limited under normal conditions (Ward and Carrel, 1979). Therefore, increasing sperm is the primary means of raising fecundity, as seen in the *tra-3(e2333)* or *fem-3(gf)* mutants (Barton et al., 1987; Hodgkin and Barnes, 1991). The *tra-3* mutant increases sperm count by delaying the sperm-to-oocyte switch until early adulthood (Hodgkin and Barnes, 1991); this delay is reflected in a right-shifted brood production curve. The earliest brood experiments performed on *cyp-35a5;fhc10* and *nhr-88;cyp-35a5;fhc10* lines revealed a similar delay in progeny production

(Figure 3.12). The shifted brood curve could also be indicative of slow development. While the *cyp-35a5;fhc10* is developmentally delayed, taking 36 hours longer to get to adult than N2, I was careful to use day 1 adults for brood experiments. However, the double mutant had a reduced brood despite this shift and the increase in brood size of the triple mutant persisted even after the brood delay phenotype disappeared, suggesting that sperm count may be raised by some other mechanism, such as an increased rate of gametogenesis. Future experiments could test this hypothesis by measuring spermatogenesis rate in the triple mutant by counting sperm present at multiple points during L4 (Murray, 2009).

Interestingly, the additive effect of the *nhr-88(tm1088), cyp-35a5(ok1985),* and *fhc10* alleles is temperature sensitive. It has been established that selfed fecundity decreases at higher temperatures despite an increase in the rate of sperm production (Murray, 2009). The reasons for this inconsistency are two-fold: first, the sperm are made for a shorter time period, such that the total number of sperm produced remains approximately constant. Second, errors in spermatogenesis or spermatid activation increase at 25˚C, such that not all sperm can successfully fertilize oocytes (Harvey and Viney, 2007). While the combination of the three mutations increases progeny production at 20˚C, at 25˚C the triple mutant shows an over 80% decrease in brood size (Table 3.1). For some reason, the sperm produced in the triple mutant are especially sensitive to increases in temperature. If faster gametogenesis is in fact the reason for increased brood at 20˚C, perhaps the additional rate increase caused by raising the temperature overwhelms the differentiation system within the gonad. If this hypothesis were correct, I would expect to see the sperm count and rate of spermatogenesis decrease at 25˚C. Unlike the brood size reduction incurred by other strains at high temperatures, that of the triple mutant cannot be rescued by the introduction of N2 sperm from 20˚C-reared males (Table 3.1). The inability of exogenous sperm to rescue fully suggests an additional defect, probably relating to sperm recruitment or oocyte health. However, as the embryos from both selfed and mated triple mutants hatch at 25˚C, it is more likely that the defect lies in oocyte recruitment of sperm. Visualizing N2 sperm via MitoTracker labeling would allow for this hypothesis to be tested, as I could measure recruitment of these wildtype sperm to the mutant embryos. In sum, I believe that NHR-88, CYP-35A5, and *fhc10(+)* work together in an N2 worm to limit sperm production, potentially by influencing rate of spermatogenesis.

The fhc10 *allele reduces the population of germ cells in mitosis*

nhr-88, cyp-35a5, and *fhc10* also act together to determine size of the mitotic region within the *C. elegans* gonad. *fhc10(+)* acts to increase the length of the region, as mutating this gene significantly decreases MR length (Table 3.2). Similarly, the normal function of CYP-35A5 is also to increase size of the mitotic region, but this effect is seen only in an *fhc10* background. NHR-88 has the opposite effect from CYP-35A5, again only in the presence of the *fhc10* allele. These data are consistent with a model in which the nuclear receptor is required for distal shift of the transition zone. Interestingly, gonads from all lines containing the *nhr-88* mutation appear wider than those of corresponding strains carrying the wildtype *nhr-88* allele, suggesting that NHR-88 may affect additional aspects of gonadal morphology.

The question remains how changes within the mitotic region are effected. Reduction in germ cell number likely results from two primary factors: increased apoptosis or decreased proliferation. As altered PUFA profiles have been shown to increase apoptosis within the germline, it will be important to count the number of germ cells in a *ced-3;cyp-35a5;fhc10* mutant. The *ced-3* mutant is missing the caspase required to initiate apoptosis and is therefore cell death defective (Ellis and Horvitz, 1986). If apoptosis were contributing to the reduction in germ cell count in this mutant, I would expect the number of cells within the mitotic region to increase. However, canonical germline apoptosis pathways affect only meiotic cells (Gumienny et al., 1999). While death of these cells could in theory feed back to shift the transition zone distally and change the number of mitotic cells, it is more likely that there is a defect within the mitotic population itself. The phenotypic similarities between *cyp-35a5;fhc10* and *cye-1* RNAi gonads, including reduced cell number and increased size of individual cells, suggests that synthetic interaction of *cyp-35a5* and *fhc10* may be affecting the cell cycle. The *C. elegans* cyclin E homolog CYE-1 promotes proliferation in the germline, where its localization is determined post-transcriptionally through interaction with RNA-binding proteins (Biedermann et al., 2009; Fay and Han, 2000). I expect that the reduction in mitotic region in *fhc10*-containing lines may be attributed to changes in localization or transcription of CYE-1. Following the hypothesis that this shortening occurs via NHR-88-dependent transcriptional changes, I looked for changes in *cye-1* expression in an *nhr-88* background by qRT-PCR. Although this experiment showed no difference in transcript levels (Figure 3.9B), repeating the experiment in different mutants might reveal a role for CYP-35A5 or *fhc10(+)* in expression of CYE-1. Based

on the fact that GLD-1 regulates CYE-1 localization post-transcriptionally (Biedermann et al., 2009), using antibodies against CYE-1 to directly visualize protein levels may prove to be more informative; if my mutants are indeed affecting cell cycle, I would anticipate seeing a restricted area of protein expression that would correspond to the smaller proliferative zone seen in those strains. An alternative test would be to add *fhc10* to a sensitized background such as the *glp-1(bn18)* hypomorph and look for loss of the proliferative zone, as demonstrated by Fox *et al*. for *cye-1* knockdown (Fox et al., 2011). Phenotypic analyses demonstrate that CYP-35A5 and NHR-88 interact with *fhc10(+)* to ensure normal gonadal morphology, although further studies are required to determine how they are affecting the mitotic germ cell population.

Balance of longevity and fertility through germline-soma communication

The Ruvkun lab identified a lipase linking germline stem cell arrest to somatic changes, including decreased fat stores and increased lifespan (Wang et al., 2008). The *cyp-35a5;fhc10* line, which I hypothesize may be affecting cell cycle progression in the germline, also exhibits these phenotypes of low fat and long life (Figure 3.9D and Table 3.3). The double mutant also has a decreased brood, thereby subscribing to the theory that increased longevity comes at the cost of fecundity, as described in the introduction. With the exception of the *nhr-88;cyp-35a5;fhc10* line, all of the strains used in these studies roughly follow this tenet. However, the triple mutant is both long-lived and has a significant increase in fecundity, offering a clear counter-example to the trade-off hypothesis (Tables 3.1 and 3.3); some *daf-2* alleles also follow this pattern (Gems et al., 1998). The data describing longevity trends in my mutants are better fit by plotting lifespan against the number of mitotic cells instead of brood size. The former comparison yields an r^2 value of 0.418 as opposed to 0.107 for the latter, even including the point for the triple mutant. Separating the data on the basis of the *nhr-88(tm1033)* allele further strengthens the correlation: the trend line for strains carrying this mutation is fit with an r^2 of 0.796, compared to 0.951 for those with the wildtype allele at that locus (Figure 3.13). This correlation indicates that it is not brood size but number of mitotic cells that must be balanced with lifespan. My hypothesis is supported by data from the literature demonstrating that removal of mitotically dividing germline stem cells by laser ablation or mutation increases lifespan, while increasing the proliferative population using tumor-forming mutants decreases longevity (Arantes-Oliveira et al., 2002). However, the worm strains used in these experiments

demonstrate an "all-or-none" approach to alterations within the germline. Although the mutants I describe cover a much smaller scope in terms of number of mitotic cells, they also represent a physiological range instead of extremes. Furthermore, the flattening of the line comparing *nhr-88* mutants suggests that NHR-88 is required for these changes to occur in the first place. I therefore speculate that the phenotypes resulting from synthetic interactions between the NR and *cyp-35a5* and *fhc10* might be interrelated via germline-soma crosstalk.

Altered PUFA profiles and sensitivity to DGLA suggest an identity for the NHR-88 ligand

Examining the epistatic relationships between the *cyp-35a5*, *fhc10*, and *nhr-88* mutants with respect to long-chain PUFA abundance reveals a requirement for NHR-88 similar to that seen for mitotic region length. The *cyp-35a5* mutant exacerbates accumulation of arachidonic acid and DGLA in an *fhc10*-containing background. These changes seem to go through the nuclear receptor, as functional NHR-88 is required for increased C20 content in both *cyp-35a5;fhc10* and *fhc10* lines (Figure 3.9C). While the *nhr-88(tm1033)* strain shows no change in expression of any PUFA biosynthesis genes, the *fhc10* mutant allele may also need to be present to affect transcription of these genes.

The altered C20 PUFA profile led me to examine sensitivity of my mutants to the sterility-inducing lipid DGLA. Despite inter-experimental variability, likely resulting from oxidation of DGLA both in the stock solution and within the plates, some trends are apparent in the data. First, the mutants with the fewest mitotic cells are those that are most sensitive to DGLA. Second, the amount of DGLA present in the lipid pool does not correspond to sensitivity to DGLA-induced sterility, as seen with the *fhc10* and *nhr-88;cyp-35a5;fhc10* mutants. Sensitivity or resistance in the original screen came about due to alterations in endogenous DGLA levels (Watts and Browse, 2006), indicating that there is a different mechanism at work in my set of mutants. Finally, presence of the *nhr-88(tm1033)* deletion reduces sensitivity to DGLA, especially at intermediate concentrations (Figure 3.10A, B and Table 3.5). These data, together with shortening of the MR in worms grown on low concentrations of DGLA (Figure 3.11), suggest a model in which DGLA or a metabolite may be responsible for altering the mitotic region and inducing sterility. Requirement of *nhr-88* for full sensitivity implicates the nuclear receptor in the recognition or transmission of the DGLA-derived signal. A possible explanation for the disparity between this NHR-88-dependent response to low levels of DGLA

and the complete sterility induced by very high DGLA concentrations may be the difference between a physiological pathway normally attuned to small changes in endogenous DGLA and a stress response to non-physiological levels of this compound.

This proposed model raises the possibility that DGLA may provide a ligand for NHR-88, an orphan nuclear receptor. NAEs are good candidate metabolites for ligands through which NHR-88 might sense nutritional status, as they are PUFA-derived and have been implicated in nutrient sensing (Lucanic et al., 2011). A transcriptional reporter of *nape-1*, one of two identified genes that encode the enzyme catalyzing the last step in NAE synthesis in worms, is expressed in non-sensory neurons in a pattern similar to that seen for NHR-88 (Lucanic et al., 2011); thus this nuclear receptor is ideally positioned to respond to these compounds. Furthermore, NAEs can be metabolized by P450s to form other bioactive compounds (Snider et al., 2010). I propose that NHR-88 responds to a DGLA-derived ligand such as an NAE within the neurons to sense organismal nutritional status. This signal is transmitted to the germline, where it may affect the germline stem cells. Changes within the mitotically dividing population in turn feed back to the soma to adjust lifespan (Figure 3.14). In analysis of germline phenotypes, *nhr-88(tm1033)* is epistatic to both *cyp-35a5(ok1985)* and *fhc10* (Figure 3.8 and Table 3.2), placing action of NHR-88 downstream of the other genes (Figure 3.14). Mutation of *cyp-35a5* increases the number of proliferating cells within the germline, suggesting that CYP-35A5 acts with NHR-88 to affect the mitotic region, possibly by metabolizing DGLA into an NHR-88 agonist. The role of *fhc10(+)* is complicated by the fact that its identity is unknown, making it impossible to predict its function. While SNP mapping has allowed me to narrow the genetic location of *fhc10* to just under 20 centimorgans, this still leaves me with hundreds of genes that could be affected. Based on its interactions with DGLA and CYP-35A5, I speculate that *fhc10* may reside within another P450 gene that also acts to metabolize a lipid-derived ligand. There are several *cyp* genes on the X chromosome and whole-genome sequencing should help to determine whether they are affected by the *fhc10* allele. Whatever its molecular identity, shortening of the MR in *fhc10* mutants suggests that *fhc10(+)* likely acts to oppose NHR-88 activity via the clearance of an agonist or the synthesis of an antagonist. In this model, NHR-88 acts as a nutrient sensor whose signal is modified by CYP-35A5 and *fhc10(+)* to maintain appropriate balance of lifespan and reproduction. Curiously, the preliminary data for sensitivity of *fhc10* and *cyp-35a5;fhc10* to DGLA-induced sterility demonstrate resistance in the presence

of the *fhc10* allele and sensitivity in the double mutant (Figure 3.10); the contradiction between DGLA sterility and mitotic region epistasis patterns further supports the hypothesis that DGLA affects these phenotypes through distinct pathways.

Experimental Procedures

Strains and maintenance

The wild-type N2 (Bristol) strain and RB1613 *cyp-35a5(ok1985)V;(fhc10)X* were provided by the Caenorhabditis Genome Center, which is funded by the NIH National Center for Research Resources (NCRR). *nhr-88(tm1033)II* was provided by the Mitani lab and *fat-3(wa22)IV* was provided by Jenny Watts. *nhr-49(nr2041)I* was a gift from Carl Johnson at Axys Pharmaceuticals. All mutants were outcrossed to N2 a minimum of 5 times. Worm maintenance was carried out at 20˚C using standard methods.

RNA extraction and qRT-PCR

Larvae were synchronized by hatching embryos collected by bleaching a gravid population on unseeded nematode growth media (NGM) plates. 20-24 hours later, the synchronized population was plated to high growth (HG) plates seeded with *Escherichia coli* strain OP50 and grown to mid-L4 at room temperature, at which point they were collected in M9, washed 5 times to remove excess bacteria, and frozen in an ethanol-dry ice bath. Samples were stored at -80˚C until ready for processing.

RNA extraction was done using the QIAGEN RNeasy Plus Mini kit (Germantown, MD). The protocol used was that for purifying total RNA from animal cells. Tissues/cells were disrupted by sonication and homogenized using a QIAshredder column (QIAGEN, Germantown, MD). cDNA synthesis was conducted using M-MuLV reverse transcriptase (20,000 units, New England BioLabs, Ipswich, MA), 1X of the provided reverse transcriptase buffer, 1mM dNTPs (Invitrogen, Carlsbad, CA), and RNaseOUT recombinant ribonuclease inhibitor (2000 units, Invitrogen, Carlsbad, CA) templated with 5µg RNA and 30µg random primers (Invitrogen, Carlsbad, CA) in a 100µl reaction incubated at 42˚C for 1 hour.

30µl PCR reactions consisting of 0.3µM primers, $1/500^{th}$ of the above cDNA reaction, 125µM dNTPs (Invitrogen, Carlsbad, CA), 1.5mM $MgCl_2$, 1X reaction buffer, and 0.75 units of Taq DNA polymerase (Invitrogen, Carlsbad, CA) were prepared in 96-well plates. Reactions were run using a Bio-Rad iCycler equipped with a MyiQ Single Color Real-Time PCR Detection System (Hercules, CA) to automatically monitor formation of double-stranded DNA product using SYBR-Green (Molecular Probes, Eugene, Oregon). qRT-PCR primers were designed

using Primer 3 software (Rozen and Skaletsky, 2000). Data shown are $\Delta\Delta C_T$ normalized to *nhr-23* expression. Statistics are the result of t-tests on the ΔC_T of the two values being compared.

Creation and characterization of Pnhr-88::GFP *expression lines*

All plasmids were constructed using standard molecular techniques. The *nhr-88* transcriptional reporter contained a promoter region corresponding to 1500 base pairs upstream of *nhr-88* driving GFP expression in the L3691 backbone. This construct was injected into N2 animals with the *rol-6(su1006)* co-injection marker following standard protocols (Mello et al., 1991). Neuronal GFP expression was compared to DiI staining pattern. The dye filling experiment was conducted by exposing worms to 10µg/µl DiI (Invitrogen, Carlsbad, CA) in 1mL of water with 5µl TritonX-100. After 3 hours of shaking at room temperature in the dark, worms were washed and plated to an NGM plate seeded with *Escherichia coli* strain OP50 for 1 hour in the dark to reduce intestinal background before mounting on agar pads. Images were acquired using a Zeiss AxioImager Z1 microscope equipped with an AxioCam 5 MRm camera and Axiovision 4.8 software (Gottingen, Germany).

Lifespan assays

Lifespans were determined by counting the number of days individual worms survived after the L4 molt. Experiments were conducted at 20˚C on *Escherichia coli* strain HT115 transformed with empty vector unless otherwise noted. HT115 was used instead of OP50 because RNAi experiments were conducted in parallel. Live animals were moved to fresh plates daily during the reproductive period, after which they were moved every two to three days. Worms were considered dead when they no longer responded to gently prodding. Bagged animals were censored. Lifespan curves and statistical data, including *P*-values from a one-way ANOVA followed by a Bonferroni multiple comparison test of relevant strains, were produced and analyzed using GraphPad Prism 5 (GraphPad Software, San Diego, CA).

Brood size assays

L4 animals were picked to individual OP50 plates on day 0. Adults were moved to new plates daily as long as they were laying embryos. Progeny plates were maintained at 20˚C until worms were L3-L4, at which point the number of larvae were counted and recorded. Individuals that

bagged while other worms in the group were still laying were censored. Statistical analyses, including *P*-values from a one-way ANOVA followed by a Bonferroni multiple comparison test of relevant strains, used GraphPad Prism 5 (GraphPad Software, San Diego, CA).

Lipid purification and analysis

To collect worms for lipid analysis, approximately 30,000 L1s synchronized by an overnight hatch on unseeded NGM plates were plated to NGM plates seeded with *Escherichia coli* strain OP50 and grown at room temperature. Once the population reached mid-L4, the worms were collected and washed 5 times with M9. After excess buffer was aspirated from the worm pellet, the sample was frozen in an ethanol-dry ice bath and transferred to -80˚C.

For fatty acid profiles and desaturation ratios, total lipids were extracted and converted to fatty acid methyl esters (FAMEs) as described (Watts and Browse, 2002). The resultant FAMEs were analyzed by gas chromatography/mass spectrometry (GC/MS) (Agilent 5975GC, 6920MS). Data were presented as relative abundance (profiles) or the ratio of abundance of C18:0 to that of C18:1n9 (desaturation ratio). To measure fat storage, total lipids were extracted and separated into neutral lipid, glycolipid, and phospholipid fractions as described (Perez and Van Gilst, 2008).

Mapping fhc10

Genetic mapping based on single nucleotide polymorphism was conducted using published protocols and primer sequences (Davis et al., 2005). In short, outcrossed *fhc10*-containing mutants were crossed to Hawaiian CB4856 males and F2 adults were sorted based on phenotype. Mutant and wildtype animals were processed in parallel for visualization of SNP alleles. Band intensity was quantified using Bio-Rad Image Lab software (Hercules, CA). Enrichment values were calculated using the formula $E=\log([band_{N2}/band_{HI}]_{mutant}/[band_{N2}/band_{HI}]_{wildtype}$, where $band_{N2}$ and $band_{HI}$ are intensities of wild-type and Hawaiian allele bands.

Characterization of germline phenotypes

Gonads were extruded from day 1 adults into a small volume of M9 on a polylysine treated slide. Once the M9 evaporated, 100µl of MeOH was pipetted on top of the gonads and the slide was left in a humidifying chamber at room temperature for 10 minutes. The MeOH was removed and

the sample was washed with 50µl of PBS for 10 minutes. Remaining liquid was removed and replaced with 7µl VectaShield mounting media with DAPI (Vector Labs, Burlingame, CA). The slides were sealed and stored at 4˚C until imaged. Z-stacks were acquired using a Zeiss AxioImager Z1 microscope equipped with an AxioCam 5 MRm camera and Axiovision 4.8 software (Gottingen, Germany).

Length of mitotic region was determined by manually counting the number of cell diameters from the beginning of the transition zone (defined by the first row with multiple crescent-shaped nuclei) to the distal tip. Total number of cells within the mitotic region was determined using a counting module designed by Tony Cooke for use with MetaMorph software (Molecular Devices, Sunnyvale, CA). Correlation of these values to lifespan was conducted using a Pearson correlation test with GraphPad Prism 5 (GraphPad Software, San Diego, CA).

DGLA supplementation

NGM plates containing varying concentrations of dihomo-gamma-linolenic acid (DGLA, from Nu-Chek Prep, Elysian, MN) and 0.1% tergitol (Sigma-Aldrich, St. Louis, MO) were prepared as described and kept in the dark (Watts et al., 2003). After 1-2 days of drying time, plates were seeded with *Escherichia coli* strain OP50 and the bacteria were allowed to grow for 2 days at room temperature. Embryos from hypochlorite treatment of gravid adults were plated and maintained at 20˚C for the rest of the experiment. DAPI staining of day 1 adults was conducted as described above. DGLA-induced sterility was assayed in day 2 adults by scoring for embryos within the uterus of individual animals. In some cases only one gonad was intact; if these animals had embryos they were counted as not sterile. DGLA uptake was measured by pooling worms grown on replicate plates and processing the samples as described above.

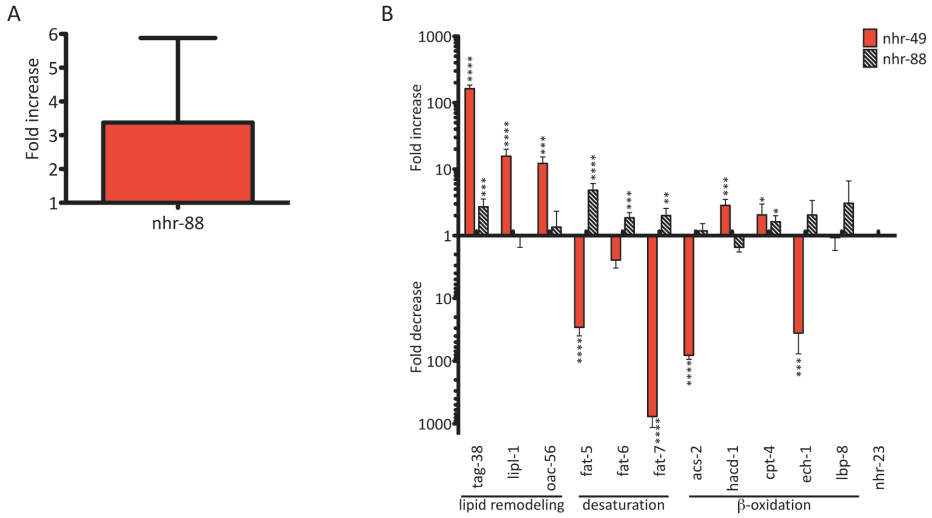

Figure 3.1. NHR-88 is not a key regulator of NHR-49 target genes. (A) qRT-PCR expression data for the *nhr-88* locus in an *nhr-49(nr2041)* mutant. The change is not significant. (B) Comparing gene expression changes of selected NHR-49-regulated genes in *nhr-49(nr2041)* and *nhr-88(tm1033)* mutants, as measured by qRT-PCR. Gene classifications are shown under the gene names. Differences shown are means from at least one experiment performed in duplicate, ± SEM when compared to an N2 population. $^{*}P < 0.05$, $^{**}P < 0.01$, $^{***}P < 0.001$, $^{****}P < 0.0001$.

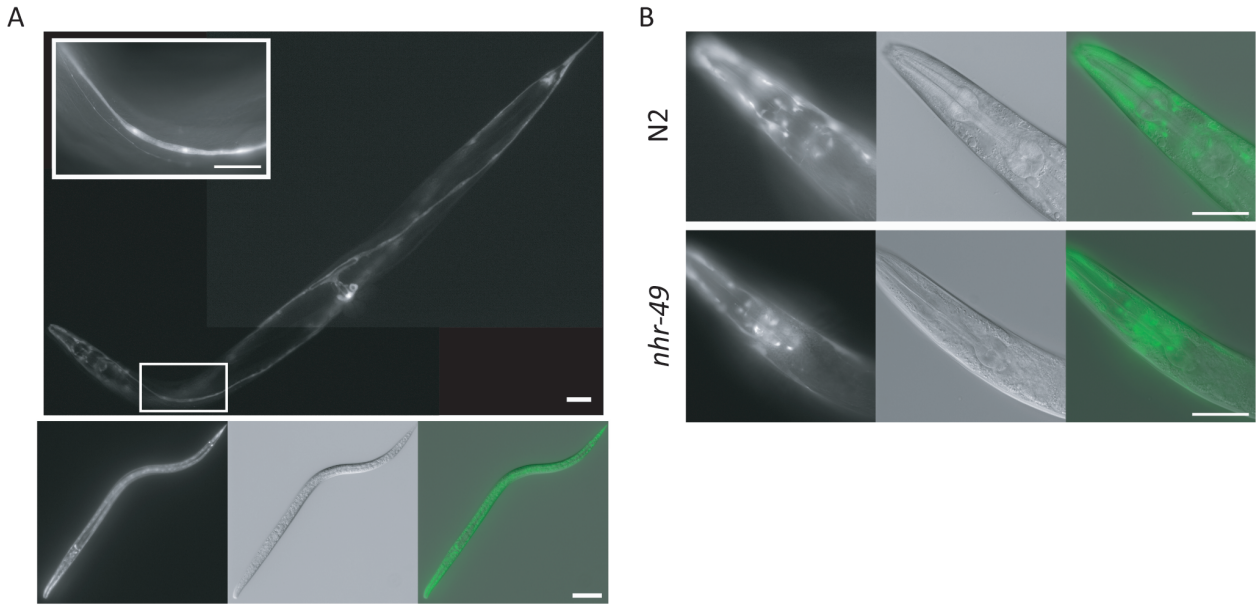

Figure 3.2. NHR-88 promoter drives neuronal and hypodermal expression. (A) Composite image of *Pnhr-88*::*GFP* in an adult worm shows neuronal and hypodermal expression (top). The lateral stripes represent GFP expression in both hypodermal cells and nerve cord (inset). This same pattern is seen in dauer animals (bottom). (B) *Pnhr-88* reporter pattern does not change in an *nhr-49(nr2041)* background. Scale bar represents 50µm in all images.

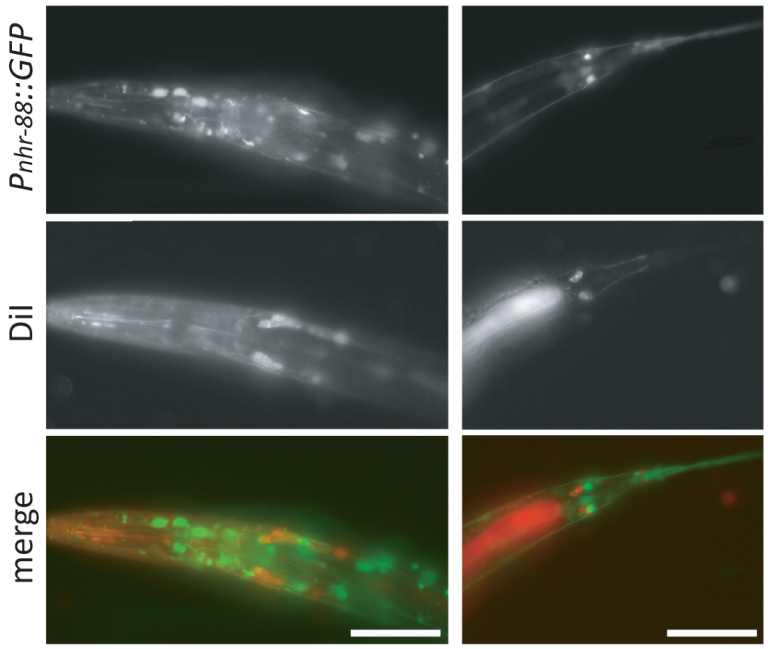

Figure 3.3. NHR-88 does not appear to act in the sensory neurons. *Pnhr-88::GFP* expression does not overlap with DiI dye-filling, which selectively stains sensory neurons. DiI also accumulates in the intestine nonspecifically. Scale bar represents 50μm.

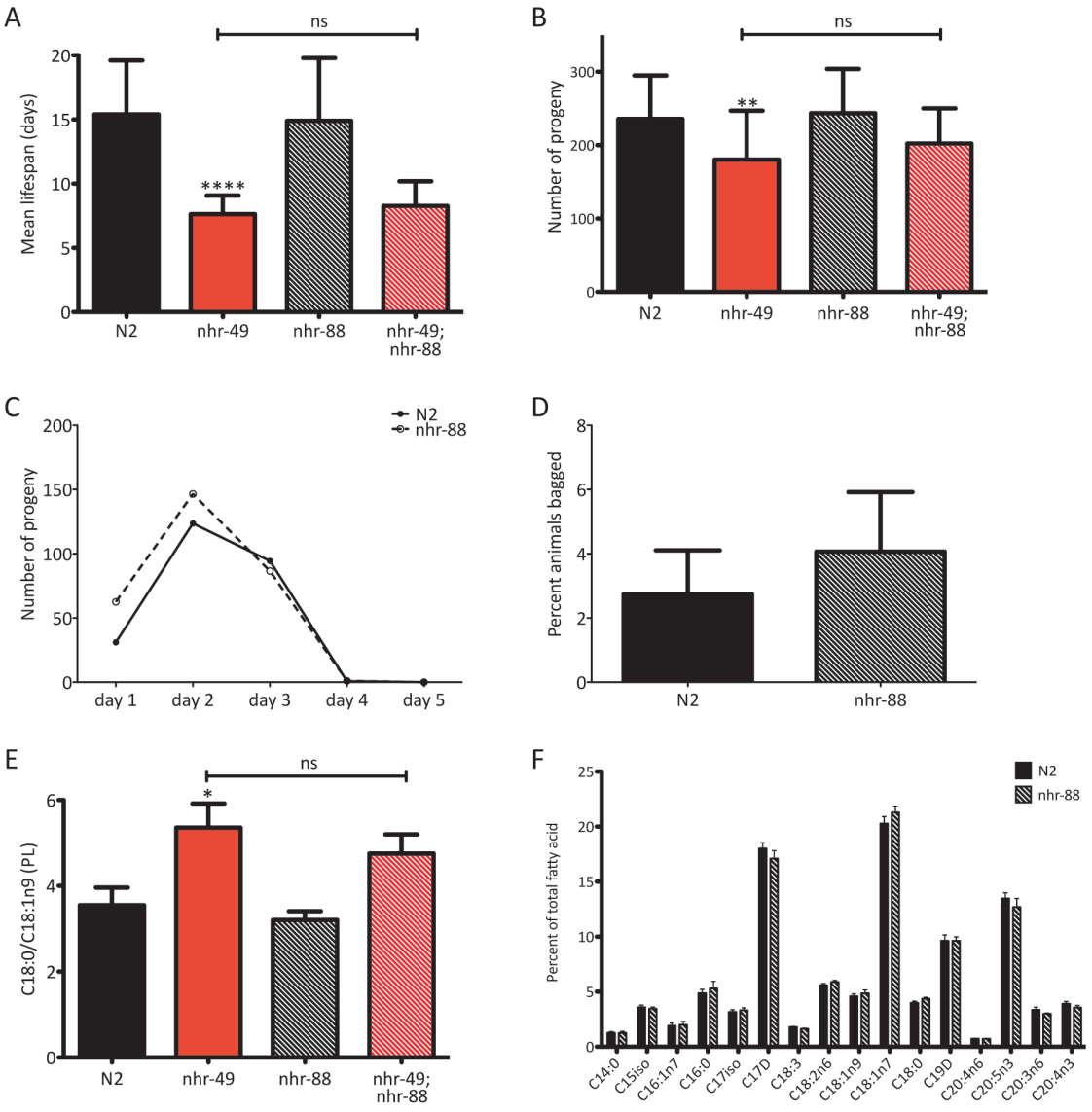

Figure 3.4. *nhr-88(tm1033)* is not epistatic to *nhr-49(nr2041)*. (A) Lifespan of *nhr-49* and *nhr-88* single and double mutants. Data shown are mean lifespans ± SD from at least 109 individuals assayed in at least 2 separate experiments. (B) Total progeny produced by *nhr-49* and *nhr-88* mutants. Shown are means from at least 23 individuals in at least 5 separate experiments. Error bars represent SD. (C) Daily brood production from a representative experiment of 4 individuals showing that *nhr-88* mutants do not experience a reproductive delay. (D) Percent of animals censored due to bagging during lifespan assays. Data shown are means of at least 5 experiments ± SEM. The difference between N2 and *nhr-88* is not significant based on a t-test. (E) Desaturation ratio of *nhr-49* and *nhr-88* mutants. Values are the ratio of C18:0 to C18:1n9 abundance in the phospholipid fraction. The mean ± SEM of at least 3 experiments are shown. (D) Fat profile of the *nhr-88(tm1033)* mutant. Means are the result of at least 10 replicates ± SEM. No lipid species is significantly changed from N2 based on 2-way ANOVA. $^{*}P < 0.05$, $^{**}P < 0.01$, $^{****}P < 0.0001$.

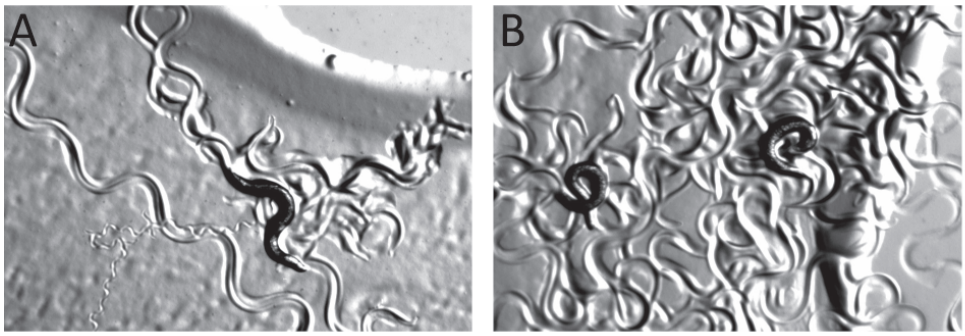

Figure 3.5. *fhc10* allele identified by uncoordinated coiler phenotype. (A) N2 animals produce normal, sinusoidal tracks. (B) Worms with the *fhc10* allele exhibit abnormal movement, including deep bends and curling.

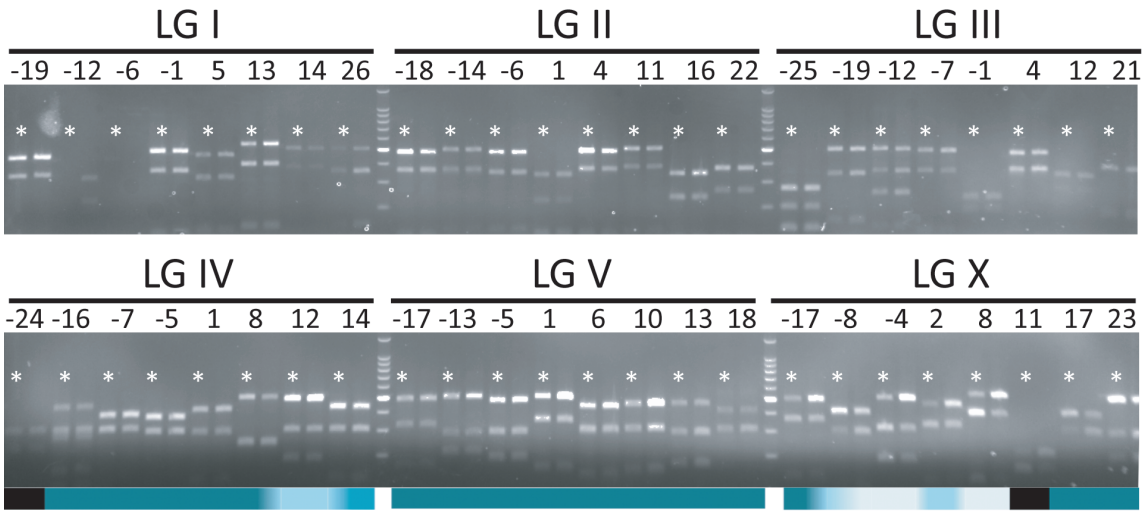

Figure 3.6. The *fhc10* allele maps to the X chromosome. DNA gel showing banding patterns produced by SNP-dependent differences in restriction sites. Lanes marked with an asterisk contain mutant-templated PCR products; alternate lanes contain PCR products from wild-type worms. Genetic positions of markers are noted above the lanes. Enrichment of N2 alleles in the mutant worms was calculated for the bottom comb and is depicted below the gel. Lighter colors denote a higher enrichment score. The high enrichment and reciprocal banding pattern shown through the middle of the X chromosome indicates linkage of *fhc10* to these SNP markers.

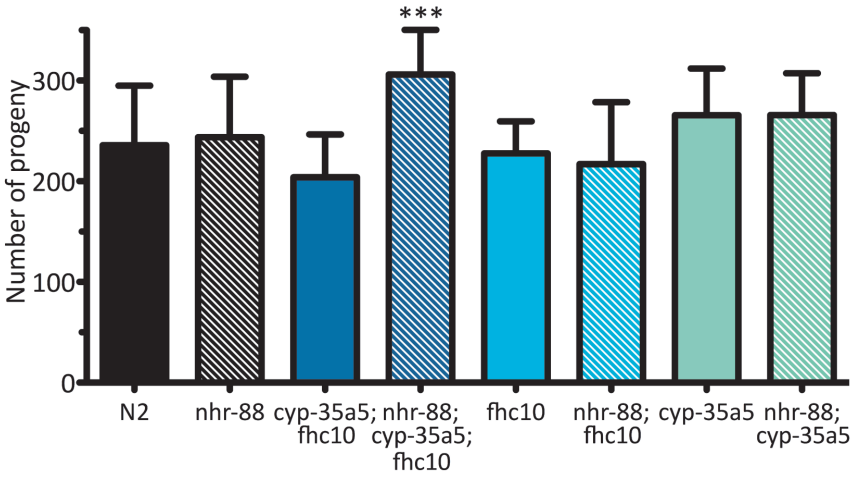

Figure 3.7. NHR-88, CYP-35A5, and *fhc10(+)* act together to regulate brood size. Average total progeny produced by mutants in this study. Brood sizes are the means of at least 9 animals assayed in a minimum of 2 experiments for *nhr-88;cyp-35a5;fhc10*, *fhc10*, *nhr-88;fhc10*, *cyp-35a5*, and *nhr-88;cyp-35a5* and at least 30 individuals in at least 9 replicates for N2, *nhr-88*, and *cyp-35a5;fhc10*. Error bars represent SD.

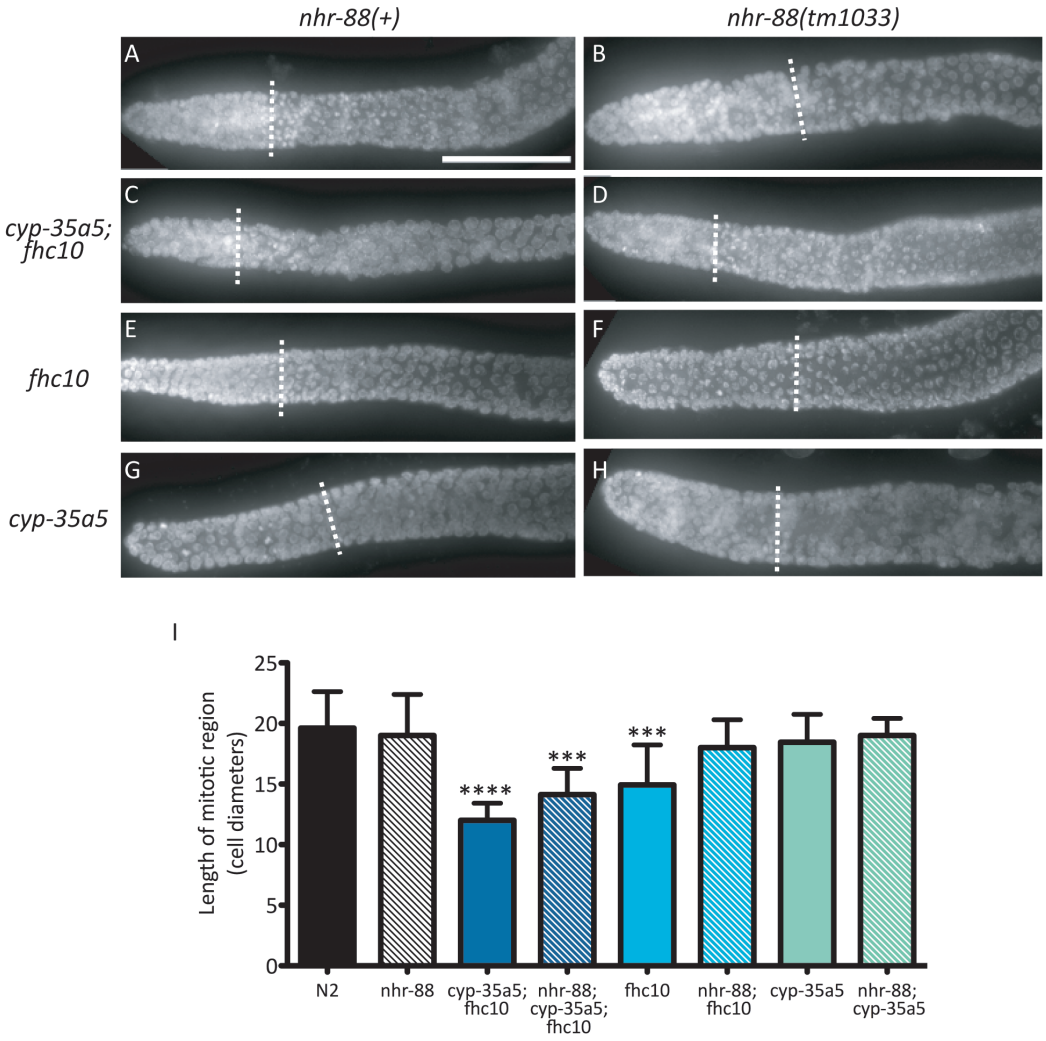

Figure 3.8. *fhc10*, *cyp-35a5*, and *nhr-88* affect mitotic cells within the gonad. Representative DAPI stained gonads extruded from N2 (A), *nhr-88* (B), *cyp-35a5;fhc10* (C), *nhr-88;cyp-35a5;fhc10* (D), *fhc10* (E), *nhr-88;fhc10* (F), *cyp-35a5* (G), and *nhr-88;cyp-35a5* (H) day 1 adults. The beginning of the transition zone is marked with a dashed line. Scale bar = 50µm. All images were acquired at 40X. (I) Quantification of length of the mitotic region. Values shown are the means ± SD of at least 7 gonads, except for *nhr-88;cyp-35a5*, which only has 2.

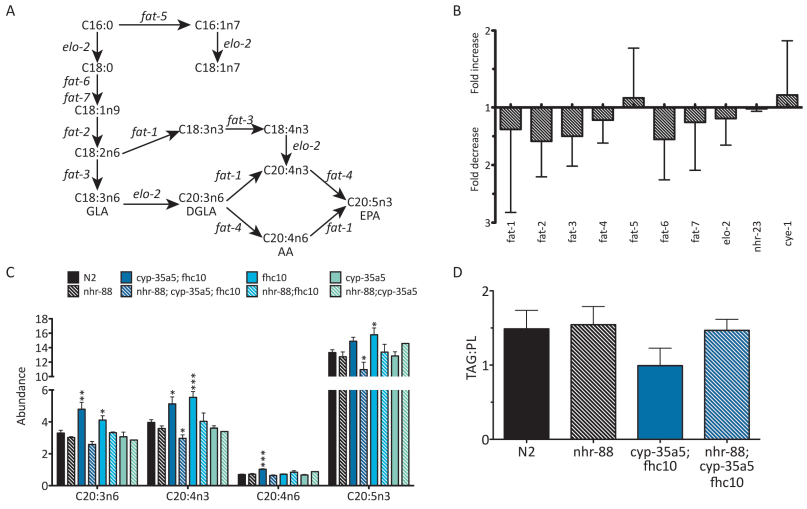

Figure 3.9. *fhc10* changes long-chain PUFA profile in an NHR-88-dependent manner. (A) *C. elegans* PUFA biosynthesis pathway. Shortened common names are shown for gamma-linolenic acid (GLA), dihomo-gamma-linolenic acid (DGLA), arachidonic acid (AA), and eicosopentaenoic acid (EPA). (B) qRT-PCR expression data of PUFA biosynthesis genes and *cye-1* in fed *nhr-88* mutants. No change is significant when compared to N2 by t-test (n=3, in duplicate). (C) Abundance of C20 PUFAs in the mutant strains used in this study. Values shown are means ± SEM, $n > 2$ except for *nhr-88;cyp-35a5*, which has only one replicate. See Table 3.4 for complete fatty acid profile. (D) Ratio of triglyceride to phospholipid as a measure of fat storage in a subset of mutants. Mean from at least 3 experiments is shown ± SEM. $^{*}P < 0.05$, $^{**}P < 0.01$, $^{***}P < 0.001$, $^{****}P < 0.0001$.

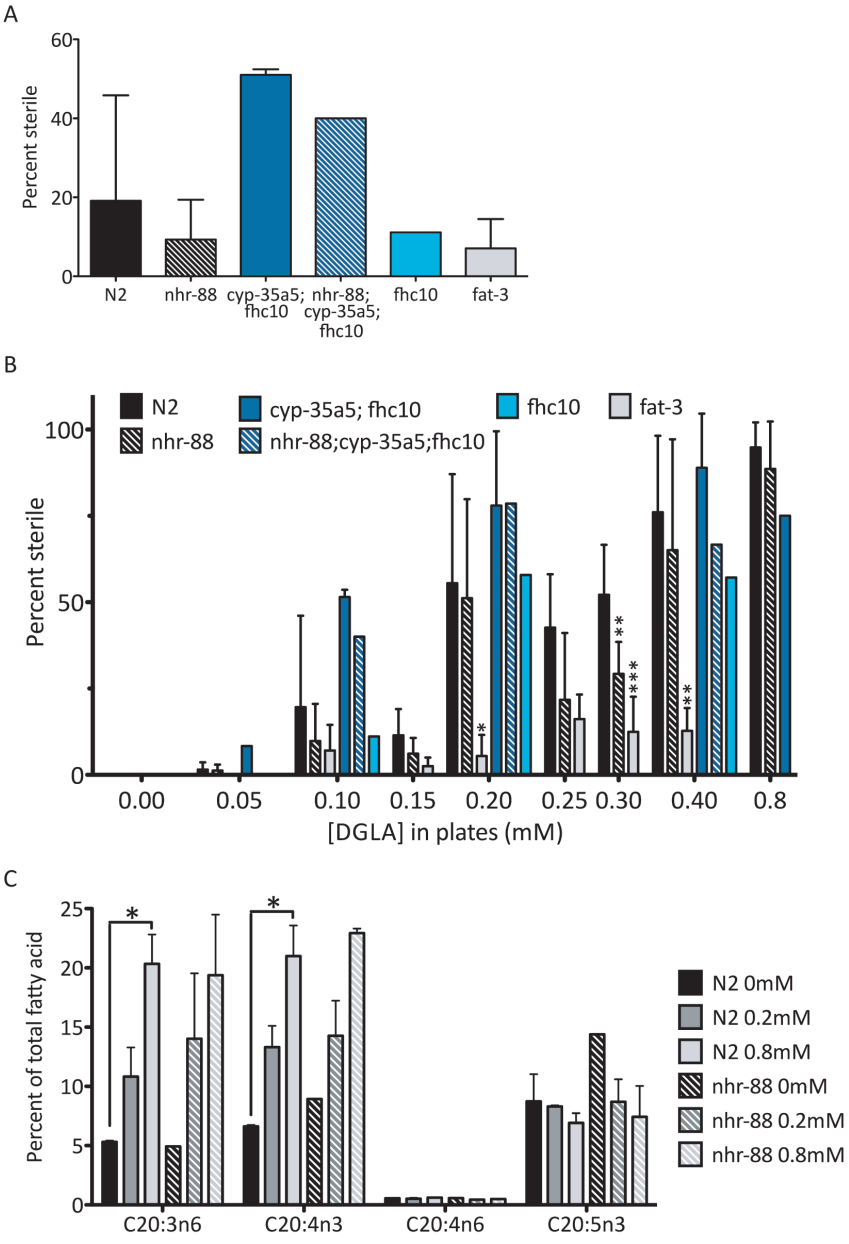

Figure 3.10. NHR-88 is required for full effect of DGLA-induced sterility. (A) Percent of animals sterile at 0.1mM DGLA. Means calculated from variable numbers of replicates (see Table 3.5 for all data and *n* values). Error bars represent SD. (B) Percent of sterile animals for all [DGLA] assayed. Mean ± SD. (C) Mean C20 PUFA species abundance ± SEM in N2 and *nhr-88* mutants grown on increasing concentrations of DGLA. Data are compiled from 2 experiments, where available (abundance of 1 *nhr-88* 0mM replicate too low to quantify). Differences between N2 and *nhr-88* are not significant when compared with a standard t-test. See Table 3.6 for complete profiles. $^{*}P < 0.05$, $^{**}P < 0.01$, $^{***}P < 0.001$

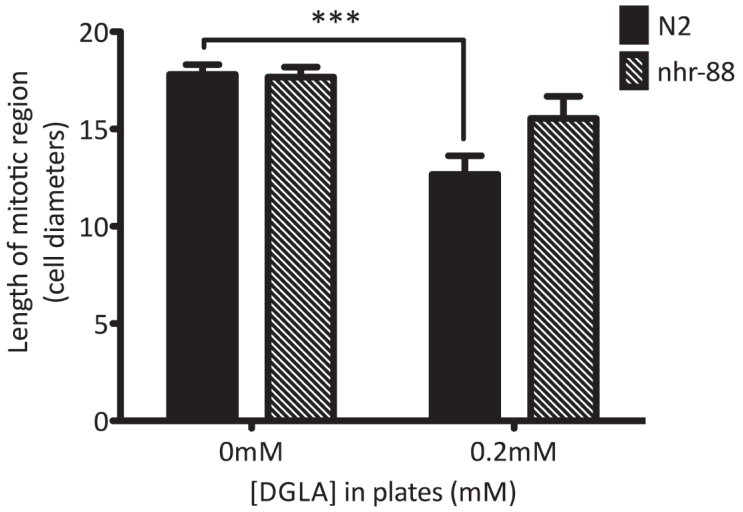

Figure 3.11. DGLA causes shortening of the mitotic region at low concentrations. Length of the mitotic region in N2 and *nhr-88* mutants grown on plates containing either 0mM or 0.2mM DGLA from embryo to day 1 of adulthood. DGLA significantly decreases the length of the mitotic region in N2 but not in *nhr-88*.

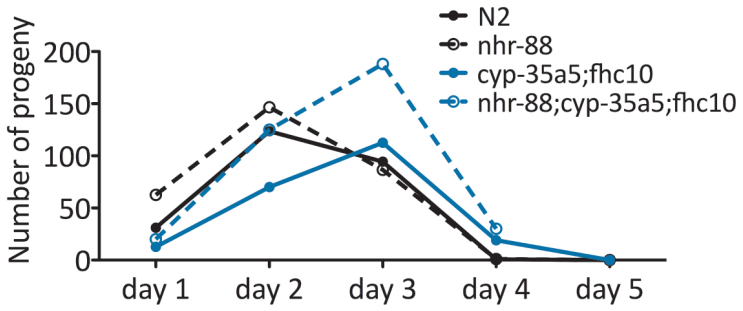

Figure 3.12. Brood delay in *cyp-35a5;fhc10* and *nhr-88;cyp-35a5;fhc10* mutants. Daily brood production from a representative experiment. Day 1 represents the first day post-L4 molt. Note the rightward shift in the brood production curves for *cyp-35a5;fhc10* and *nhr-88; cyp-35a5;fhc10*.

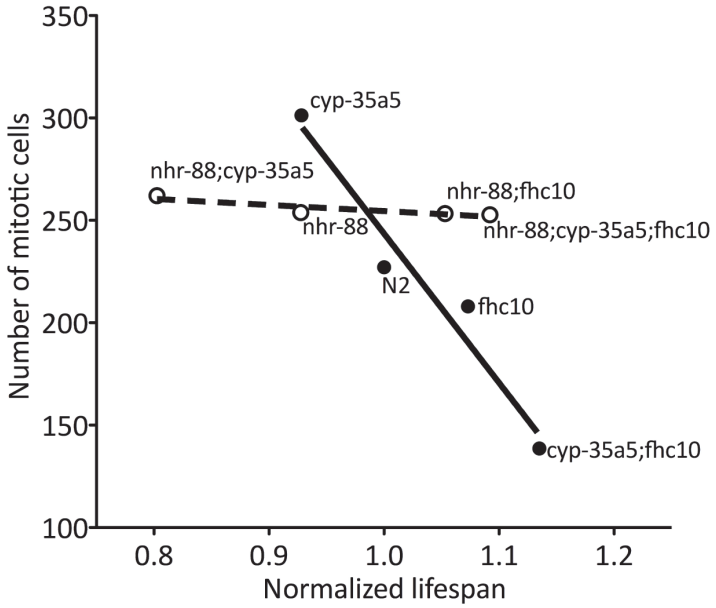

Figure 3.13. Lifespan and number of mitotic cells are inversely related only in the presence of NHR-88. Lifespan normalized to inter-experimental N2 controls (see Table 3.3 for explanation) plotted against number of cells within the mitotic region of the germline. Mutants are separated into two classes: those with the wildtype *nhr-88* allele (filled circles fit with solid line, r^2=.951) and those with *nhr-88(tm1033)* in their genetic background (open circles fit with dashed line, r^2=.796). These correlations suggest that NHR-88 is required for changing the number of mitotic cells and transmitting this information to the somatic tissues, at least within these mutant backgrounds.

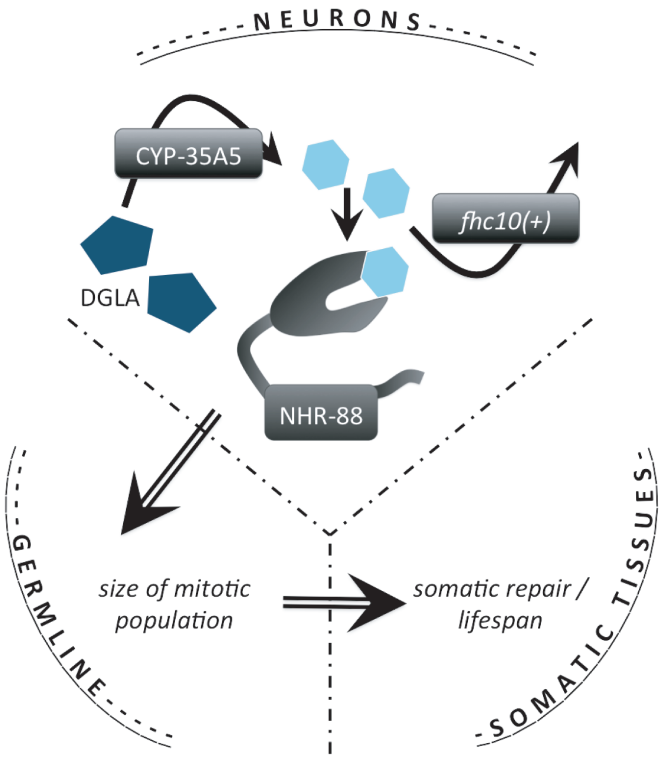

Figure 3.14. Model: NHR-88 signal to mitotic population is altered by *fhc10(+)* and CYP-35A5 activity. The role of NHR-88 in the neurons is to read nutritional status through local changes in DGLA concentration. NHR-88 passes this information to the germline to affect the number of germ cells maintained within the mitotic region, which in turn helps to determine lifespan of the organism. As described in the text, data are consistent with a model in which CYP-35a5 produces a DGLA-derived agonist while *fhc10(+)* counters NHR-88 activity, possibly by clearing this molecule.

Table 3.1. Temperature-dependent fecundity controlled by NHR-88, CYP-35A5, and *fhc10(+)*.

	Selfed brood size				Mated brood size	
	20˚ C		25˚ C		25˚ C	
	mean ± SD	n_{ind} (n_{exp})	mean ± SD	n_{ind} (n_{exp})	mean ± SD	n_{ind} (n_{exp})
N2	246.5 ± 53.5	52 (13)	128.4 ± 38.1****	20 (6)	344.3 ± 118.5****	4 (1)
nhr-88	248.7 ± 59.0	43 (8)	155.3 ± 40.9****	11 (3)	521.3 ± 104.1****	4 (1)
cyp-35a5;fhc10	200.8 ± 41.7***	36 (8)	36.2 ± 16.3****	9 (3)	183.3 ± 44.1***	3 (1)
nhr-88;cyp-35a5;fhc10	298.3 ± 50.3***	22 (6)	49.6 ± 24.2****	8 (3)	94.0 ± 95.1	4 (1)
fhc10	227.6 ± 32.0	9 (2)	133.8 ± 46.0	8 (2)	n.d.	
nhr-88; fhc10	217.0 ± 261.5	9 (2)	183.1 ± 29.7	7 (2)	n.d.	
cyp-35a5	265.5 ± 46.4	15 (2)	196 ± 29.0	4 (1)	254 ± 74.3	5 (1)
nhr-88;cyp-35a5	266.8 ± 41.5	12 (2)	175.3 ± 21.7*	4 (1)	382.4 ± 81.1****	5 (1)

$^{*}P < 0.05$, $^{***}P < 0.001$, $^{****}P < 0.0001$, n.d. = not determined.
Significance values shown are based on comparison to N2 for 20˚C mutant broods, to 20˚C broods for 25˚C, and to selfed 25˚C broods for mated broods at 25˚C.

Table 3.2. Quantification of changes within the mitotic region.

	Length (cell diameters)		Cell number	
	mean ± SD	n_{ind} (n_{exp})	mean ± SD	n_{ind} (n_{exp})
N2	19.6 ± 3.0	13 (4)	227.1 ± 35.7	8 (4)
nhr-88	19.0 ± 3.4	13 (4)	253.8 ± 40.1	10 (4)
cyp-35a5;fhc10	12.0 ± 1.4****	13 (4)	138.6 ± 50.7**	17 (4)
nhr-88;cyp-35a5;fhc10	14.1 ± 2.32***	7 (2)	252.7 ± 85.5	3 (2)
fhc10	14.9 ± 3.3***	28 (2)	208.0 ± 27.0	8 (2)
nhr-88; fhc10	18.0 ± 02.3	8 (2)	253.3 ± 50.9	8 (2)
cyp-35a5	18.5 ± 2.3	11 (1)	301.3 ± 92.3*	7 (1)
nhr-88;cyp-35a5	19.0 ± 1.4	2 (1)	262	1 (1)

$^{**}P < .01$, $^{***}P < 0.001$, $^{****}P < 0.0001$

Table 3.3. Mutant lifespan data from replicate experiments.

		Mean lifespan ± SD	Ratio to N2	Maximum lifespan	*n*
07.23.10	N2	15.3 ± 4.6	1.000	27	56
	nhr-88(tm1033)	14.8 ± 6.5	0.967	26	48
	cyp-35a5(ok1985);fhc10	15.3 ± 8.5	1.000	35	53
10.18.10	N2	16.0 ± 4.0	1.000	25	58
	nhr-88	15.3 ± 4.07	0.956	24	40
	cyp-35a5;fhc10	18.7 ±5.5**	1.169	31	57
	nhr-88;cyp-35a5;fhc10	17.1 ± 4.1	1.069	25	51
01.12.11	N2	14.9 ± 4.0	1.000	21	59
	nhr-88	14.7 ± 3.6	0.987	24	52
	cyp-35a5;fhc10	19.7 ± 7.5***	1.322	37	53
	nhr-88;cyp-35a5;fhc10	16.6 ± 5.0	1.114	31	54
04.07.11	N2	16.0 ± 3.3	1.000	22	50
	nhr-88	12.8 ± 4.4***	0. 800	24	46
	cyp-35a5	14.9 ± 3.3	0.931	26	46
	nhr-88;cyp-35a5	12.9 ± 2.9***	0.806	22	42
06.08.11	N2	19.4 ± 5.1	1.000	26	20
	cyp-35a5;fhc10	20.0 ± 7.6	1.03	26	19
	fhc10	20.8 ± 8.5	1.072	44	43
	nhr-88;fhc10	20.4 ± 5.0	1.052	28	47

		Mean lifespan ± SEM	Ratio to N2	Maximum lifespan	*n*
all experiments	N2	15.6 ± 0.8†	1.000	27	5
	nhr-88	14.4 ± 0.5	0.923	26	4
	cyp-35a5;fhc10	18.4 ± 1.1	1.179	37	4
	nhr-88;cyp-35a5;fhc10	16.9 ± 0.3	1.083	31	2
	fhc10	20.8‡	1.072	44	1
	nhr-88;fhc10	20.4‡	1.052	28	1
	cyp-35a5	14.9	0.931	26	1
	nhr-88;cyp-35a5	12.9	0.806	22	1

†Mean from 06.08 was excluded as an outlier.
‡Normalized to N2 control from 6.08 experiment.

Table 3.4. Complete fat profiles of mutants used in this study.

	N2	nhr-88	cyp-35a5; fhc10	nhr-88; cyp-35a5; fhc10	fhc10	nhr-88;fhc10	cyp-35a5	nhr-88; cyp-35a5
n	16	12	3	3	4	2	2	1
C14:0	1.2 ± 0.07	1.2 ± 0.12	1.2 ± 0.1	1.2 ± 0.12	1.6 ± 0.22	1.1 ± 0.17	1.2 ± 0	1.2
C15iso	3.6 ± 0.19	3.5 ± 0.13	3.9 ± 0.14	3.0 ± 0.16	4.2 ± 0.34	3.1 ± 0.14	3.5 ± 0.18	3.2
C16:1n7	1.9 ± 0.18	1.9 ± 0.26	1.9 ± 0.04	2.1 ± 0.27	2.2 ± 0.28	1.6 ± 0.05	1.9 ± 0.23	1.8
C16:0	4.9 ± 0.26	5.2 ± 0.54	3.2 ± 0.07*	5.9 ± 0.28	4.0 ± 0.21	4.6 ± 0.02	4.4 ± 0.31	4.8
C17iso	3.2 ± 0.16	3.4 ± 0.19	5.6 ± 0.43****	2.9 ± 0.11	3.6 ± 0.32	3.4 ± 0.4	3.5 ± 0.22	3.2
C17D	18.1 ± 0.51	17.0 ± 0.61	14.4 ± 0.22**	18.8 ± 1.12	15.7 ± 0.31*	18.5 ± 2.27	17.6 ± 0.13	15.9
C18:3	1.8 ± 0.05	1.6 ± 0.04	1.4 ± 0.01**	1.7 ± 0.08	1.7 ± 0.16	1.7 ± 0.17	1.8 ± 0.1	1.5
C18:2n6	5.5 ± 0.1	5.9 ± 0.12*	5.3 ± 0.25	5.3 ± 0.27	5.4 ± 0.35	5.9 ± 0.22	5.9 ± 0.26	6.0
C18:1n9	4.6 ± 0.28	4.7 ± 0.29	3.0 ± 0.17*	4.8 ± 0.43	4.3 ± 0.5	3.7 ± 0.66	4.4 ± 0.19	4.8
C18:1n7	20.4 ± 0.69	21.5 ± 0.5	21.9 ± 0.86	22.5 ± 0.67	20.3 ± 0.59	19.5 ± 1.26	22.1 ± 0.2	21.7
C18:0	4.0 ± 0.13	4.4 ± 0.1*	3.4 ± 0.17	4.4 ± 0.19	3.5 ± 0.37	4.7 ± 0.26	4.2 ± 0.2	4.5
C19D	9.5 ± 0.42	9.6 ± 0.3	9.1 ± 0.3	10.0 ± 0.39	7.4 ± 1*	10.7 ± 0.44	9.5 ± 0.12	9.5
C20:4n6	0.7 ± 0.03	0.7 ± 0.04	1.0 ± 0.03***	0.6 ± 0.03	0.7 ± 0.02	0.8 ± 0.09	0.7 ± 0.03	0.9
C20:5n3	13.3 ± 0.39	12.8 ± 0.66	14.9 ± 0.56	11.0 ± 1.02*	15.8 ± 0.94*	13.4 ± 1.09	12.9 ± 0.57	14.6
C20:3n6	3.3 ± 0.17	3.0 ± 0.06	4.8 ± 0.43**	2.6 ± 0.19	4.1 ± 0.27*	3.3 ± 0.05	3.1 ± 0.29	2.9
C20:4n3	4.0 ± 0.18	3.6 ± 0.16	5.1 ± 0.44*	3.0 ± 0.22*	5.5 ± 0.36***	4 ± 0.52	3.6 ± 0.15	3.4

$^{*}P < .05$, $^{**}P < .01$, $^{***}P < 0.001$, $^{****}P < 0.0001$

Table 3.5 DGLA-induced sterility data from individual experiments

		0 mM	0.05 mM	0.1 mM	0.15 mM	0.2 mM	0.25 mM	0.3 mM	0.4 mM	0.8 mM
05.25.11*	N2	0.0				77.8			100.0	92.3
05.31.11*	*cyp35a5;fhc10*	0.0				83.3			100.0	100.0
06.03.11*	N2	0.0	28.0			100.0			100.0	100.0
	nhr-88	0.0	0.0			41.4			55.0	93.8
	cyp35a5;fhc10	0.0	52.6			83.3			100.0	75.0
06.11.11*	N2	0.0	8.3	47.6		92.3			75.0	
	nhr-88	0.0	0.0	25.7		66.7			100.0	
	cyp35a5;fhc10	0.0	8.3	50.0		76.9			77.8	
	nhr88;cyp35a5;fhc10	0.0	0.0	40.0		78.6			66.7	
	fhc10	0.0	0.0	11.1		57.9			57.1	
09.21.11*	N2	0.0	2.0	8.3		56.8			75.0	93.0
	nhr-88	0.0	2.0	0.0		6.0			73.3	80.6
09.25.11*	N2	0.0	3.1	12.5		66.1			78.9	94.5
	nhr-88	0.0	3.1	3.7		5.4			17.9	47.8
10.07.11*	N2	0.0	0.0	2.0		32.7			77.4	100.0
	nhr-88	0.0	1.5	0.0		40.7			100.0	100.0
10.16.11	N2	0.0	0.0	0.0		34.9			71.9	100.0
		0.0				14.3			82.9	95.0
	nhr-88	0.0	0.0	0.0		29.6			94.2	86.0
		0.0	0.0			40.0			84.2	90.9
10.21.11	N2	0.0	3.3	91.0		82.2			94.3	100.0
		0.0	0.0	78.9		82.9			83.3	75.0
		0.0	1.4	20.7		89.7			98.1	82.2
	nhr-88	0.0	0.0	32.4		100.0			90.2	82.9
		0.0	1.5	11.4		71.4			94.0	87.0
		0.0	6.4	30.8		91.2			96.3	95.2

		0 mM	0.05 mM	0.1 mM	0.15 mM	0.2 mM	0.25 mM	0.3 mM	0.4 mM	0.8 mM
10.21.11, continued	N2†	0.0	3.0	6.0		67.3			50.0	100.0
		0.0	1.7	2.7		89.1			98.8	96.1
		0.0	0.0	36.6		76.3			98.4	97.4
		0.0	0.0	13.3		86.4			93.1	96.9
	nhr-88†	0.0	2.6	12.1		78.3			95.6	99.0
		0.0	0.0	0.0		70.9			81.8	98.4
		0.0	2.1	6.9		83.3			96.2	95.6
		0.0	4.0	8.7		83.1			81.3	95.1
		0.0		1.4		86.7				
11.18.11	N2†	0.0	0.0	4.9	5.7	11.3	40.0	42.1	22.9	0.0
		0.0	3.2	9.1	25.0	15.7	22.4	34.1	49.2	0.0
		0.0	0.0	3.4	3.6	23.5	32.7	67.3	64.9	0.0
		0.0	0.0	0.0	14.3	21.8	41.5	68.8	55.9	0.0
		0.0	1.3	2.0	10.6	14.1	66.7	43.1	38.2	0.0
		0.0	0.0	5.4	9.5	30.4	52.5	57.5	65.4	0.0
	nhr-88†	0.0	1.2	0.0	14.5	31.7	5.8	17.7	13.7	0.0
		0.0	0.0	9.6	5.4	20.6	0.0	31.3	35.6	0.0
		0.0	0.0	4.6	0.0	29.5	23.7	18.9	18.8	0.0
		0.0	0.0	5.8	7.5	23.1	12.5	34.8	38.5	0.0
		0.0	0.0	6.5	3.2	40.0	40.4	44.1	27.3	0.0
		0.0	0.0	8.5	4.2	28.1	15.4	26.0	26.1	0.0
			0.0		8.1	57.9	54.2	32.0	46.9	
	fat-3	0.0	0.0	15.6	5.0	2.0	14.9	2.4	20.0	0.0
		0.0	0.0	2.1	0.0	12.5	9.8	22.7	7.1	0.0
		0.0	0.0	3.4	2.6	1.9	23.8	12.2	11.1	0.0

		0 mM	0.05 mM	0.1 mM	0.15 mM	0.2 mM	0.25 mM	0.3 mM	0.4 mM	0.8 mM
Mean ± SEM (n) all experiments	N2	0 (21)	1.5 ± 2.1 (18)	19.6 ± 26.5 (19)	11.5 ± 7.6 (6)	52.6 ± 33.3 (21)	42.6 ± 15.4 (6)	52.2 ± 14.5 (6)	73.3 ± 25.3 (22)	91.7 ± 14.1 (15)
	nhr-88	0 (20)	1.2 ± 1.7 (20)	8.8 ± 10.1 (19)	6.1 ± 4.6 (7)	54.5 ± 27.5 (21)	21.7 ± 19.4 (7)	29.3 ± 9.3 (7)	68.6 ± 30.9 (20)	92.1 ± 6.5 (12)
	cyp35a5;fhc10	0 (2)	8.3 (1)	51 ± 1.4 (2)		72 ± 15.1 (3)		92.6 ± 12.8 (3)	100 (1)	0 ± 0 (2)
	nhr88;cyp35a5;fhc10	0 (1)	0 (1)	40 (1)		78.6 (1)			66.7 (1)	
	fhc10	0 (1)	0 (1)	11.1 (1)		57.9 (1)			57.1 (1)	
	fat-3	0 (3)	0 ± 0 (3)	7.1 ± 7.5 (3)	2.5 ± 2.5 (3)	5.5 ± 6.1 (3)	16.2 ± 7.1 (3)	12.5 ± 10.1 (3)	12.8 ± 6.6 (3)	0 ± 0 (3)

†Worms used in these replicates came from freshly-thawed stocks.
*Worms plated on multiple plates were assayed together, yielding one measurement from a pooled population.

Table 3.6. Complete fat profile of DGLA-treated animals.

	N2			*nhr-88*		
[DGLA]	0mM	0.2mM	0.8mM	0mM	0.2mM	0.8mM
C14:0	2.1 ± 1.1	2 ± 0.75	1.9 ± 0.64	3.1	2 ± 0.96	2.5 ± 0.21
C15iso	3.5 ± 0.48	5.2 ± 1.13	5 ± 1.42	4.2	6.9 ± 1.18	5.4 ± 1.6
C16:1n7	1.3 ± 0.21	2.4 ± 0.7	3 ± 0.8	3.7	3 ± 0.94	3.5 ± 0.29
C16:0	7.2 ± 3.41	5.2 ± 0.75	6.1 ± 0.33	4.6	5.7 ± 0.74	6.3 ± 0.41
C17iso	2.6 ± 0.22	2.1 ± 0.04	1.5 ± 0.08	2.6	2 ± 0.05	1.3 ± 0.01
C17D	20.7 ± 3.59	12.2 ± 2.32	7.1 ± 1.61	16.1	10.2 ± 1.05	6.8 ± 0.95
C18:3	1.3 ± 0.67	1.1 ± 0.41	0.9 ± 0.13	0.5	0.8 ± 0.13	0.7 ± 0.1
C18:2n6	2.8 ± 0.29*	5.6 ± 0.08	4.5 ± 0.85	4.3	5.6 ± 0.68	4.5 ± 1.05
C18:1n9	3.1 ± 0.5	5.9 ± 0.51	5.4 ± 0.48	3.1	6 ± 0.53	4.2 ± 0.73
C18:1n7	18.2 ± 1.62	11.5 ± 0.81	5.5 ± 1.29	17.9	9.5 ± 0.19	5.7 ± 0.33
C18:0	6.6 ± 2.03	5.5 ± 0.45	5.5 ± 1.29	4	3.9 ± 0.18	5 ± 0.51
C19D	9.5 ± 1.67	8.5 ± 1.4	4.8 ± 1	7	6.9 ± 0.42	3.9 ± 0.88
C20:4n6	0.6 ± 0.03	0.5 ± 0.08	0.6 ± 0.04	0.6	0.4 ± 0	0.5 ± 0.03
C20:5n3	8.7 ± 2.3	8.3 ± 0.1	6.9 ± 0.83	14.4	8.7 ± 1.9	7.4 ± 2.61
C20:3n6	5.3 ± 0.1*	10.8 ± 2.46	20.3 ± 2.48	4.9	14 ± 5.52	19.4 ± 5.11
C20:4n3	4 ± 0.11*	13.3 ± 1.8	21 ± 2.58	8.9	14.3 ± 2.97	22.9 ± 0.39

*$P < .05$

Chapter IV: NHR-88 acts downstream of NHR-49 to regulate the adult reproductive diapause

Organisms have evolved myriad ways to survive periods of nutrient deprivation. The adult reproductive diapause (ARD) in *Caenorhabditis elegans* is an example of an alternative life history that protects reproductive longevity in the case of long-term food deprivation. To date, the nuclear receptor NHR-49 is the only known regulator of this diapause. By analyzing microarrays of fasted animals, I defined several additional modules of the NHR-49 starvation response that may play a role in executing the ARD phenotype. I also discovered that NHR-49 drives expression of *nhr-88*, another nuclear receptor, in response to fasting. *nhr-88* deletion animals enter ARD at a reduced rate and animals that do enter show hallmarks of a defective diapause, including missing embryos and mislocalization of sperm. As many *nhr-88* ARD phenotypes are shared with *nhr-49* mutants, I propose that a subset of NHR-49 fasting targets is actually regulated through NHR-88.

Introduction

The *Caenorhabditis elegans* nuclear receptor NHR-49, like its mammalian homologs HNF4α and PPARα, is a key regulator of glucose and lipid metabolism. Therefore it is a critical player in the fasting response, allowing animals to adapt to reduced nutrient availability via mobilization of fat stores. As expected, *nhr-49* mutants are starvation sensitive; however, this sensitivity stems not only from the inability to appropriately regulate general fasting-specific metabolic changes that are independent of starvation-resistant fates, but also from defective entry into one of these protective states – the adult reproductive diapause (ARD) (Angelo and Van Gilst, 2009; Van Gilst et al., 2005b). While *nhr-49* worms are capable of entering both L1 and dauer diapauses, the long-term survival of these early-stage arrested animals has not been determined.

ARD is a long-lived, non-aging diapause that occurs when food is withdrawn at the mid-L4 stage; wild-type worms starved just before this window will arrest as L4s, while those starved after will not arrest and eventually dying as a result of internal hatching of embryos ("bagging") (Angelo and Van Gilst, 2009). Markers of a healthy arrest are a single embryo held within each arm of the gonad, cessation of fertilization events, and extreme plasticity within both the germline and soma. Throughout the first ten days of starvation the number of germ cells drops

from over 1000 to about 35 per gonad arm, with the volume of the gonad decreasing accordingly (Angelo and Van Gilst, 2009). Electron microscopy of wild-type arrested adults has recently revealed extreme remodeling within somatic tissues as well, including disappearance of fat stores, loss of intestinal villi, and alterations of hypodermal structure (Giana Angelo, unpublished data). This somatic plasticity is completely absent in the *nhr-49* mutant, leading to the classification of these mutants as "slowly starving" as opposed to "arrested".

Amazingly, these changes are reversed once animals are re-fed. After just 72 hours back on food, the germline is repopulated and the animal begins reproducing with minimal loss of fecundity, especially if exogenous sperm are provided (Angelo and Van Gilst, 2009). Furthermore, recovered ARD animals, even those starved for extended periods of time, go on to live a normal adult lifespan of approximately 18 days (Angelo and Van Gilst, 2009). Thus the adult reproductive diapause is similar to the dauer diapause, which also protects longevity during extreme periods of starvation (Kim and Paik, 2008). However, while the dauer pathways are very well characterized, *nhr-49* is the only known regulator of ARD entry; there is no overlap in requirement of dauer genes tested to date (Giana Angelo, unpublished data).

The cellular adaptations that occur in ARD animals during starvation are likely to be conserved in the mammalian fasting response, making *C. elegans* an excellent system in which to study these changes. I aimed to improve ARD as a genetically tractable model system by identifying novel regulators of the diapause phenotype that would allow separation from the pleiotropy of the *nhr-49* mutant. To expand the network of ARD-related genes, I analyzed microarrays done on fasted worms and defined several categories of genes that make up the NHR-49 fasting response, including another nuclear receptor. As described in Chapter 3, NHR-88 is a *C. elegans* nuclear receptor that impacts the germline. Although it does not interact with *nhr-49* in fed animals, I found that *nhr-88* is activated in an NHR-49-dependent manner upon removal from food, and may in turn regulate some aspects of the ARD phenotype.

Results

Expanding the NHR-49-dependent fasting response

While the fasting-dependent transcriptional changes effected by NHR-49 on fat and glucose metabolism genes had been previously defined, I was interested in identifying NHR-49 targets required for entry into the adult reproductive diapause (ARD). To this end, I analyzed

microarrays comparing fed to fasted N2 and *nhr-49(nr2041)* worms that had been done by Giana Angelo. As RNA for these experiments was harvested from animals starved at a time point similar to that for ARD entry, I reasoned that the expression profile may include genes important for the diapause. Using a 5-fold cut-off, the microarray shows 483 genes to be significantly up-regulated and 50 significantly down-regulated upon fasting in the N2 background (Tables 4.1 and 4.2). Of these, over 95% were dependent on NHR-49 for their change (Tables 4.1 and 4.2). Even if NHR-49 does not directly regulate these genes, they will still implicate processes that are important for the diapause.

To get a better sense for the types of genes required for the ARD fasting response, I categorized genes meeting the cut-off into categories based on reported phenotypes and gene ontology annotations available on WormBase (Figure 4.1 and Table 4.3). I then designed primers to use in qRT-PCR to confirm the role of NHR-49 in the fasting-dependent changes in a 166-gene subset of targets falling into 12 categories (Figure 4.1). Although there was overrepresentation of other gene groups (such as serpentine receptors), I chose to focus on gene classes that had clear connections to physiological changes associate with ARD. For example, since embryonic arrest/delay and halting of reproductive activities, including oocyte production, are required for entry into ARD, and tissue remodeling and protection of longevity are associated with maintenance of the diapause, I retested the effect of fasting on genes involved in yolk metabolism, reproduction, and cell cycle (Figure 4.2), as well as on autophagy and aging-related genes (Figure 4.3). The data were extremely variable and expression changes between fasted animals and fed controls of the same genotype were relatively minor, making it difficult to define category-wide trends; however, there were some interesting differences between N2 and the *nhr-49* mutant, especially when taken in context of the *nhr-49* starvation phenotype. For example, there are some autophagy genes that are fasting-induced only in an N2 background, which may help to explain the accumulation of cell corpses in starving *nhr-49* animals (see Discussion for exploration of other divergences). I also assayed expression changes in groups of genes with less defined roles in ARD, including those involved in neuronal signaling, metal processing, P-granule formation, lipid metabolism, osmoregulation, cuticle formation, and a group of nematode-specific genes (Figures 4.4 and 4.5). Again, experimental variability, likely stemming from RNA quality, makes expression data for these categories difficult to interpret.

NHR-88 acts downstream of NHR-49 to regulate select ARD phenotypes

NHR-49 does not appear to regulate NHR-88 in the fed state, as the preliminary microarray data could not be confirmed by qRT-PCR (see Chapter 3). However, I did identify a role for NHR-49 in the fasting-dependent activation of NHR-88. When N2 animals are removed from food for 8 hours, qRT-PCR shows that expression of *nhr-88* increases approximately 4-fold (Figure 4.6). This activation is abrogated in an *nhr-49* mutant, implicating NHR-49 in the response (Figure 4.6).

I next explored the possibility that misregulation of NHR-88 might cause a subset of *nhr-49* fasting phenotypes. Starving *nhr-88(tm1033)* mutants results in a diapause-like state very similar to the *nhr-49* starving adult phenotype. In preliminary, qualitative experiments, I noticed fewer ARD animals on starved *nhr-88* plates than on N2 controls. I also found that most of the ARD adults that I looked at by DIC microscopy did not have embryos held *in utero* (Figure 4.7). This observation suggests that, as with *nhr-49* animals, only the small percentage of *nhr-88* worms that avoid bagging due to inviable or absent embryos can survive starvation. Additionally, sperm continue to localize to the proximal oocyte, demonstrating an inability to halt fertilization (Figure 4.7A). As I was careful to stage L4 animals before starvation to ensure that they were within the ARD entry window and I could differentiate arrested L4s and bagging adults in addition to the diapause-like animals, the defects described above likely result from *nhr-88* regulation of ARD.

Although *nhr-88* mutants cannot properly enter ARD, examination of slowly starving adults shows the maintenance phase to be grossly intact. I see a reduction in germ cell number as starvation progresses, a hallmark of a healthy diapause (Figure 4.7B); shrinking of the germline also occurs in *nhr-49* animals (Angelo and Van Gilst, 2009). Re-feeding of slowly starving adults shows additional defects in the recovery phase. While *nhr-88* mutants are able to repopulate their germlines, indicating that NHR-88 is not involved in the maintenance of the putative germline stem cell population during starvation (Figure 4.7C), both selfed and mated brood sizes are reduced compared to that reported for recovered N2 ARD animals (Figure 4.7D). Furthermore, recovered animals accumulate what appears to be yolk within the body cavity (Figure 4.7C), another phenotype shared with *nhr-49* mutants (Angelo and Van Gilst, 2009). The similarities between the adult starvation responses of *nhr-88* and *nhr-49* mutants, in combination with qRT-PCR data showing an NHR-49-dependent activation of *nhr-88* upon

removal from food at mid-L4, suggest a role for NHR-88 in coordinating some aspects of the diapause.

Discussion

NHR-49 is a key coordinator of the *C. elegans* fasting response; expanding upon the regulation of previously identified lipid and glucose metabolism genes, I have defined several other fasting-dependent modules that may be involved in entry into the adult reproductive diapause. I also discovered that *nhr-88* is activated during starvation in an NHR-49-dependent manner. Finally, I found that *nhr-88* mutants enter a false diapause very similar to that entered by *nhr-49* animals, suggesting a role for NHR-88 in ARD, possibly downstream of NHR-49.

Newly defined fasting response categories coincide with ARD phenotypes

Based on preliminary microarray data collected by Giana Angelo, I defined 12 gene categories showing fasting-dependent changes in expression level and retested the 166 genes within these classifications (Figure 4.1). qRT-PCR confirmed a role for most of these retested genes in the fasting response. As the time point at which worms are removed from food is the same for these qRT-PCR experiments and ARD induction, it is likely that a portion of genes identified as fasting-induced or repressed are important for entry into the diapause. Others may be part of a non-specific fasting response. Comparison of genes regulated during L4 fasting with genes reported to be enriched in the dauer diapause reveals less than 10% overlap, suggesting that the majority of targets are specific to the L4 time point (Liu et al., 2004; Wang and Kim, 2003). This hypothesis is supported by the fact that the newly defined fasting modules make sense in the context of the physiological changes required for proper arrest. However, even genes that change significantly demonstrate relatively minor differences in expression levels. As only about a third of a population starved during mid-L4 will continue to the diapause, I would expect to see more dramatic expression level changes if I were to enrich for arrested adults. Another possibility is that these small changes reflect tissue specificity.

While gene classes do not appear to be co-regulated, expression changes of specific genes can inform future studies of the diapause. For example, since ovulation halts during ARD, no new oocytes need to be made, thus dispensing with the need to make and transport yolk to the germline. Accordingly, expression is decreased for three of the six vitellogenin genes, which

encode lipoproteins that form the basis of yolk droplets (Figure 4.2A, Table 4.3). The other three are not reduced, suggesting that the *vit* genes do not experience coordinated regulation. There are also a number of other genes involved in reproduction, including several sperm proteins. As there are no new fertilization events after entry into ARD, I would expect that expression of these genes might decrease. Even though spermatogenesis has finished by the time an animal enters ARD, there may be changes within the pre-diapause L4 that ensure cessation of fertilization activities. While this is the trend seen for some major sperm proteins, like *msp-76* and *msp-59*, others, such as *msp-56*, increase slightly or do not change (Figure 4.2B, Table 4.3). For both the yolk and reproduction-related genes, I would expect misregulation in an *nhr-49* background based on the *nhr-49* mutant phenotypes of yolk accumulation upon recovery and continued localization of sperm to the proximal oocyte. However, these genes do exhibit some change in the mutant line, possibly because the yolk and sperm phenotypes are involved in recovery and maintenance instead of the entry time point or due to regulators other than NHR-49. Another hallmark of diapause entry is apparent embryonic arrest; it is therefore unsurprising that a number of cell cycle genes were implicated in the fasting response (Figure 4.2C, Table 4.3). As this arrest does not occur in *nhr-49* animals, I would anticipate NHR-49 to be required for expression changes within this category; however, most cell cycle genes experience similar expression differences in N2 and *nhr-49* mutants. One gene that is NHR-49-dependent is *cdc-25.3*, an inducer of mitosis. Interestingly, expression of this gene is increased during fasting, suggesting that removal from food does not lead to exit from the cell cycle for all tissues. Given that most cells are post-mitotic in an L4 animal and that germ cell number decreases during starvation (indicating that this cell population halts the cell cycle), the increased expression of this inducer may be an artifact of tissue remodeling occurring at the L4-to-adult transition.

During the maintenance phase of the diapause, tissue remodeling occurs in both the germline and soma, presumably to provide the energy required to keep the worm alive and preserve germline stem cells. It therefore makes sense that I see upregulation of some genes involved in autophagy and protein catabolism (Figure 4.3A, Table 4.3). The fact that these genes, especially the autophagy-related *ced-10* and *lgg-2*, are not induced fully in the *nhr-49* background may help to explain the genetic basis for lack of somatic remodeling and accumulation of germline cell corpses in the mutant. For example the *ced-10* GTPase is required in the engulfing cell for autophagy to occur (Reddien and Horvitz, 2000); its reduced expression

may account for the accumulation of cell corpses in proximal gonad of *nhr-49* starved worms. Additionally, mechanisms to protect longevity must be at work during starvation, since worms can survive for many times their normal lifespan away from food and yet still have a normal lifespan refed. This hypothesis is supported by overlap between fasting-regulated genes and genes with reported roles in aging (Golden et al., 2008) (Figure 4.3B, Table 4.3).

Finally, these data may provide novel insights into the mechanism of ARD. For example, a possible method for coordinating the diapause between tissues is suggested by neuronal genes that show altered expression profiles when food is removed. Regulation of the dopamine receptor *dat-1* and a predicted dopamine monooxygenase (which should theoretically metabolize dopamine) suggest that dopamine signaling may be downregulated during fasting (Figure 4.4A, Table 4.3). Since dopamine is known to regulate food-searching behaviors in *C. elegans* (Hills et al., 2004), it would make sense that removal from food would induce changes in this signaling pathway. Three neuropeptides also increase expression a few fold, implicating them in transmission of a fasting signal (Figure 4.4A, Table 4.3). Heme has also been put forth as the diapause signal, due to the fact that heme-starved worms share several phenotypes with starved, arrested animals (personal communication with Giana Angelo and Wayne Van Voorhies). While there are some fasting-regulated genes implicated in metabolism of heme itself, such as the intestinal heme transporter *hrg-4* (Rajagopal et al., 2008), there are many other genes that simply bind heme and that exhibit a greater magnitude of change, including a number of cytochrome P450s (Figure 4.4B, Table 4.3).

Another observation that may provide the basis for further study is the fasting-dependent upregulation of several proteins associated with P-granules, germline-specific organelles made up of RNA and proteins that are thought to be involved in post-transcriptional regulation (Figure 4.4C) (Updike and Strome, 2010). Taken together with experiments conducted by Bargavi Thyagarajan (a post-doctoral fellow in the Van Gilst lab) demonstrating that ARD animals are able to recover even when transcription is blocked chemically or genetically, upregulation of P-granule stabilizing genes such as the RNA helicases *glh-1* and *glh-4* suggests that mRNAs may be stored during starvation. However, as with all of the modules included on the qRT-PCR panel, not every gene behaves the same way, and there are P-granule genes that are fasting-repressed as well (Figure 4.4C, Table 4.3). Although these inconsistencies complicate my

analysis, I believe that they are also providing insight into which members of these gene families may be specific to the fasting response.

The final groups of genes included on the qRT-PCR panel are not associated with known ARD phenotypes. It will be important to clarify whether activation of lipid metabolism and osmoregulation genes is specific to ARD or if they are activated as part of the global fasting response (Figure 4.5A, B). If the former, these qRT-PCR data may lead to the identification of new pathways involved in diapause entry. Similarly, fasting-dependent regulation of collagen-related genes suggests that cuticular remodeling may be a hallmark of ARD (Figure 4.5C). Future experiments could test the ability of osmoregulation or collagen mutants to enter the diapause. Lastly, a number of nematode-specific genes are fasting-regulated (Figure 4.5D). Interestingly, expression of the *nspd* family is increased in N2 but decreased in *nhr-49* fasted worms, while the *nspe* expression goes down in both backgrounds. This differential regulation suggests that the families are involved in different processes, potentially demonstrating functions for members of this uncharacterized gene class. Likewise, these studies have also paved the way for characterization of a number of other unnamed genes with roles in the fasting response.

NHR-88 is required for healthy diapause, possibly downstream of NHR-49

I found that, contrary to what is seen in the fed state, NHR-49 is responsible for activation of NHR-88 in fasted animals (Figure 4.6). As both NHR-88 and NHR-49 are derived from an HNF4-like ancestor, this regulation demonstrates the subsequent specialization of supplementary nuclear receptors. In lieu of direct regulation of all ARD target genes, NHR-49 instead exerts its control through increased expression of NHR-88, allowing for amplification of the ARD entry signal. This finding led me to characterize the role of NHR-88 in the primary NHR-49-dependent starvation response: the adult reproductive diapause. While at this point my data is preliminary, I have been able to draw several parallels between slowly starving *nhr-49* mutant adults and *nhr-88* animals that have entered a pseudo-diapause. One such similarity is the absence or inviability of embryos within the uterus. As presence of embryos is one of the markers used to identify an ARD animal, especially at low magnification, it is difficult to distinguish arrested L4s from adults. I propose that future experiments be done in a reporter strain with LAG-2::GFP marking the distal tip cell, as the gonad retracts in an adult but not in an L4. Use of this transgenic strain would allow more reliable identification of ARD animals.

Another commonality is the presence of a yolk-like substance in recovered animals; a GFP reporter line carrying a translational GFP fusion of the vitellogenin *vit-2* would permit me to confirm the accumulation of yolk in the *nhr-88* mutant.

Despite showing a number of defects in ARD entry and maintenance, both the *nhr-49* and *nhr-88* mutants are able to decrease gonad volume during starvation (Figure 4.7B) (Angelo and Van Gilst, 2009). While both strains can effectively reduce cell number, only *nhr-49* mutants accumulate cell corpses in the proximal gonad, suggesting a role for the nuclear receptor in phagocytosis of the cleared cells (Angelo and Van Gilst, 2009). I have not had the opportunity to perform electron microscopy on my *nhr-88* mutants to investigate the role of this nuclear receptor in ARD processes outside of the gonad, such as the somatic plasticity that characterizes the wild-type diapause. Performing qRT-PCR on *nhr-88* mutants using my fasting gene primer panel will further elucidate which NHR-49 targets may be regulated through NHR-88, as will phenotypic or expression-based epistasis experiments. Regardless of the degree of overlap, studying ARD in the *nhr-88* mutant will allow for selective investigation of this phenotype away from more global defects caused by an *nhr-49* deletion, thus permitting us to extend our knowledge of the metabolic pathways that respond to fasting. This knowledge in turn may elucidate new features of the mammalian fasting response.

Experimental Procedures

Strains and maintenance

The wild-type N2 (Bristol) strain was provided by the Caenorhabditis Genome Center, which is funded by the NIH National Center for Research Resources (NCRR). *nhr-88(tm1033)II* was provided by the Mitani lab. *nhr-49(nr2041)I* was a gift from Carl Johnson at Axys Pharmaceuticals. All mutants were outcrossed to N2 a minimum of 5 times. Worm maintenance was carried out at 20˚C using standard methods.

Microarray analysis

At mid-L4, worm plates were split into two groups. Worms from one set were collected, washed thoroughly with M9 to remove food, and plated to unseeded NGM plates; the other set of worms remained on food. After 8 hours, worms were harvested in parallel, washed twice with M9, and frozen in liquid nitrogen. For RNA preparation, worms were thawed at 65°C for 10 min, and

RNA was isolated using Trizol/chloroform. cDNA synthesis was conducted using M-MuLV reverse transcriptase (20,000 units, New England BioLabs, Ipswich, MA), 1X of the provided reverse transcriptase buffer, 1mM dNTPs (Invitrogen, Carlsbad, CA), and RNaseOUT recombinant ribonuclease inhibitor (2000 units, Invitrogen, Carlsbad, CA) templated with 5µg RNA and 30µg random primers (Invitrogen, Carlsbad, CA) in a 100µl reaction incubated at 42˚C for 1 hour. RNA was then labeled with Cy3 or Cy5 and hybridized to Washington University manufactured *C. elegans* microarrays. Data was obtained from two independent biological replicates and analyzed using GenePix Pro 6.0 software. Ratios were calculated using background corrected, and normalized data (global mean). Annotation and characterization of target gene functions was done manually based on phenotypes, expression data, and gene ontology information available on WormBase. A 5-fold cut-off was chosen to limit the fasting-induced gene list to a reasonable size, while still having fasting-repressed genes that met the criterion. Raw data is not available, so statistical tests cannot be performed and this data should be viewed as preliminary.

RNA extraction and qRT-PCR

Larvae were synchronized by hatching embryos collected by bleaching a gravid population on unseeded nematode growth media (NGM) plates. 20-24 hours later, the synchronized population was plated to high growth (HG) plates seeded with *Escherichia coli* strain OP50 and grown to mid-L4 at room temperature. At mid-L4, worm plates were split into two groups. Worms from one set were collected, washed thoroughly with M9 to remove food, and plated to unseeded NGM plates; the other set of worms remained on food. After 8 hours, worms were collected in M9, washed 5 times to remove excess bacteria, and frozen in an ethanol-dry ice bath. Samples were stored at -80˚C until ready for processing.

RNA extraction was done using the QIAGEN RNeasy Plus Mini kit (Germantown, MD). The protocol used was that for purifying total RNA from animal cells. Tissues/cells were disrupted by sonication and homogenized using a QIAshredder column (QIAGEN, Germantown, MD). cDNA synthesis was conducted using M-MuLV reverse transcriptase (20,000 units, New England BioLabs, Ipswich, MA), 1X of the provided reverse transcriptase buffer, 1mM dNTPs (Invitrogen, Carlsbad, CA), and RNaseOUT recombinant ribonuclease inhibitor (2000 units,

Invitrogen, Carlsbad, CA) templated with 5µg RNA and 30µg random primers (Invitrogen, Carlsbad, CA) in a 100µl reaction incubated at 42˚C for 1 hour.

30µl PCR reactions consisting of 0.3µM primers, 1/500th of the above cDNA reaction, 125µM dNTPs (Invitrogen, Carlsbad, CA), 1.5mM $MgCl_2$, 1X reaction buffer, and 0.75 units of Taq DNA polymerase (Invitrogen, Carlsbad, CA) were prepared in 96-well plates. Reactions were run using a Bio-Rad iCycler equipped with a MyiQ Single Color Real-Time PCR Detection System (Hercules, CA) to automatically monitor formation of double-stranded DNA product using SYBR-Green (Molecular Probes, Eugene, Oregon). qRT-PCR primers were designed using Primer 3 software (Rozen and Skaletsky, 2000). Data shown are mean $\Delta\Delta C_T$ values ± SEM from 3 biological replicates for N2 and *nhr-49* fed samples, 2 replicates for N2 fasted, and 3 replicates for *nhr-49* fasted. All replicates were run in duplicate and normalized to *nhr-23* expression. Statistics are the result of t-tests on the ΔC_T of the two values being compared.

Adult reproductive diapause

To induce adult reproductive diapause, a synchronized population was starved at mid-L4 as described (Angelo and Van Gilst, 2009). Starvations were maintained on sterilely poured NGM plates at 20˚C. Individual animals were picked to NGM plates seeded with *Escherichia coli* strain OP50 for recovery. For recovery brood size assays, adults were moved to new plates daily as long as they were laying embryos and progeny plates were maintained at 20˚C until worms were L3-L4, at which point the number of larvae were counted and recorded. In the case of mated broods, ARD animals were allowed to recover for 36 hours before 4-6 N2 males were added to the plate. Statistical analyses, including *P*-values from an unpaired t-test test, used GraphPad Prism 5 (GraphPad Software, San Diego, CA).

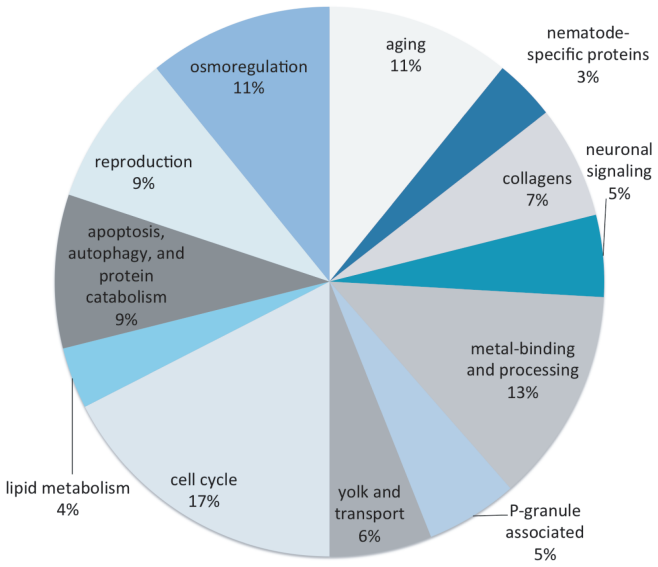

Figure 4.1. Fasting-regulated gene classes. Manually curated categories of genes included in qRT-PCR primer panels used to retest fasting-dependent expression level changes in 8-hour fasted L4 N2s. Categories are based on WormBase annotations.

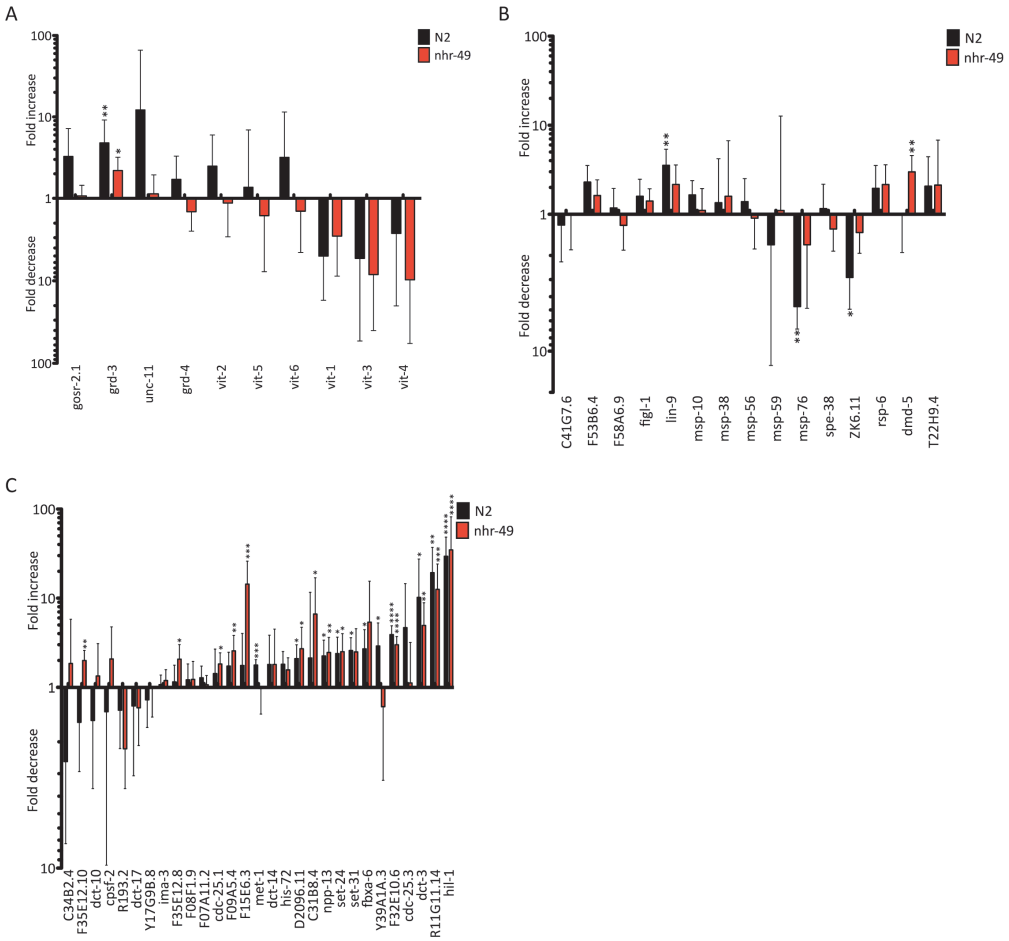

Figure 4.2. Expression changes of genes implicated in adult reproductive diapause entry processes. qRT-PCR data showing fasting-dependent expression level changes of genes involved in yolk production (A), reproduction (B), and cell cycle progression (C) in N2 and *nhr-49(nr2041)*. Data shown are mean $\Delta\Delta C_T$ values ± SEM from 3 biological replicates for N2 and *nhr-49* fed samples, 2 replicates for 8-hour N2 fasted, and 3 replicates for 8-hour *nhr-49* fasted. See Table 4.3 for gene descriptions. $^{*}P < .05$, $^{**}P < .01$, $^{***}P < 0.001$, $^{****}P < 0.0001$.

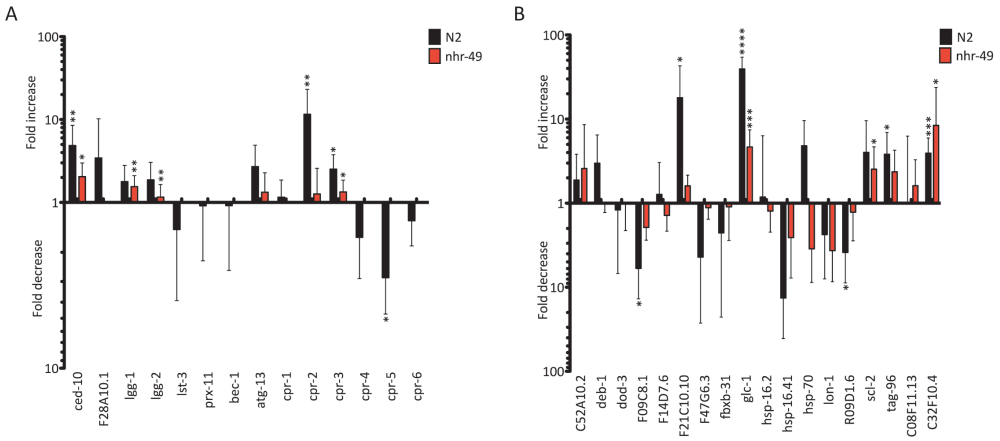

Figure 4.3. Fasting-dependent changes in expression of gene categories associated with the maintenance phase of ARD. qRT-PCR shows that expression of autophagy (A) and aging-related (B) genes changes during fasting in both N2 and *nhr-49(nr2041)* animals. Data shown are mean $\Delta\Delta C_T$ values ± SEM from 3 biological replicates for N2 and *nhr-49* fed samples, 2 replicates for 8-hour N2 fasted, and 3 replicates for 8-hour *nhr-49* fasted. See Table 4.3 for gene descriptions. $^{*}P < .05$, $^{**}P < .01$, $^{***}P < 0.001$, $^{****}P < 0.0001$.

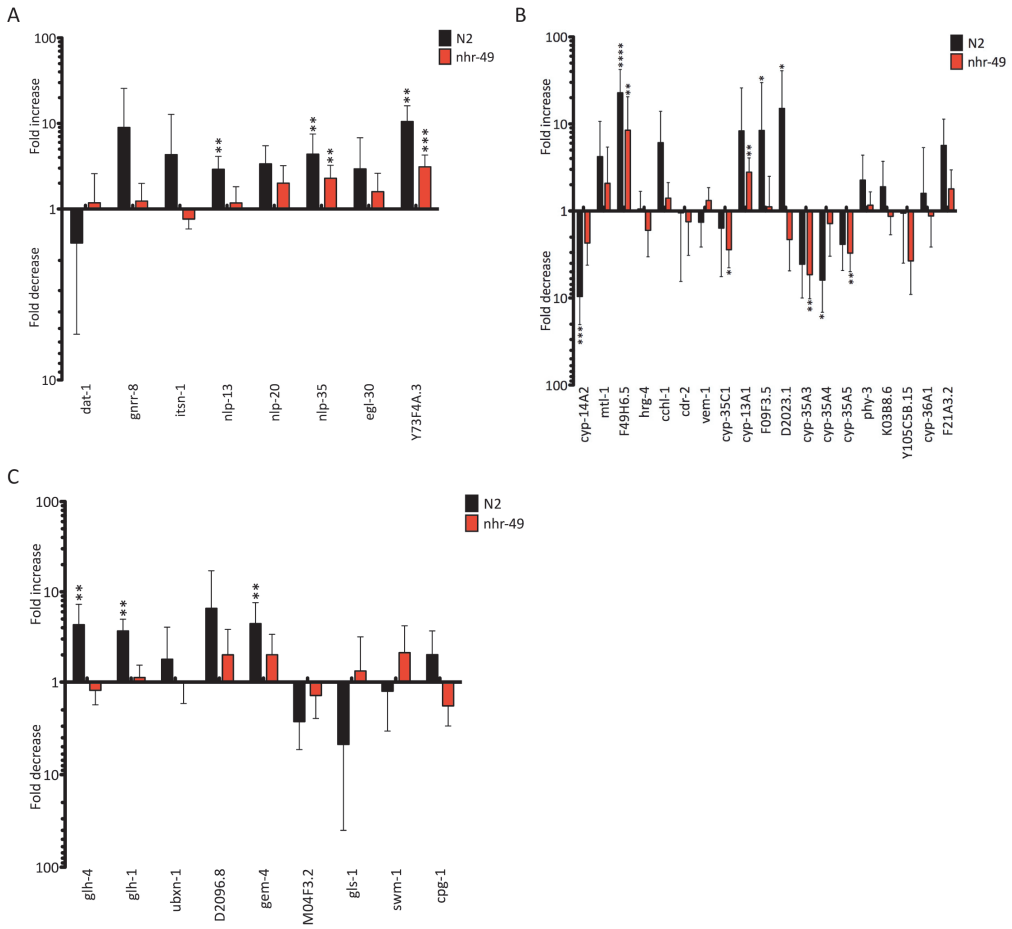

Figure 4.4. Expression data of genes with unknown roles in ARD. qRT-PCR data comparing expression levels of genes involved in neuronal signaling (A), metal processing and binding (B), and P-granule formation (C) in N2 and *nhr-49* fasted animals. Data shown are mean $\Delta\Delta C_T$ values ± SEM from 3 biological replicates for N2 and *nhr-49* fed samples, 2 replicates for 8-hour N2 fasted, and 3 replicates for 8-hour *nhr-49* fasted. $^{*}P < .05$, $^{**}P < .01$, $^{***}P < 0.001$, $^{****}P < 0.0001$.

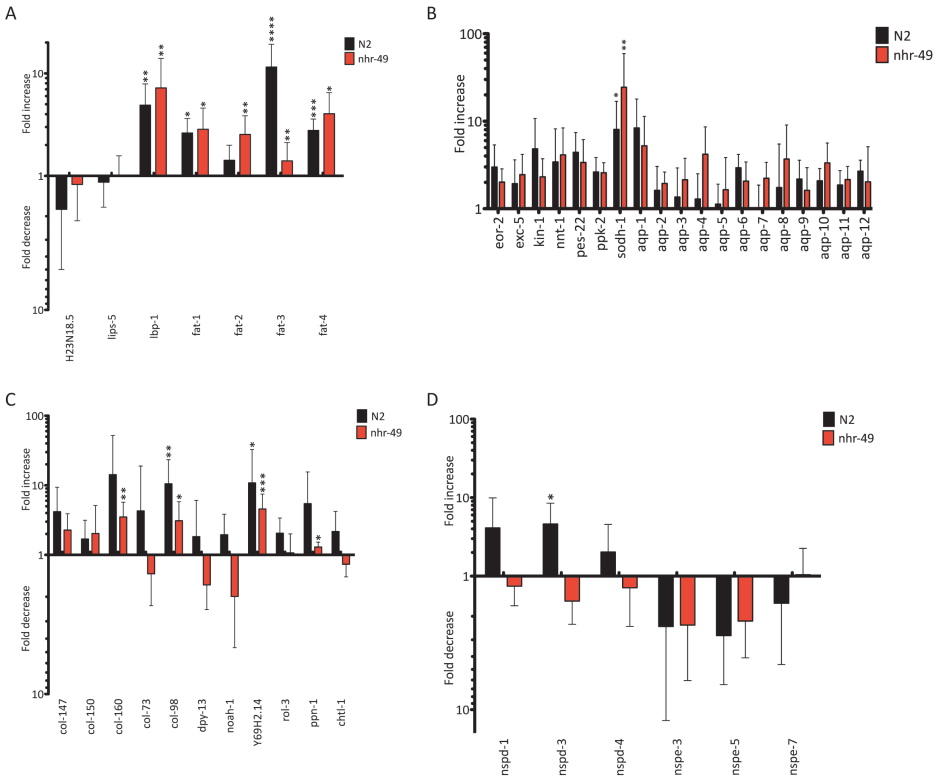

Figure 4.5. Expression level changes of gene classes not associated with ARD phenotypes. qRT-PCR-measured expression changes show that genes involved in lipid metabolism (A), genes important for osmoregulation (B), collagen-related genes (C), and unspecified nematode-specific genes (D) are all affected by fasting in N2 and *nhr-49(nr2041)* mutants. See Table 4.3 for gene descriptions. $^{*}P < .05$, $^{**}P < .01$, $^{***}P < 0.001$, $^{****}P < 0.0001$.

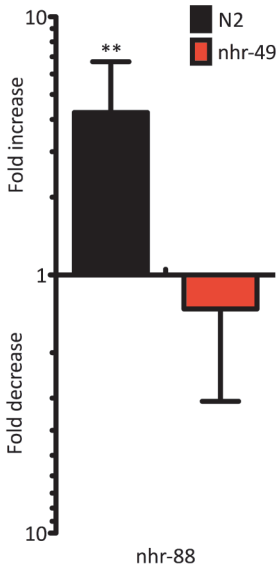

Figure 4.6. NHR-88 is fasting-induced in an NHR-49-dependent manner. Expression level of *nhr-88* in fasted N2 and *nhr-49(nr2041)* animals. Values shown are mean ± SEM from at least 3 replicates. $^{**}P < .01$.

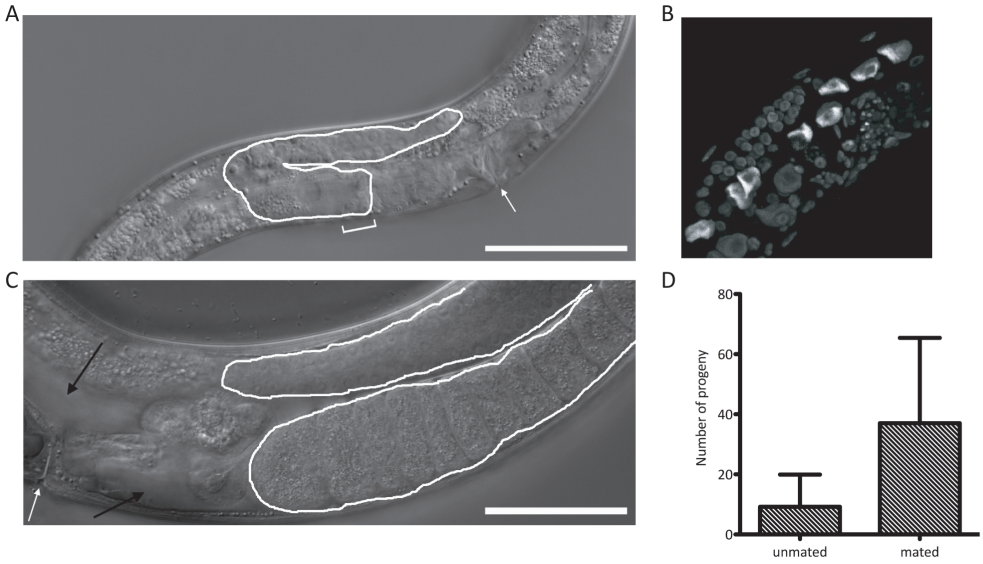

Figure 4.7. NHR-88 is required for healthy ARD. (A) 5-day starved *nhr-88* mutant arrested without embryos and continues to localize sperm to the proximal oocyte (bracket). The mutants are able to reduce their germline volume. (B) DAPI staining of an 11-day starved *nhr-88* mutant shows appropriate reduction in germ cell number. Larger nuclei belong to somatic tissues. (C) An *nhr-88(tm1033)* animal recovered for 5 days after a 10 day starvation demonstrates recovery defects including stacked oocytes and yolk accumulation (black arrows). White outlines mark the gonad and white arrows show location of the vulva in both DIC images. (D) 10-day starved *nhr-88* recovered mutants have a greatly reduced brood that is only partially rescued by introduction of endogenous sperm by mating. Values shown are mean ± SD of 5 animals. The difference between mated and unmated broods is not significant.

Table 4.1. Fasting-induced genes.

Gene name	WormBase annotation notes	Fold change (N2)	Fold change (*nhr-49*)
sodh-1	alcohol dehydrogenase, class V	96.60	29.76
acs-2	acyl coA synthetase	75.23	1.23
scl-2	defense-related protein	69.27	7.04
F46C5.1*		41.36	21.96
hsp-16.2	heat shock protein	37.83	1.35
F26F12.5*		35.04	1.71
ZK381.2*	extracellular protein with cysteines	30.12	0.97
C18E3.4		29.06	1.05
hsp-16.41	heat shock protein	27.89	1.59
Y32B12A.4		25.45	2.23
srxa-17	serpentine receptor, class X	24.56	0.95
F09F7.6*		24.55	3.22
C06G3.3*		22.76	3.67
F08F1.9	predicted G2/Mitotic-specific cyclin A	22.72	0.86
F47G9.4	spermatogenesis-related	22.51	1.05
F47G6.3	spermatogenesis-related	22.43	1.17
str-155	seven TM receptor	21.53	0.94
srz-29	serpentine receptor, class Z	21.47	0.96
B0238.1	predicted carboxylesterase	20.73	1.49
math-49	meprin-associated Traf homology	20.21	2.38
twk-25	twik family of potassium channels	20.06	1.16
srbc-73	serpentine receptor, class BC	20.00	1.13
srm-1	serpentine receptor, class M	19.81	0.78
srh-110	serpentine receptor, class H	19.74	0.88
dmd-5	doublesex/MAB-3 domain	19.66	0.86
F43C11.7	predicted E3 ubiquitin ligase	19.57	5.34
C07G3.10		19.51	1.14
ZC395.5*	involved in embryonic development	19.38	17.88
unc-62	male tail and vulval morphogenesis	19.29	0.68
C54G10.4	mitochondrial carrier protein	19.20	0.87

Gene name	WormBase annotation notes	Fold change (N2)	Fold change (*nhr-49*)
clec-78*	c-type lectin	19.16	1.00
gap-3	GTPase activating protein	19.13	0.71
spp-7	saposin-like protein	19.09	1.06
F14D7.6	predicted transporter	18.99	1.12
sago-1	argonaute strain	18.80	1.57
pfd-4	prefoldin; age-regulated; oogenesis-enriched	18.69	1.04
F35G2.2	predicted mitochondrial endoribonuclease	18.67	0.96
C34D4.5	transposon	18.66	0.97
gyg-3	glycogenin-like	18.38	0.91
srp-7	serpin; hermaphrodite-enriched	18.38	1.13
F25E5.4	predicted trypsin	18.35	1.31
Y102A5C.2		18.32	1.02
sru-28	serpentine receptor, class U	17.99	1.07
git-1	GTPase activating protein	17.98	0.94
C49F5.7*		17.98	2.78
T22H9.4		17.75	0.88
ceh-19	C elegans homeobox	17.74	1.32
tag-96	GHMP family galactokinase	17.66	1.23
npr-12	neuropeptide receptor family	17.66	0.89
kin-15	protein kinase	17.63	0.96
fbxc-4	F-box C protein	17.48	0.82
F56D2.8	male soma-enriched	17.37	1.23
F20A1.9	putative DEAD-box helicase	17.13	1.07
nlp-13	predicted neuropeptide; with pharyngeal expression	17.08	1.26
C36A4.5	microtubule-associated protein; oogenesis-enriched	17.07	1.13
ubxn-6	UBX-containing protein	16.79	0.86
M04F3.2	paralog to P-granule proteins	16.72	0.67
R11G11.14	triglyceride lipase-cholesterol esterase	16.54	17.39
Y53C10A.1		16.11	0.67
spe-38	spermatogenesis-related	16.11	1.70

Gene name	WormBase annotation notes	Fold change (N2)	Fold change (*nhr-49*)
figl-1	fidgetin-like; required for persistence of germline	16.08	1.09
C52A10.2	predicted carboxylesterase	15.96	1.23
Y10G11A.1	nucleotidase domains	15.91	0.76
C52B11.4		15.86	0.81
wdr-23	WD repeat protein	15.81	1.04
F21C10.11		15.79	4.33
F48D6.4*		15.75	3.25
kpc-1	Kex-2 proprotein convertase	15.46	2.28
nhr-230	nuclear hormone receptor	15.45	1.24
kcnl-2	calcium-activated potassium channel	15.40	0.80
W01B6.5	protein tyrosine kinase	15.28	1.21
F55B11.4		15.26	1.59
W09C3.4	predicted RNA polymerase III; oogenesis-enriched	15.26	1.02
srj-4	serpentine receptor, class J	15.22	1.14
F48D6.4*		15.13	2.97
set-31*	trithorax/polycomb domain-containing; oogenesis-enriched	15.12	0.65
srw-22	serpentine receptor, class W	15.08	1.05
math-23	meprin-associated Traf homology ,possibly involved in apoptosis	15.04	2.89
Y57G11C.8	spermatogenesis-enriched	14.99	1.32
Y73B6BL.23		14.95	1.48
nhr-242	hormone receptor	14.91	0.69
nca-2	putative nematode calcium channel	14.86	0.98
mdt-27	mediator; oogenesis-related	14.85	0.83
C32H11.5	predicted alpha helical protein	14.75	0.76
C16D9.4		14.74	1.78
sel-8	suppressor/enhancer of lin-12	14.68	0.73
T20F5.6	predicted E3 ubiquitin ligase	14.64	0.88
B0507.3		14.64	1.31
C24G7.1	predicted non-voltage gated ion channels	14.63	0.78
srh-220	serpentine receptor, class H	14.58	0.94

Gene name	WormBase annotation notes	Fold change (N2)	Fold change (*nhr-49*)
C10F3.4	predicted hydrolase	14.56	1.09
F10H6.10		14.54	1.92
abcf-2*	ABC transporter	14.53	4.64
ZK1240.4	predicted E3 ubiquitin ligase	14.53	0.74
obr-2	oxysterol binding protein; spermatogenesis-related	14.52	1.46
cchl-1	cytochrome C heme-lyase	14.45	0.97
gei-7	isocitrate lyase/malate synthase	14.44	4.95
ccch-2	zinc finger transcription factor	14.42	1.27
F08F8.9		14.38	1.09
ced-10	GTPase required for programmed cell death and DTC migration	14.27	0.75
ttr-21	transthyretin-related	14.19	1.20
F54D12.4	oogenesis-enriched	14.13	0.90
F21H7.3		14.13	0.74
C35A5.2		14.12	1.05
fsn-1	F-box synaptic protein; oogenesis-enriched	14.09	0.60
srs-2	seryl tRNA synthetase; required for germline development	14.07	0.96
Y41E3.11	predicted scaffold-specific factor	13.80	1.07
fbxa-118	F-box A protein	13.80	1.06
rol-3	protein tyrosine kinase	13.78	0.89
F48D6.4*		13.78	3.42
cdc-25.1	M-phase inducer with strong expression in germline and embryos;	13.77	1.04
scl-27	SCP-like extracellular protein	13.73	0.88
H25K10.5	predicted receptor	13.72	1.03
egl-30	G-protein subunit	13.64	1.01
F35E12.10	paralog to dct-17	13.62	1.06
amph-1	amphiphysin homolog	13.60	1.70
pqe-1	polyQ toxicity enhancer	13.60	1.26
nas-9	metalloprotease	13.54	1.32
C47C12.4	predicted Ras related/Rac-GTP binding protein; mixed oogenesis-somatic microarray	13.54	0.77

Gene name	WormBase annotation notes	Fold change (N2)	Fold change (*nhr-49*)
fncm-1	Fanconi Anemia complex homolog	13.50	1.01
F58H7.1		13.49	0.87
npr-16	neuropeptide receptor family	13.47	1.36
rsp-6	splicing factor; roles in embryogenesis and reproduction	13.38	0.81
srbc-61	serpentine receptor, class BC	13.34	1.07
nhr-32	hormone receptor	13.26	1.36
D1022.4	dienelactone hydrolase domain	13.26	0.81
spp-10	saposin-like protein; predicted to activate sphingomyelinphosphodiesterase and glucosylceramidase	13.25	1.68
F25E5.8		13.23	2.43
twk-9*	twik family of potassium channels	13.20	1.15
sdz-31	skn-1-dependent zygotic transcript	13.14	0.62
C39D10.8		13.14	0.99
F58G1.2	involved in embryonic development and hermaphrodite genitalia development	13.12	1.07
B0207.6	predicted GTPase	13.12	0.86
clec-256	c-type lectin	13.10	1.39
B0564.3	bestrophin	13.03	6.54
ZK616.7	protein tyrosine phosphatase	13.02	1.27
gstk-2	glutathione s-transferase kappa	13.02	1.69
F49C12.4	predicted secreted small molecules methylase	12.98	0.93
fat-3	desaturase	12.96	3.70
ulp-2	ubiquitin-like protease	12.96	1.00
D2062.7		12.94	0.92
pqn-83	prion-like domain bearing protein	12.88	0.88
F56H11.2		12.88	1.13
unc-30	homeodomain-containing protein related to PTX1	12.87	1.37
itfa-2	intraflagellar transport associated	12.78	1.12
smr-1	splicing factor SPF30	12.73	1.42
prx-11	peroxisome assembly factor	12.71	0.71
F01F1.1	predicted leucine permease transcriptional regulator	12.67	0.86
dpy-13*	collagen	12.67	0.77
K03H6.1	predicted serpentine receptor, class W	12.60	1.01
snf-10	sodium neurotransmitter symporter family	12.60	1.37
fipr-17	fungus-induced protein-related; male soma-enriched	12.59	0.78
ragc-1	predicted small GTPase involved in nuclear protein import; oogenesis-related	12.58	0.97
R05G6.5	involved in nucleotide-triphosphate synthesis	12.58	1.16
pkc-2	protein kinase C; hermaphrodite soma-enriched	12.56	1.24
ztf-9	zinc finger transcription factor	12.55	0.69
ZK550.4	transcription initiation factor IIE	12.50	0.80
hyls-1	human hydrolethalus syndrome homolog	12.48	0.94
ers-1	glutamyl/glutaminyl tRNA synthetase	12.46	1.09
Y116A8B.1		12.43	0.77
idh-1*	isocitrate dehydrogenase; oogenesis-related	12.43	0.44
tag-253*		12.42	2.91
smi-1	ortholog of gemin2	12.40	1.29
T12A7.7	homologous to serpentine receptor, class H	12.38	1.25
sma-2	SMAD protein; reproduction-related	12.38	2.43
gnrr-8	human GnRH receptor-related	12.37	1.35
his-72	histone	12.34	0.60
F07B7.14	predicted cysteine rich protein	12.32	0.88
K04C1.2	paralogous to polycomb group	12.28	0.86

Gene name	WormBase annotation notes	Fold change (N2)	Fold change (*nhr-49*)
nspd-4	nematode specific peptide family, group D; spermatogenesis-enriched	12.24	2.07
noah-1	paralog of cuticulin-like cutl-17	12.17	1.35
F22B8.7	uncharacterized Fe-S protein; spermatogenesis-related	12.14	0.83
gei-7	isocitrate lyase/malate synthase	12.14	2.85
B0513.4	hermaphrodite soma-enriched	12.14	0.92
Y7A9A.1	predicted gamma-glutamyltransferase	12.11	1.07
C30H6.10		12.05	1.38
unc-11	clathrin adaptor protein	12.03	0.79
C14C10.6	predicted membrane protein	12.01	1.20
srz-61	serpentine receptor, class Z	12.01	1.00
C27A7.3	predicted phosphodiesterase	11.99	1.38
far-7	fatty acid/retinol binding protein	11.97	16.10
cpt-4*	carnitine palmitoyl transferase	11.95	0.82
C08B6.2		11.92	0.88
C10C5.5	predicted metalloexopeptidase; male soma-enriched	11.90	2.93
srv-29	serpentine receptor, class V	11.90	1.14
ins-1	insulin-related	11.89	1.51
ttr-15*	transthyretin-related family	11.84	2.21
src-2	tyrosine kinase	11.82	0.68
dct-10	daf-16/FOXO-controlled; affects germline tumor formation	11.82	0.94
B0310.2		11.81	1.81
C44H9.8		11.80	1.77
Y73F4A.3*		11.74	2.25
C09B8.8		11.73	0.96
lst-3*	predicted DNA-binding protein; predicted role in apoptosis	11.67	0.79
pqn-21	prion-like domain bearing protein	11.66	1.06
srw-61	serpentine receptor, class W	11.62	1.25
dhs-9	short-chain dehydrogenase	11.60	1.26
mrck-1	serine/threonine-protein kinase; oogenesis-related	11.60	1.20
C35C5.8*		11.54	4.72
fbxc-7*	F-box C protein	11.53	2.37
F56D5.9		11.51	1.10
srsx-39	serpentine receptor, class SX	11.49	1.11
F22B7.9*	predicted methyltransferase	11.49	2.62
itsn-1	synaptic vesicle recycling	11.49	0.68
str-255	seven transmembrane receptor	11.48	1.12
pkd-2	in male-specific sensory neurons	11.47	0.77
C32H11.7		11.44	1.06
clec-167	C-type lectin	11.44	0.74
aqp-1	aquaglyceroporin	11.41	0.84
oac-57	o-acyltransferase	11.40	1.03
F35H12.4	predicted phosphatidylinositol kinase	11.39	1.03
D2023.1*	hermaphrodite soma-enriched	11.39	0.91
F09A5.4	related to cell-cycle associated protein Mob1-1	11.38	1.43
emb-27	APC, Cdc16 subunit	11.35	0.83
eif-3.F	translation initiation factor 3	11.35	1.06
F29B9.11		11.31	1.47
dhhc-1	DHHC-type zinc finger TF	11.30	0.97
K10G9.1	predicted permease; spermatogenesis-enriched	11.25	2.59
D2096.11	involved in cell-cycle arrest; paralog to csp-2, vab-10	11.24	0.95
C03B1.2		11.24	0.90
clec-11	c-type lectin	11.23	1.79
C53B7.6		11.22	0.87
K02G10.5	predicted organic anion transporter	11.16	1.05
K10D3.6		11.11	8.46
wdr-23	WD40 repeat-containing	11.09	0.79
lin-9	involved in germline/genitalia development	11.08	1.28
srw-140	serpentine receptor, class W	11.07	1.22
exc-5	guanine nucleotide exchange involved in excretory cell growth	11.04	0.78

Gene name	WormBase annotation notes	Fold change (N2)	Fold change (*nhr-49*)
clec-42	C-type lectin	11.03	0.70
Y71H2AR.3		11.03	1.53
B0273.1	spermatogenesis-enriched	11.01	0.97
T02D1.7	predicted seven transmembrane receptor	11.00	0.95
met-1	histone methyltransferase	10.87	0.65
C09H10.5		10.83	0.82
kin-26	predicted protein tyrosine kinase; spermatogenesis-enriched	10.82	1.19
T23D5.3		10.81	1.18
brp-1	poly-Q protein	10.77	1.30
clec-76	C-type lectin	10.77	9.83
mtx-2	metaxin	10.77	1.07
nhr-127	nuclear receptor in seam cells	10.75	0.99
tag-335	hexapeptide transferase domain	10.75	0.82
srg-32*	serpentine receptor, class G	10.69	1.60
tag-345	predicted microtubule binding protein; oogenesis-enriched	10.67	1.05
C46H11.7*	paralog of pharyngeal toxin	10.67	0.77
fbxa-215	F-box A protein	10.66	0.68
oac-31	o-acyltransferase	10.65	0.80
eor-2	involved in excretory cell growth	10.58	0.84
C17E7.9		10.58	1.38
sph-1	synaptophysin; involved in vesicle transport	10.57	1.46
W05B10.4	involved in signal transduction	10.57	1.67
W01B6.6	spermatogenesis-enriched	10.54	1.21
nlp-20	neuropeptide	10.54	1.56
pes-22	monocarboxylate porter	10.50	1.01
mig-6	required for DTC migration	10.49	2.47
Y48G1BL.6	predicted RNA-binding protein	10.46	0.57
T05C7.1	paralog of frm-1	10.45	0.85
F33D4.7	involved in embryonic development	10.44	0.92
C50B8.1	RNA-recognition motif domain	10.40	1.58
isp-1	iron-sulfur protein in mitochondrial Complex III	10.40	1.99

Gene name	WormBase annotation notes	Fold change (N2)	Fold change (*nhr-49*)
zig-5*	immunoglobulin	10.31	1.43
R102.7*		10.31	1.06
F49C12.6	sugar transport domains	10.30	0.95
T26E4.4*	paralog of glycosyltransferase	10.28	0.62
dcaf-1	oogenesis-enriched	10.28	0.88
phy-3	proline hydroxylase	10.27	1.05
C01A2.6		10.24	1.17
srj-15	serpentine receptor, class J	10.24	1.22
F55G1.7	oogenesis-enriched	10.23	1.14
Y17G9B.8	paralog of HAT SAGA-associated factor; hermaphrodite enriched	10.20	1.34
C47B2.2	uracil phosphoribosyltransferase	10.19	1.31
F17B5.1*	related to thioredoxins; hermaphrodite enriched	10.18	6.07
srw-113	serpentine receptor, class W	10.11	1.13
Y102A5C.4		10.10	1.25
Y37E11AL.3		10.09	0.93
grd-3	groundhog (hedgehog-like)	10.07	0.68
nlp-35*	neuropeptide	10.06	1.36
Y9C2UA.1	male sex enriched	10.04	1.32
F21C10.10	spermatogenesis enriched	10.04	1.87
Y18D10A.1	DNA-binding motif	10.03	1.12
C36B1.6		10.02	4.40
gls-1	P-granule component	9.95	1.09
mlt-9	involved in molting	9.95	0.87
cdr-2	cadmium responsive	9.92	1.57
ergo-1	oogenesis-enriched	9.86	0.74
Y38H6C.16	involved in sterol metabolism	9.84	0.82
Y24D9A.1	predicted RNA pol II elongation factor	9.84	1.02
C52E4.5*	predicted glycosyl hydrolases	9.83	0.81
C06B3.6*		9.82	4.59
F08D12.3		9.79	1.28
F55D12.6	spermatogenesis-enriched with ribosomal protein S2 conserved site	9.78	1.33

Gene name	WormBase annotation notes	Fold change (N2)	Fold change (*nhr-49*)
T23F6.5		9.73	0.70
srw-63	serpentine receptor, class W	9.72	1.11
K11H12.7		9.69	1.04
Y41D4B.16	has transmembrane glycoprotein	9.63	1.17
srh-75*	serpentine receptor, class H	9.60	0.72
kin-6	protein kinase	9.60	1.32
F55G11.10		9.59	1.06
F21D5.7	involved in reproduction	9.56	1.16
hsp-70	heat shock protein	9.55	0.58
F59F3.4	predicted sodium channel; male-sex enriched	9.55	1.47
C45B2.8		9.54	0.74
T08B6.1	predicted splicing factor	9.54	0.98
K03B8.6	hermaphrodite soma-enriched	9.51	1.27
T22F3.11	predicted permease	9.39	87.24
smg-3	predicted nonsense-mediated mRNA decay protein	9.38	0.96
cpr-4	cysteine protease	9.37	2.86
acs-11	acyl-coA synthetase	9.37	1.27
C53B7.3		9.37	2.37
bre-1	GDP-mannose dehydratase	9.37	0.90
D1044.7	Ca^{++} binding EGF domains	9.36	1.20
D2096.11	involved in cell-cycle arrest; paralog to csp-2, vab-10	9.34	0.78
lem-3	ankyrin repeat	9.32	0.80
cpsf-2	mRNA cleavage and polyadenylation complex subunit	9.31	1.09
srt-44	serpentine receptor, class T	9.27	0.91
T28F4.5	death-associated protein homolog	9.22	3.90
K07A12.4	oogenesis related	9.18	0.79
srv-30	serpentine receptor, class V	9.17	1.15
C09H10.9	spermatogenesis-enriched	9.15	1.23
fbxb-31	F-box B protein	9.13	1.04
B0491.5		9.10	0.93
lpd-6*	predicted nucleolar protein required for fat storage; oogenesis-enriched	9.08	1.08

Gene name	WormBase annotation notes	Fold change (N2)	Fold change (*nhr-49*)
ppk-2	non-essential PIP4K	9.04	1.12
T25B9.6	spermatogenesis-enriched	9.04	1.12
sig-7	predicted peptidyl prolyl cis-trans isomerase	9.02	1.18
Y6D1A.1	transposon-encoded protein	9.00	0.92
pqn-21	Q/N-rich domain	8.99	0.77
egl-30	G-protein subunit	8.98	0.99
plk-2	POLO kinase	8.85	1.20
C23G10.11*	involved in embryonic development	8.85	27.69
deb-1	vinculin ortholog expressed in somatic gonad	8.85	1.05
T22B11.3	protein tyrosine kinase	8.81	1.12
T26C5.3*	predicted acetyl-coA transporter	8.80	1.19
K05C4.7	oogenesis-enriched	8.75	0.85
ZK616.3		8.71	1.15
Y47D3B.1	involved in oviposition	8.69	0.80
C51E3.9		8.69	1.19
srx-51	serpentine receptor, class X	8.63	0.79
srh-111	serpentine receptor, class H	8.55	0.98
zig-8	immunoglobulin	8.47	1.12
ZK1055.4	predicted glycosyltransferase	8.44	0.96
T12G3.5	predicted mitochondrial ribosomal subunit	8.39	1.10
thoc-3	transcription factor/nuclear export; oogenesis-enriched	8.36	0.90
C35A5.8	mixed oogenesis-somatic	8.36	0.94
W03C9.1	spermatogenesis-enriched	8.33	1.12
rgl-1	predicted guanine-nucleotide releasing factor	8.32	1.10
T12A2.2	predicted oligosaccharide transferase	8.31	0.89
F10D7.5	may be involved in glp-1/lin-12 signaling	8.23	1.24
coh-4	cohesin	8.20	0.64
ima-3	importin alpha required for meiotic prophase	8.15	1.57

Gene name	WormBase annotation notes	Fold change (N2)	Fold change (*nhr-49*)
T07F8.1	paralog of RNAi-related protein	8.12	1.04
mbf-1	transcriptional coactivator	8.07	1.14
C05E7.2		8.07	1.31
vem-1	heme-binding domain involved in neuron outgrowth	8.07	0.84
C18A3.1	predicted DNA methyltransferase; oogenesis-enriched	7.94	0.80
M60.4	male soma enriched	7.89	3.85
ZC443.3		7.89	8.77
C50F4.14	putative GDP-fucose transporter	7.84	1.04
F11F1.5		7.81	1.35
C35C5.9		7.80	3.01
F13H10.6		7.79	1.50
H23L24.2	spermatogenesis-related	7.76	0.83
F29C4.2	cyt C oxidase domain; positively regulates growth rate	7.73	1.42
ZC449.3	predicted MAPKK	7.71	1.24
gosr-2.1	Golgi SNAP receptor complex; oogenesis-related	7.68	0.69
F42A9.3	spermatogenesis-enriched	7.64	1.57
C34B2.4	Enigma-related; spermatogenesis-enriched	7.53	1.42
R03H10.4	extracellular protein	7.52	0.89
cyp-37B1*	cytochrome P450 CYP4/CYP19/CYP26 subfamilies	7.51	5.45
clec-82	c-lectin	7.51	1.99
nhr-38	hormone receptor	7.45	1.16
C32E12.1	spermatogenesis-enriched	7.42	1.29
F41E6.5	glycolate oxidase	7.34	2.73
F53A9.8*	paralog of RNA-splicing protein	7.32	4.08
D2096.8*	related to nucleosome assembly protein; oogenesis-related	7.29	1.81
F53B6.4	predicted major sperm protein	7.28	1.32
F10E9.12	copper amine oxidase domain	7.28	3.95
zig-2	immunoglobulin	7.26	1.22
C28H8.5	ShK-domain like	7.23	0.95

Gene name	WormBase annotation notes	Fold change (N2)	Fold change (*nhr-49*)
Y46B6A.10	serine/threonine kinase; oogenesis-related	7.22	1.30
alh-1	aldehyde dehydrogenase	7.20	1.38
T05D4.2	F-box domain; oogenesis-e	7.19	0.68
set-24	SET domain-containing	7.15	0.41
spp-2	saposin-like protein; ortholog of interferon gamma receptor	7.08	1.82
Y69H2.14	probable collagen protein	7.06	1.15
col-98	collagen	7.03	1.69
T20G5.4	bestrophin	6.98	1.13
D2023.5	mercaptopyruvate or thiosulfate sulfurtransferase; oogenesis-enriched	6.97	0.98
dlc-1	dynein light chain	6.92	1.93
K03H6.5	serpentine receptor, class W domains	6.89	1.05
F37A4.1	predicted alpha/beta hydrolase BAT5	6.88	1.28
col-160	collagen	6.87	2.99
F07A11.2	putative glucosamine-fructose 6-phosphate aminotransferase	6.83	0.74
C41G7.6	paralog of major sperm proteins	6.76	1.81
Y38H6C.9	F-box A paralog	6.75	1.06
dat-1	dopamine transporter	6.74	0.80
glc-1	glutamate-gated chloride channel	6.73	4.89
dct-14	daf-16/FOXO controlled; affects germline tumors	6.70	0.78
D2096.11	growth arrest-specific domain	6.68	0.73
cdc-25.3	M-phase inducer phosphatase	6.68	0.45
W06F12.2	involved in embryonic development	6.65	1.28
F32E10.6	chromatin-associated	6.59	0.95
K01G12.3	hermaphrodite-enriched	6.56	0.59
col-147	collagen	6.53	1.55
cpr-1	cysteine protease	6.52	2.42
F55H12.4		6.52	2.52
F09F3.5	predicted peroxidase/oxygenase	6.48	1.14

Gene name	WormBase annotation notes	Fold change (N2)	Fold change (*nhr-49*)
F26F12.3		6.48	2.73
F16F3.5		6.47	1.90
lgc-50	ligand-gated ion channel	6.43	1.50
dpy-6	required for normal morphology	6.42	0.60
M01H9.3*		6.35	2.28
vet-6	spectrin repeat domain	6.32	0.70
col-73*	collagen	6.30	0.90
oac-24*	o-acyltransferase	6.30	1.07
C16E9.1*	Von Willebrand factor domain	6.30	1.41
vps-36	vacuolar protein sorting	6.27	1.19
Y38E10A.2		6.26	0.92
F23D12.2	F-box domain; oogenesis-enriched	6.19	0.77
F09E10.7	male soma enriched	6.17	2.17
fbxa-24	F-box A protein; male soma enriched	6.16	3.32
Y26H9A.11		6.15	2.90
F16H6.8	paralog of c-lectins	6.15	1.45
F34D6.1	F-box domain	6.14	1.24
elo-1	fatty acid elongation	6.12	1.12
F59G1.4		6.10	1.32
C32F10.4		6.10	4.89
oac-38*	o-acyltransferase; oogenesis-related	6.08	1.05
str-156	seven transmembrane receptor	6.07	0.98
Y4C6B.2	predicted amino acid transporter	6.05	2.02
Y73F8A.5	fibrillin-related	6.03	1.20
rps-23	small ribosomal subunit; required for germline development	5.98	2.84
ilys-3	invertebrate lysozyme	5.92	10.16
Y71A12B.11		5.89	0.78
ttyh-1	cell surface protein	5.88	0.87
trap-4	translocon associated protein; involved in reproduction	5.77	0.45
abf-1	antibacterial factor	5.77	0.90
R102.6		5.77	1.34
Y54F10BM.2		5.75	1.33

Gene name	WormBase annotation notes	Fold change (N2)	Fold change (*nhr-49*)
coq-6	ubiquinone synthesis	5.73	0.84
ttr-44*	transthyretin related	5.66	4.23
F53C3.13	lipid phosphate phosphatase	5.66	1.46
K04F1.9*		5.66	0.70
ptr-8	sterol-sensing domain; weakly required for L4 to adult molt	5.64	1.69
dod-3*	downstream of daf-16; age-related	5.64	6.00
scl-19	SCP-like extracellular protein	5.60	1.04
alh-1	aldehyde dehydrogenase	5.58	1.21
kin-1	protein kinase	5.56	1.42
C44B7.10	predicted acetyl-coA hydrolase	5.55	1.08
gpa-13	G-protein, alpha subunit	5.53	0.94
chtl-1	choline transporter-like; male soma enriched	5.52	0.37
W09G12.7		5.50	2.03
B0294.1*		5.50	1.13
lgc-37	ligand-gated ion channel involved in spermatogenesis	5.48	1.04
Y55B1BR.4	predicted serine kinase or guanylate kinase	5.47	0.81
acl-4	phosphate acyltransferase	5.47	0.58
npp-13	nuclear pore complex protein	5.39	0.80
F14H3.12	serine/threonine kinase	5.38	2.45
F53C3.11	involved in embryonic development	5.34	1.25
unc-119	secreted growth factor in DTC and axonal migration	5.32	1.31
F45D3.3		5.25	13.56
srd-74	serpentine receptor, class D	5.24	0.95
K01A11.1	involved in embryonic development	5.22	0.94
K03D3.2*		5.22	3.62
T28B8.1	male soma enriched	5.19	2.83
acs-19	acyl coA synthetase	5.18	0.71
C34G6.6	lipid biding serum glycoprotein domains	5.16	1.27

Gene name	WormBase annotation notes	Fold change (N2)	Fold change (*nhr-49*)
noah-1	NompA homolog involved in molting	5.16	0.79
W05G11.4	predicted cytosolic cysteine protease	5.15	0.77
C14F11.1	predicted aspartate aminotransferase/glutamic oxaloacetic transaminase	5.14	0.85
srj-19	serpentine receptor, class J	5.13	1.15
Y39A1A.3	mitosis-related	5.10	1.40
lgg-2	involved in autophagy	5.09	3.07
M151.3	paralog of oogenesis-related	5.09	0.36
ttr-8	transthyretin related	5.08	1.04
C50F4.8		5.05	2.68
T27D12.1	permease	5.05	1.87
krs-1*	lysyl tRNA synthetase	5.04	0.66
M02D8.4	predicted asparagine synthase	5.02	2.75
F28A10.1	putative methylasetransferase; inhibits germline apoptosis	5.02	1.39
F49H6.3	metal transport	5.01	1.54
D2030.2	putative ATP-dependent Clp-type protease	5.01	2.45
Y51B9A.3	spermatogenesis-related	5	1.18

*denotes dauer-enriched gene (Liu et al., 2004; Wang and Kim, 2003).
Microarray experiments conducted by Giana Angelo.

Table 4.2. Fasting-repressed genes.

Gene name	WormBase annotation notes	Fold change	Fold change (*nhr-49*)
cut-2*	grl-16 paralog	10.56	0.27
lon-3*	cuticle collagen	9.97	0.26
ZK6.11	paralog of *dod* genes; age-related	9.15	0.37
vit-3*	yolk lipoprotein	9.06	0.26
F58A6.9	major sperm protein	8.13	1.70
ubxn-1	predicted ubiquitin regulatory protein	7.65	0.65
R08E5.3	SAM-dependent methyltransferase	7.28	0.97
ZK697.8	transthyretin hydrolase domain	7.25	1.01
R12E2.14*		7.23	0.98
H23N18.5	phospholipase A domain	6.71	0.43
vit-4	predicted lipoprotein	6.70	0.22
gln-2	glutamine synthetase	6.64	1.10
nspd-1	nematode specific protein family, group d	6.62	1.90
T06E4.9		6.61	0.67
col-150*	collagen	6.55	1.51
msp-59	major sperm protein	6.34	4.37
F35E12.8*	paralog to dct-17; age-related	6.25	0.65
grl-16	ground-like domain (hedgehog related)	6.25	1.16
C35A5.3	permease	6.24	0.22
cyp-35C1	cytochrome P450 CYP2	6.22	0.07
F36A4.11		6.15	0.95
T10G3.4	paralog to 7TM receptors	6.12	1.05
C38D9.3	transposon	6.09	0.96
F52G3.4	DNA helicase	6.06	0.97
H10E21.4	related to calmodulin	6.05	1.03
msp-56	major sperm protein	6.01	4.11
msp-10	major sperm protein	5.99	1.51
srbc-11	serpentine receptor, class BC	5.96	1.04
F47F2.1	predicted cAMP-dependent PKA subunit	5.87	0.84
nspd-3	nematode specific protein family, group d	5.87	2.27
C56C10.4	predicted fibronectin	5.84	0.87
lbp-8	lipid binding protein	5.83	0.16
cpr-6*	cysteine protease	5.83	0.64
D1054.9		5.70	0.89
grd-4	groundhog (hedgehog-like); predicted role in vesicle trafficking	5.63	0.78
col-17*	collagen	5.57	0.45
vit-6	yolk lipoprotein	5.55	1.36
C02E7.6*	paralogous to grl-16	5.55	0.35
Y5H2B.3	oogenesis-related	5.37	0.46
msp-38	major sperm protein	5.34	3.26
msp-76	major sperm protein	5.24	4.70
T20D4.17	predicted secreted cysteine-rich protein	5.21	1.07
col-172	collagen	5.18	1.02
C23F12.3		5.15	0.72
fbxb-114	F-box B protein	5.14	0.77
F26F2.4		5.08	0.67
C56G3.2	predicted aldo/keto reductase	5.06	1.22
C02E7.7	paralogous to grl-16	5.02	0.67
col-109	cuticular collagen	5.00	0.83

*denotes dauer-enriched gene (Liu et al., 2004; Wang and Kim, 2003).
Microarray experiments conducted by Giana Angelo.

Table 4.3. WormBase annotation notes of genes included on the qRT-PCR fasting panel.

	Gene name	WormBase annotation notes
yolk production and transport	gosr-2.1	Golgi SNAP receptor complex; oogenesis-related
	grd-3	groundhog (hedgehog-like)
	unc-11	clathrin adaptor protein involved
	grd-4	groundhog (hedgehog-like)
	vit-2	yolk protein gene
	vit-5	yolk protein gene
	vit-6	yolk protein gene
	vit-1	yolk protein gene
	vit-3	yolk protein gene
	vit-4	yolk protein gene
reproduction-related	C41G7.6	predicted major sperm protein
	F53B6.4	predicted major sperm protein
	F58A6.9	major sperm protein
	figl-1	fidgetin-like; required for persistence of germline
	lin-9	involved in germline/genitalia development
	msp-10	major sperm protein
	msp-38	major sperm protein
	msp-56	major sperm protein
	msp-59	major sperm protein
	msp-76	major sperm protein
	spe-38	spermatogenesis-related
	ZK6.11	age-related
	rsp-6	splicing factor with roles in embryogenesis and reproduction
	dmd-5	doublesex/MAB-3 domain
	T22H9.4	involved in sex differentiation
cell cycle	C34B2.4	involved in meiotic chromosome segregation
	F35E12.10	paralog of dct-17

	Gene name	WormBase annotation notes
cell cycle-related	dct-10	DAF-16 controlled; affects germline tumor formation
	cpsf-2	mRNA cleavage and polyadenylation complex subunit; involved in cell division
	R193.2	involved in positive regulation of growth rate
	dct-17	DAF-16 controlled; affects germline tumors
	Y17G9B.8	predicted HAT factor; hermaphrodite-enriched
	ima-3	importin alpha required for meiotic prophase
	F35E12.8	paralog to dct-17
	F08F1.9	predicted G2/mitotic-specific cyclin A
	F07A11.2	predicted glucosamine-fructose 6-phosphate aminotransferase involved in cell division
	cdc-25.1	M-phase inducer with strong expression in germline and embryos
	F09A5.4	homology to cell cycle-associated protein Mob1-1
	F15E6.3	involved in reproduction
	met-1	histone methyltransferase
	dct-14	DAF-16 controlled; affects germline tumors
	his-72	histone
	D2096.11	involved in cell-cycle arrest
	C31B8.4	paralog of dct-3
	npp-13	nuclear pore complex protein; required for establishment of mitotic spindle orientation
	set-24	SET domain-containing
	set-31	oogenesis-enriched
	fbxa-6	involved in cell division and oogenesis
	Y39A1A.3	Zn ribbon-containing protein implicated in mitosis
	F32E10.6	chromatin-associated; involved in embryonic development
	cdc-25.3	M-phase inducer phosphatase
	dct-3	DAF-16 controlled; affects germline tumor formation
	R11G11.14	triglyceride lipase-cholesterol esterase involved in meiotic chromosome segregation
	hil-1	histone H1

	Gene name	WormBase annotation notes
autophagy, apoptosis, and protein catabolism	ced-10	GTPase required for programmed cell death; involved in distal tip cell migration
	F28A10.1	putative small molecule methylasetransferase that inhibits germline apoptosis
	lgg-1	MT-associated anchor protein involved in autophagy and membrane trafficking
	lgg-2	MT-associated protein involved in autophagy
	lst-3	predicted DNA-binding protein; putative role in apoptosis
	math-23	meprin-associated Traf homology; possibly involved in apoptosis
	prx-11	peroxisome assembly factor
	bec-1	autophagy-related
	atg-13	autophagy-related
	cpr-1	cysteine protease
	cpr-4	cysteine protease
	cpr-6	cysteine protease
	cpr-3	cysteine protease
	cpr-5	cysteine protease
aging-associated	C52A10.2	predicted carboxylesterase
	deb-1	vinculin ortholog; expressed in somatic gonad
	dod-3	downstream of daf-16; decreases with age
	F09C8.1	phospholipase
	F14D7.6	predicted transporter
	F21C10.10	spermatogenesis-enriched
	F47G6.3	spermatogenesis-enriched
	fbxb-31	F-box B protein
	glc-1	glutamate-gated chloride channel
	hsp-16.2	heat shock protein
	hsp-16.41	heat shock protein
	hsp-70	heat shock protein
	lon-1	defense-related protein
	R09D1.6	chitinase
	scl-2	defense-related protein
	tag-96	GHMP family galactokinase
	C08F11.13	Integral membrane O-acyltransferase
	C32F10.4	unknown

	Gene name	WormBase annotation notes
neuronal signaling	dat-1	dopamine transporter
	gnrr-8	related to human GnRH receptor
	itsn-1	required for synaptic vesicle recycling
	nlp-13	predicted neuropeptide
	nlp-20	neuropeptide
	nlp-35	neuropeptide
	egl-30	G-protein subunit
	Y73F4A.3	predicted dopamine beta-monooxygenase
metal binding and processing	cyp-14A2	cytochrome P450
	cyp-37B1	cytochrome P450
	mtl-1	predicted metallothionein
	F49H6.5	molybdenum cofactor biosynthesis
	hrg-4	mediates heme homeostasis
	cchl-1	cytochrome c heme-lyase
	cdr-2	cadmium responsive
	vem-1	contains heme-binding domain
	cyp-35C1	cytochrome P450
	cyp-13A1	cytochrome P450
	F09F3.5	contains heme-binding domain
	D2023.1	contains heme-binding domain
	cyp-35A3	cytochrome P450
	cyp-35A4	cytochrome P450
	cyp-35A5	cytochrome P450
	phy-3	proline hydroxylase; iron-binding
	Y105C5B.15	purple acid phosphatase; metal-binding
	cyp-36A1	cytochrome P450
	F21A3.2	purple acid phosphatase; metal-binding
P-granule-associated	glh-4	putative germline RNA helicase
	glh-1	required with glh-4
	ubxn-1	predicted ubiquitin regulatory protein
	D2096.8	related to nucleosome assembly protein; mixed oogenesis-somatic microarray
	gem-4	antagonizes GON-2 in gonadal cell division
	M04F3.2	paralog to P-granule associated proteins
	gls-1	P-granule component
	swm-1	involved in spermatogenesis
	cpg-1	P-granule-associated

	Gene name	WormBase annotation notes
lipid metabolism	H23N18.5	phospholipase A domain
	lips-5	lipase-related
	lbp-1	FABP
	fat-1	desaturase
	fat-2	desaturase
	fat-3	desaturase
	fat-4	desaturase
osmoregulation	eor-2	putative involvement in excretory cell growth
	exc-5	GEF; involved in excretory cell growth
	kin-1	protein kinase; expressed in excretory cell
	nnt-1	nicotinamide nucleotide transhydrogenase
	pes-22	monocarboxylate porter; expressed in excretory cell
	ppk-2	non-essential PIP4K in excretory cell and reproductive system
	sodh-1	alcohol dehydrogenase, class V
	aqp-1	aquaporin
	aqp-2	aquaporin
	aqp-3	aquaporin
	aqp-4	aquaporin
	aqp-5	aquaporin
	aqp-6	aquaporin
	aqp-7	aquaporin
	aqp-8	aquaporin
	aqp-9	aquaporin

	Gene name	WormBase annotation notes
osmo	aqp-10	aquaporin
	aqp-11	aquaporin
	aqp-12	aquaporin
collagen and cuticle-related	col-147	collagen
	col-150	collagen
	col-160	collagen
	col-73	collagen
	col-98	collagen
	dpy-13	collagen
	noah-1	NompA homolog involved in molting
	Y69H2.14	probable collagen protein
	rol-3	protein tyrosine kinase involved in cuticle development
	ppn-1	involved in cuticle development
	chtl-1	predicted choline transporter involved in cuticle development
nematode specific proteins	nspd-1	nematode specific protein family, group D
	nspd-3	nematode specific protein family, group D
	nspd-4	nematode specific peptide family, group D; enriched in spermatogenesis
	nspe-3	nematode specific protein family, group E
	nspe-5	nematode specific protein family, group E
	nspe-7	nematode specific protein family, group E

Chapter V: Conclusions and Perspectives

In this dissertation, I have presented data that augments understanding of a nutrient-sensing network organized by nuclear receptors, likely via interaction with metabolic intermediate-derived ligands and possibly regulated by miRNAs. By using the *C. elegans* nuclear receptors NHR-49 and NHR-88, I have been able to study feeding and fasting responses in an *in vivo* system that is more genetically tractable than mammalian models. This model system allowed the creation of transgenic strains and isolation of new mutations that affect metabolic homeostasis, while common metabolic pathways permit my findings to be relevant in other organisms. I highlight my major conclusions and speculate on further experimental directions below.

Chapter II: Sensitivity to NHR-49 protein level reveals role for miRNAs in adult reproductive diapause

While setting out to explore the structure-function relationship of NHR-49, I discovered the extreme sensitivity of the worm to levels of this protein. There is precedent for this phenomenon in the *C. elegans* nuclear receptor field; as seen with *nhr-49*, worms mutant for *nhr-40* have the same phenotype as those overexpressing the protein (Brozova et al., 2006). The authors put forth several hypotheses that may also apply to NHR-49, including that the phenotype might result from increased expression of downstream targets or dominant negative activity of the transgenic NR (Brozova et al., 2006). For example, overexpression of NHR-49 may change the ratio of homodimer to heterodimer pairs in partners capable of interacting with DNA in either conformation or increase the number of NHR-49 homodimers present. These changes could alter responsiveness to different ligands; potential consequences are illustrated by the mammalian retinoic acid receptors (RARs) and retinoid X receptors (RXRs). RXR can act as either a homo- or heterodimer with RAR, but a subset of its ligands are recognized only by the heterodimer (Kurokawa et al., 1994). Furthermore, the heterodimer binds DNA more tightly than the homodimer, so excess RXR/RAR heterodimers can displace the homodimer, making the cell less receptive to RXR/RXR-specific ligands (Kurokawa et al., 1994). While there is not yet enough known about independent activity of NHR-49 heterodimer partners, regulatory targets of the NHR-49 homodimer, or ligand specificity for the various dimer configurations, a model such as this could explain toxicity of the NHR-49 overexpression construct.

Interestingly, toxicity of overexpression constructs is mitigated by addition of genomic regions including introns and the 3'UTR. Due to the existence of two miRNAs predicted to target *nhr-49* and a precedent for miRNA regulation of NRs in both worms (Hammell et al., 2009) and mammals (Yang and Wang, 2011), I interpreted this result as probable miRNA regulation of NHR-49 protein levels. However, the genomic elements could play some other role in improving outcome of transgenic worms. For example, they could contain recognition sites for RNA-binding proteins that prevent effective transcription of the transgene; while the outcome would be the same as that caused by miRNA targeting, it could explain the lack of fed phenotypes seen in the miRNA mutants. Future experiments stemming from these data could go in two directions. Firstly, using the knowledge that constructs containing genomic sequence and introduced at lower copy number both permit partial rescue of the *nhr-49* lifespan phenotype, the original aim of selectively disrupting NHR-49 domains and assaying phenotypic and regulatory outcome should now be possible. Secondly, the requirement for the genomic sequences remains unexplained. Experiments such as quantifying NHR-49 protein in miRNA mutants and transgenic lines expressing NHR-49 cDNA or genomic constructs with or without the 3'UTR could answer the question of whether the introns or 3'UTR actually reduce expression levels, which region is required to do so, and whether the predicted NHR-49-targeting miRNAs are involved in titration of NHR-49 protein levels. These studies require an antibody against NHR-49 to allow detection of the endogenous protein.

In investigating the interaction of mir-243 and mir-797 with NHR-49, I discovered that both miRNAs are required for normal recovery from the adult reproductive diapause, thereby describing the first phenotypes for these knockout strains. Due to phenotypic similarities between recovered miRNA knockout animals and refed *nhr-49* mutants, I propose that some aspects of diapause recovery may originate in miRNA control of *nhr-49* expression. Furthermore, I hypothesize that these and other *C. elegans* miRNAs may actually switch to serving as translational activators during diapause states, as seen with the mammalian miRNAs miR369-3 and let-7 in arrested cell cultures (Vasudevan et al., 2007). The miRNA mutants also have phenotypes that, while distinct from each other, seem to implicate mir-243 and mir-797 in maintenance of differentiation states in different cell types. Specifically, the presence of what appear to be unfused seam cells in *mir-247&797* adults and undifferentiated spermatocytes within the body cavity of *mir-243* adults both indicate that differentiation of these tissues either

did not occur at the appropriate time or was not maintained. Knowing which target genes are responsible for these phenotypes will help to elucidate whether dedifferentiation is actually occurring. A candidate RNAi screen in which predicted mir-243 and mir-797 targets are knocked down during recovery from ARD may reveal phenotypes matching the miRNA deletion mutants. These genes could then be tested for miRNA regulation by looking for changes in protein expression or localization. However, it is also possible that the phenotypes result from the misregulation of multiple targets, in which case a pooled RNAi approach might be more effective. Finally, identification of miRNAs affecting only ARD recovery provides the means for a kind of selective modulation of NHR-49 pathways, which was the original goal of my project. The miRNA mutants allow the study of processes required for recovery outside the context of metabolic misregulation seen in *nhr-49* mutants, thereby preserving the other aspects of the fasting response. While the adult reproductive diapause itself is not conserved in mammals, the involved physiological processes such as autophagy and redistribution of fat stores are key components of the mammalian fasting response, and information learned from studying the regulation of ARD phenotypes in *C. elegans* may also apply to higher organisms.

Chapter III: NHR-88, CYP-35A5, and fhc10(+) *interact to determine fertility, fecundity, and longevity in* C. elegans

A large portion of my thesis work has focused on characterizing NHR-88, a nuclear receptor about which very little was known. While I found that the single mutant behaves like wild-type in the assays I performed, I discovered synthetic interactions between *nhr-88* and two other genes that affect fecundity, fat metabolism, germline organization, and longevity. The first gene, which the Ashrafi lab reported to be negatively regulated by NHR-88 (Jones, 2009), encodes the cytochrome P450 CYP-35A5. The second gene has yet to be identified, as the mutation was isolated from the background of the *cyp-35a5* deletion strain. Single nucleotide polymorphism mapping has narrowed down the location of the mutation to the X chromosome. I have samples prepared for submission to a full-genome sequencing facility; the sequence data will hopefully allow me to identify candidate genes on the X chromosome. After further narrowing the candidates by comparing RNAi knock-down phenotypes to those of the mutant, rescue experiments should allow definitive identification of the gene affected by *fhc10*. Once the molecular identity of *fhc10* is known, it will be important to remake the *cyp-35a5;fhc10* and *nhr-*

88;cyp-35a5;fhc10 mutants to confirm that the phenotypic interactions seen in these strains are not the result of yet another background mutation.

NHR-88, CYP-35A5, and *fhc10(+)* work together to regulate processes affecting multiple tissues: changes in brood size and mitotic population are germline- and/or somatic gonad-related, alterations in lipid profile most likely involve metabolic enzymes in the intestine, and changes in lifespan probably result from enhanced or deficient repair of somatic tissues. Furthermore, a transcriptional reporter of *nhr-88* is found exclusively in neurons and the hypodermis. It will be important to verify this expression using translational reporters or antibody staining, but current data suggest that NHR-88 is acting cell non-autonomously to coordinate metabolic outputs. Additionally, introducing a reporter construct at low copy number by microparticle bombardment or MosSCI will circumvent germline silencing of high-copy arrays, thereby allowing determination of whether NHR-88 is expressed in germ cells. Finally, tissue-specific knockouts of all three genes could help to define the tissues in which they are required, while microarray experiments could shed light on the genes targeted by NHR-88 in response to signals from CYP-35A5 and *fhc10(+)*.

Analysis of longevity and germline phenotypes of *nhr-88*, *cyp-35a5*, and *fhc10* mutants singly and in combination led me to discover a correlation between average number of cells within the mitotic region and mean lifespan of the strain. Not only is NHR-88 necessary for this inverse relationship to exist, but it is also required for changes to the mitotic region based on genotype. Based on these data, I hypothesize that NHR-88 is critical in communicating information about germ cell status to the somatic tissues and vice versa. This model could be bolstered by examining life span of double mutants containing the *nhr-88* deletion and a mutation affecting germline proliferation. If NHR-88 is indeed required for germline-soma communication, inducing over- or under-proliferation using *gld-1* or *glp-1* alleles should not affect longevity in an *nhr-88* mutant background. Additionally, antibody staining of mutant gonads to determine localization of key mitotic and meiotic factors such as CYE-1, REC-8, or HIM-3, will permit more reliable demarcation of the transition zone than is possible through DAPI staining alone and may also reveal misregulation of factors that could explain the shortening of the mitotic region.

The single significant phenotype I found for the *nhr-88(tm1033)* mutant was resistance to sterility induced by the fatty acid dihomo-gamma-linolenic acid (DGLA). Although high

concentrations of DGLA lead to complete loss of the germline, I discovered that life-long exposure to low concentration causes a reduction in the length of the mitotic region similar to that seen in the *cyp-35a5;fhc10* mutant raised under normal conditions; mutation of *nhr-88* seems to have a slight protective effect against this phenotype as well. While preliminary data suggest that the double mutant is more sensitive to DGLA-induced sterility than wild-type, it will be important to confirm these findings and expand analysis of mitotic region changes to the full panel of mutants. Besides providing a phenotype for the *nhr-88* mutant, these DGLA results also have implications for identification of the NHR-88 ligand. Like every *C. elegans* NR but DAF-12, NHR-88 is an orphan receptor. Its requirement for the full effect of DGLA raises the possibility that the metabolite bound by NHR-88 is DGLA-derived. If future experiments identify target genes of NHR-88, activation or repression of NHR-88 could be assayed more directly using a luciferase reporter system in mammalian cells or the ligand sensor system used to identify the HNF4α ligand in flies (Palanker et al., 2009). Finally, DGLA is a good candidate for a nutrient status proxy given that its relative abundance within the worm changes with food source and availability (Brooks et al., 2009; Van Gilst et al., 2005b). When combined with preliminary observations suggesting that food source affects the mitotic region, these data support a model in which NHR-88 acts as an environmental nutrient sensor to coordinate metabolic outputs of somatic repair and progeny production. The genetic interactions with *cyp-35a5* are also intriguing, as they echo the self-regulatory network existing between mammalian nutrient-sensing nuclear receptors and the cytochrome P450s that metabolize their ligands. Thus the relationships that I have defined between NHR-88, CYP-35A5, *fhc10(+)*, and a DGLA-derived ligand in *C. elegans* provide a model system for regulation of a nutrient-controlled response system whose mechanism is likely to be conserved in higher organisms.

Chapter IV: NHR-88 acts downstream of NHR-49 to regulate the adult reproductive diapause

Work for this chapter began with analysis and characterization of *C. elegans* fasting response genes, as determined by 5-fold changes on microarrays done by Giana Angelo, a post-doctoral fellow in the Van Gilst lab. These data led me to identify 533 genes with putative roles in the fasting response, most of which were also NHR-49-dependent. In lieu of retesting every hit, I chose to focus on a subset of 166 genes, which I characterized into 12 fasting-regulated modules that covered processes from reproduction and yolk synthesis to autophagy to cell cycle.

These modules complement the physiological changes that must occur during the adult reproductive diapause, suggesting that they may be involved in induction of the diapause. Furthermore, the set of genes I identified as NHR-49-regulated during fasting, namely genes involved in apoptosis, cell cycle regulation, and RNA processing, are strikingly similar to the noncanonical targets recently identified for the mammalian receptor HNF4α (Bolotin et al., 2010). Based on the functional homology that exists between HNF4α and NHR-49 in the fed state, it is likely that these new fasting modules are also involved in the starvation response in mammalian tissues.

To confirm both the role of these genes in the fasting response and their dependence on NHR-49, I designed qRT-PCR primers to assay expression levels in fed and fasted N2 and *nhr-49* worms. Unfortunately, my qRT-PCR data show a lot of variability, likely due to technical issues affecting RNA quality caused by protocol changes that occurred at the time of these experiments. With the data as they are, fewer genes show NHR-49-dependence and the magnitude of changes that I see are lower than those seen by microarray. Once these experiments have been repeated to define the fasting response at late L4/ARD entry, future experiments could look at expression changes at other ARD time points. For example, the autophagy and apoptosis genes may increase during the maintenance phase as tissue remodeling occurs, while genes encoding P-granule-associated proteins might show the greatest change during recovery, if mRNAs are being stored and protected during starvation.

This fasting qRT-PCR panel will also be very useful to define the role of NHR-88 in the fasting response. I have shown expression data demonstrating that NHR-88 is upregulated upon removal from food in an NHR-49-dependent manner. I have also characterized a number of ARD defects in *nhr-88* mutants, all of which are also seen in *nhr-49* animals. Genes similarly misregulated in both mutants will help to identify genetic mediators of ARD-specific processes such as cessation of fertilization and maintenance of yolk homeostasis. Besides helping to elucidate ARD regulation on a genetic level, the necessity for *nhr-88* will prove to be a powerful tool for studying the cellular mechanisms of the diapause.

Broader implications

My dissertation research has focused on the development of new *C. elegans* models in which to study aspects of the mammalian nutrient response system. I first describe the work I

have done to improve the viability of the adult reproductive diapause as a model for nutrient receptor control of protective adaptations to starvation. Identification of two miRNAs required for normal recovery and a nuclear receptor involved in both entry and recovery phases will allow for investigation of the diapause away from the general infirmity of the *nhr-49* strain. I have also identified gene classes whose expression levels change upon fasting at mid-L4 that may also play a role in the diapause. These novel regulators and downstream targets may in turn inform studies of HNF4α and PPARα-coordinated fasting responses in mammalian tissues. Likewise, understanding of the processes required for an organism or tissue to maintain metabolic homeostasis in the face of variable nutritional status, such as the multi-organ network defined by NHR-88, CYP-35A5, and *fhc10(+)*, is an important goal that may ultimately have broader implications for treatment of human metabolic disorders. The network defined by these genes echoes the interactions between mammalian NRs and P450 genes, thereby validating *C. elegans* as a model system for exploration of nuclear receptor control of adaptation to variations in nutritional status.

Aarnio, V., Lehtonen, M., Storvik, M., Callaway, J.C., Lakso, M., and Wong, G. (2011). Caenorhabditis Elegans Mutants Predict Regulation of Fatty Acids and Endocannabinoids by the CYP-35A Gene Family. Front Pharmacol *2*, 12.

Aggelidou, E., Iordanidou, P., Demetriades, C., Piltsi, O., and Hadzopoulou-Cladaras, M. (2006). Functional characterization of hepatocyte nuclear factor-4 alpha dimerization interface mutants. Febs J *273*, 1948-1958.

Almeida, M.I., Reis, R.M., and Calin, G.A. (2011). MicroRNA history: Discovery, recent applications, and next frontiers. Mutat Res.

Altun, Z.F.a.H., D.H. (2009). Epithelial system, seam cells. In WormAtlas, L.A. Herndon, ed.

Alvarez-Saavedra, E., and Horvitz, H.R. (2010). Many families of C. elegans microRNAs are not essential for development or viability. Curr Biol *20*, 367-373.

Anderson, J.L., Reynolds, R.M., Morran, L.T., Tolman-Thompson, J., and Phillips, P.C. (2011). Experimental Evolution Reveals Antagonistic Pleiotropy in Reproductive Timing but Not Life Span in Caenorhabditis elegans. J Gerontol A Biol Sci Med Sci.

Angelo, G., and Van Gilst, M.R. (2009). Starvation protects germline stem cells and extends reproductive longevity in C. elegans. Science *326*, 954-958.

Arantes-Oliveira, N., Apfeld, J., Dillin, A., and Kenyon, C. (2002). Regulation of life-span by germ-line stem cells in Caenorhabditis elegans. Science *295*, 502-505.

Arnold, K., Bordoli, L., Kopp, J., and Schwede, T. (2006). The SWISS-MODEL workspace: a web-based environment for protein structure homology modelling. Bioinformatics *22*, 195-201.

Ashrafi, K., Chang, F.Y., Watts, J.L., Fraser, A.G., Kamath, R.S., Ahringer, J., and Ruvkun, G. (2003). Genome-wide RNAi analysis of Caenorhabditis elegans fat regulatory genes. Nature *421*, 268-272.

Bain, D.L., Heneghan, A.F., Connaghan-Jones, K.D., and Miura, M.T. (2007). Nuclear receptor structure: implications for function. Annu Rev Physiol *69*, 201-220.

Barton, M.K., Schedl, T.B., and Kimble, J. (1987). Gain-of-function mutations of fem-3, a sex-determination gene in Caenorhabditis elegans. Genetics *115*, 107-119.

Beitel, G.J., Lambie, E.J., and Horvitz, H.R. (2000). The C. elegans gene lin-9,which acts in an Rb-related pathway, is required for gonadal sheath cell development and encodes a novel protein. Gene *254*, 253-263.

Bertrand, S., Brunet, F.G., Escriva, H., Parmentier, G., Laudet, V., and Robinson-Rechavi, M. (2004). Evolutionary genomics of nuclear receptors: from twenty-five ancestral genes to derived endocrine systems. Mol Biol Evol *21*, 1923-1937.

Bethke, A., Fielenbach, N., Wang, Z., Mangelsdorf, D.J., and Antebi, A. (2009). Nuclear hormone receptor regulation of microRNAs controls developmental progression. Science *324*, 95-98.

Biedermann, B., Wright, J., Senften, M., Kalchhauser, I., Sarathy, G., Lee, M.H., and Ciosk, R. (2009). Translational repression of cyclin E prevents precocious mitosis and embryonic gene activation during C. elegans meiosis. Dev Cell *17*, 355-364.

Bolotin, E., Liao, H., Ta, T.C., Yang, C., Hwang-Verslues, W., Evans, J.R., Jiang, T., and Sladek, F.M. (2010). Integrated approach for the identification of human hepatocyte nuclear factor 4alpha target genes using protein binding microarrays. Hepatology *51*, 642-653.

Brenner, S. (1974). The genetics of Caenorhabditis elegans. Genetics *77*, 71-94.

Brock, T.J., Browse, J., and Watts, J.L. (2006). Genetic regulation of unsaturated fatty acid composition in C. elegans. PLoS genetics *2*, e108.

Brooks, K.K., Liang, B., and Watts, J.L. (2009). The influence of bacterial diet on fat storage in C. elegans. PLoS One *4*, e7545.

Brozova, E., Simeckova, K., Kostrouch, Z., Rall, J.E., and Kostrouchova, M. (2006). NHR-40, a Caenorhabditis elegans supplementary nuclear receptor, regulates embryonic and early larval development. Mech Dev *123*, 689-701.

Cassada, R.C., and Russell, R.L. (1975). The dauerlarva, a post-embryonic developmental variant of the nematode Caenorhabditis elegans. Dev Biol *46*, 326-342.

Chakravarthy, M.V., Lodhi, I.J., Yin, L., Malapaka, R.R., Xu, H.E., Turk, J., and Semenkovich, C.F. (2009). Identification of a physiologically relevant endogenous ligand for PPARalpha in liver. Cell *138*, 476-488.

Chawla, A., Repa, J.J., Evans, R.M., and Mangelsdorf, D.J. (2001). Nuclear receptors and lipid physiology: opening the X-files. Science *294*, 1866-1870.

Chen, W.S., Manova, K., Weinstein, D.C., Duncan, S.A., Plump, A.S., Prezioso, V.R., Bachvarova, R.F., and Darnell, J.E., Jr. (1994). Disruption of the HNF-4 gene, expressed in visceral endoderm, leads to cell death in embryonic ectoderm and impaired gastrulation of mouse embryos. Genes Dev *8*, 2466-2477.

Crittenden, S.L., Eckmann, C.R., Wang, L., Bernstein, D.S., Wickens, M., and Kimble, J. (2003). Regulation of the mitosis/meiosis decision in the Caenorhabditis elegans germline. Philos Trans R Soc Lond B Biol Sci *358*, 1359-1362.

Davis, M.W., Hammarlund, M., Harrach, T., Hullett, P., Olsen, S., and Jorgensen, E.M. (2005). Rapid single nucleotide polymorphism mapping in C. elegans. BMC Genomics *6*, 118.

Dernburg, A.F., Zalevsky, J., Colaiacovo, M.P., and Villeneuve, A.M. (2000). Transgene-mediated cosuppression in the C. elegans germ line. Genes Dev *14*, 1578-1583.

Dhe-Paganon, S., Duda, K., Iwamoto, M., Chi, Y.I., and Shoelson, S.E. (2002). Crystal structure of the HNF4 alpha ligand binding domain in complex with endogenous fatty acid ligand. J Biol Chem *277*, 37973-37976.

Di Marzo, V., and Matias, I. (2005). Endocannabinoid control of food intake and energy balance. Nat Neurosci *8*, 585-589.

Dillin, A., Crawford, D.K., and Kenyon, C. (2002). Timing requirements for insulin/IGF-1 signaling in C. elegans. Science *298*, 830-834.

Duda, K., Chi, Y.I., and Shoelson, S.E. (2004). Structural basis for HNF-4alpha activation by ligand and coactivator binding. J Biol Chem *279*, 23311-23316.

Ellis, H.M., and Horvitz, H.R. (1986). Genetic control of programmed cell death in the nematode C. elegans. Cell *44*, 817-829.

Fay, D.S., and Han, M. (2000). Mutations in cye-1, a Caenorhabditis elegans cyclin E homolog, reveal coordination between cell-cycle control and vulval development. Development *127*, 4049-4060.

Feige, J.N., Gelman, L., Michalik, L., Desvergne, B., and Wahli, W. (2006). From molecular action to physiological outputs: peroxisome proliferator-activated receptors are nuclear receptors at the crossroads of key cellular functions. Prog Lipid Res *45*, 120-159.

Flatt, T., Min, K.J., D'Alterio, C., Villa-Cuesta, E., Cumbers, J., Lehmann, R., Jones, D.L., and Tatar, M. (2008). Drosophila germ-line modulation of insulin signaling and lifespan. Proc Natl Acad Sci U S A *105*, 6368-6373.

Forman, B.M., Chen, J., and Evans, R.M. (1997). Hypolipidemic drugs, polyunsaturated fatty acids, and eicosanoids are ligands for peroxisome proliferator-activated receptors alpha and delta. Proc Natl Acad Sci U S A *94*, 4312-4317.

Fox, P.M., Vought, V.E., Hanazawa, M., Lee, M.H., Maine, E.M., and Schedl, T. (2011). Cyclin E and CDK-2 regulate proliferative cell fate and cell cycle progression in the C. elegans germline. Development *138*, 2223-2234.

Fraser, A.G., Kamath, R.S., Zipperlen, P., Martinez-Campos, M., Sohrmann, M., and Ahringer, J. (2000). Functional genomic analysis of C. elegans chromosome I by systematic RNA interference. Nature *408*, 325-330.

Frokjaer-Jensen, C., Davis, M.W., Hopkins, C.E., Newman, B.J., Thummel, J.M., Olesen, S.P., Grunnet, M., and Jorgensen, E.M. (2008). Single-copy insertion of transgenes in Caenorhabditis elegans. Nature genetics *40*, 1375-1383.

Garrison, W.D., Battle, M.A., Yang, C., Kaestner, K.H., Sladek, F.M., and Duncan, S.A. (2006). Hepatocyte nuclear factor 4alpha is essential for embryonic development of the mouse colon. Gastroenterology *130*, 1207-1220.

Gems, D., Sutton, A.J., Sundermeyer, M.L., Albert, P.S., King, K.V., Edgley, M.L., Larsen, P.L., and Riddle, D.L. (1998). Two pleiotropic classes of daf-2 mutation affect larval arrest, adult behavior, reproduction and longevity in Caenorhabditis elegans. Genetics *150*, 129-155.

Gerisch, B., and Antebi, A. (2004). Hormonal signals produced by DAF-9/cytochrome P450 regulate C. elegans dauer diapause in response to environmental cues. Development *131*, 1765-1776.

Gissendanner, C.R., Crossgrove, K., Kraus, K.A., Maina, C.V., and Sluder, A.E. (2004). Expression and function of conserved nuclear receptor genes in Caenorhabditis elegans. Dev Biol *266*, 399-416.

Golden, T.R., Hubbard, A., Dando, C., Herren, M.A., and Melov, S. (2008). Age-related behaviors have distinct transcriptional profiles in Caenorhabditis elegans. Aging cell *7*, 850-865.

Goudeau, J., Bellemin, S., Toselli-Mollereau, E., Shamalnasab, M., Chen, Y., and Aguilaniu, H. (2011). Fatty acid desaturation links germ cell loss to longevity through NHR-80/HNF4 in C. elegans. PLoS Biol *9*, e1000599.

Griffiths-Jones, S. (2004). The microRNA Registry. Nucleic Acids Res *32*, D109-111.

Griffiths-Jones, S., Grocock, R.J., van Dongen, S., Bateman, A., and Enright, A.J. (2006). miRBase: microRNA sequences, targets and gene nomenclature. Nucleic Acids Res *34*, D140-144.

Griffiths-Jones, S., Saini, H.K., van Dongen, S., and Enright, A.J. (2008). miRBase: tools for microRNA genomics. Nucleic Acids Res *36*, D154-158.

Grigo, K., Wirsing, A., Lucas, B., Klein-Hitpass, L., and Ryffel, G.U. (2008). HNF4 alpha orchestrates a set of 14 genes to down-regulate cell proliferation in kidney cells. Biol Chem *389*, 179-187.

Gronemeyer, H., Gustafsson, J.A., and Laudet, V. (2004). Principles for modulation of the nuclear receptor superfamily. Nat Rev Drug Discov *3*, 950-964.

Guex, N., and Peitsch, M.C. (1997). SWISS-MODEL and the Swiss-PdbViewer: an environment for comparative protein modeling. Electrophoresis *18*, 2714-2723.

Gumienny, T.L., Lambie, E., Hartwieg, E., Horvitz, H.R., and Hengartner, M.O. (1999). Genetic control of programmed cell death in the Caenorhabditis elegans hermaphrodite germline. Development *126*, 1011-1022.

Gupta, R.K., and Kaestner, K.H. (2004). HNF-4alpha: from MODY to late-onset type 2 diabetes. Trends Mol Med *10*, 521-524.

Hadzopoulou-Cladaras, M., Kistanova, E., Evagelopoulou, C., Zeng, S., Cladaras, C., and Ladias, J.A. (1997). Functional domains of the nuclear receptor hepatocyte nuclear factor 4. J Biol Chem *272*, 539-550.

Hahn-Windgassen, A., and Van Gilst, M.R. (2009). The Caenorhabditis elegans HNF4alpha Homolog, NHR-31, mediates excretory tube growth and function through coordinate regulation of the vacuolar ATPase. PLoS genetics *5*, e1000553.

Hammell, C.M., Karp, X., and Ambros, V. (2009). A feedback circuit involving let-7-family miRNAs and DAF-12 integrates environmental signals and developmental timing in Caenorhabditis elegans. Proc Natl Acad Sci U S A *106*, 18668-18673.

Harvey, S.C., and Viney, M.E. (2007). Thermal variation reveals natural variation between isolates of Caenorhabditis elegans. J Exp Zool B Mol Dev Evol *308*, 409-416.

Hayhurst, G.P., Lee, Y.H., Lambert, G., Ward, J.M., and Gonzalez, F.J. (2001). Hepatocyte nuclear factor 4alpha (nuclear receptor 2A1) is essential for maintenance of hepatic gene expression and lipid homeostasis. Mol Cell Biol *21*, 1393-1403.

Hills, T., Brockie, P.J., and Maricq, A.V. (2004). Dopamine and glutamate control area-restricted search behavior in Caenorhabditis elegans. J Neurosci *24*, 1217-1225.

Hodgkin, J., and Barnes, T.M. (1991). More is not better: brood size and population growth in a self-fertilizing nematode. Proc Biol Sci *246*, 19-24.

Hoekstra, M., van der Sluis, R.J., Kuiper, J., and Van Berkel, T.J. (2011). Nonalcoholic fatty liver disease is associated with an altered hepatocyte microRNA profile in LDL receptor knockout mice. J Nutr Biochem.

Hsin, H., and Kenyon, C. (1999). Signals from the reproductive system regulate the lifespan of C. elegans. Nature *399*, 362-366.

Huang, J.C. (2008). The role of peroxisome proliferator-activated receptors in the development and physiology of gametes and preimplantation embryos. PPAR Res *2008*, 732303.

Humphrey, W., Dalke, A., and Schulten, K. (1996). VMD: visual molecular dynamics. J Mol Graph *14*, 33-38, 27-38.

Jenkins, N.L., McColl, G., and Lithgow, G.J. (2004). Fitness cost of extended lifespan in Caenorhabditis elegans. Proc Biol Sci *271*, 2523-2526.

Jia, K., Albert, P.S., and Riddle, D.L. (2002). DAF-9, a cytochrome P450 regulating C. elegans larval development and adult longevity. Development *129*, 221-231.

Johnson, T.E., Mitchell, D.H., Kline, S., Kemal, R., and Foy, J. (1984). Arresting development arrests aging in the nematode Caenorhabditis elegans. Mech Ageing Dev *28*, 23-40.

Jones, K. (2009). Genetic Analysis of TOR complex 2 signaling. In Department of Physiology (San Francisco, CA, University of California, San Francisco).

Kalkuhl, A., Kaestner, K., Buchmann, A., and Schwarz, M. (1996). Expression of hepatocyte-enriched nuclear transcription factors in mouse liver tumours. Carcinogenesis *17*, 609-612.

Kamath, R.S., Fraser, A.G., Dong, Y., Poulin, G., Durbin, R., Gotta, M., Kanapin, A., Le Bot, N., Moreno, S., Sohrmann, M.*, et al.* (2003). Systematic functional analysis of the Caenorhabditis elegans genome using RNAi. Nature *421*, 231-237.

Kelly, W.G., Xu, S., Montgomery, M.K., and Fire, A. (1997). Distinct requirements for somatic and germline expression of a generally expressed Caernorhabditis elegans gene. Genetics *146*, 227-238.

Kersten, S., Seydoux, J., Peters, J.M., Gonzalez, F.J., Desvergne, B., and Wahli, W. (1999). Peroxisome proliferator-activated receptor alpha mediates the adaptive response to fasting. J Clin Invest *103*, 1489-1498.

Kiefer, F., Arnold, K., Kunzli, M., Bordoli, L., and Schwede, T. (2009). The SWISS-MODEL Repository and associated resources. Nucleic Acids Res *37*, D387-392.

Kim, S., and Paik, Y.K. (2008). Developmental and reproductive consequences of prolonged non-aging dauer in Caenorhabditis elegans. Biochem Biophys Res Commun *368*, 588-592.

Kim, V.N., and Nam, J.W. (2006). Genomics of microRNA. Trends Genet *22*, 165-173.

Kimble, J., and Crittenden, S.L. (2007). Controls of germline stem cells, entry into meiosis, and the sperm/oocyte decision in Caenorhabditis elegans. Annu Rev Cell Dev Biol *23*, 405-433.

Kimble, J., and Sharrock, W.J. (1983). Tissue-specific synthesis of yolk proteins in Caenorhabditis elegans. Dev Biol *96*, 189-196.

Kozomara, A., and Griffiths-Jones, S. (2011). miRBase: integrating microRNA annotation and deep-sequencing data. Nucleic Acids Res *39*, D152-157.

Kubagawa, H.M., Watts, J.L., Corrigan, C., Edmonds, J.W., Sztul, E., Browse, J., and Miller, M.A. (2006). Oocyte signals derived from polyunsaturated fatty acids control sperm recruitment in vivo. Nat Cell Biol *8*, 1143-1148.

Kurokawa, R., DiRenzo, J., Boehm, M., Sugarman, J., Gloss, B., Rosenfeld, M.G., Heyman, R.A., and Glass, C.K. (1994). Regulation of retinoid signalling by receptor polarity and allosteric control of ligand binding. Nature *371*, 528-531.

Kuwabara, P.E., and Perry, M.D. (2001). It ain't over till it's ova: germline sex determination in C. elegans. Bioessays *23*, 596-604.

Lausen, J., Thomas, H., Lemm, I., Bulman, M., Borgschulze, M., Lingott, A., Hattersley, A.T., and Ryffel, G.U. (2000). Naturally occurring mutations in the human HNF4alpha gene impair the function of the transcription factor to a varying degree. Nucleic Acids Res *28*, 430-437.

Lazarevich, N.L., Cheremnova, O.A., Varga, E.V., Ovchinnikov, D.A., Kudrjavtseva, E.I., Morozova, O.V., Fleishman, D.I., Engelhardt, N.V., and Duncan, S.A. (2004). Progression of HCC in mice is associated with a downregulation in the expression of hepatocyte nuclear factors. Hepatology *39*, 1038-1047.

Liang, B., Ferguson, K., Kadyk, L., and Watts, J.L. (2010). The role of nuclear receptor NHR-64 in fat storage regulation in Caenorhabditis elegans. PLoS One *5*, e9869.

Liu, T., Zimmerman, K.K., and Patterson, G.I. (2004). Regulation of signaling genes by TGFbeta during entry into dauer diapause in C. elegans. BMC Dev Biol *4*, 11.

Lu, P., Rha, G.B., Melikishvili, M., Wu, G., Adkins, B.C., Fried, M.G., and Chi, Y.I. (2008). Structural basis of natural promoter recognition by a unique nuclear receptor, HNF4alpha. Diabetes gene product. J Biol Chem *283*, 33685-33697.

Lucanic, M., Held, J.M., Vantipalli, M.C., Klang, I.M., Graham, J.B., Gibson, B.W., Lithgow, G.J., and Gill, M.S. (2011). N-acylethanolamine signalling mediates the effect of diet on lifespan in Caenorhabditis elegans. Nature *473*, 226-229.

Martinez, N.J., Ow, M.C., Reece-Hoyes, J.S., Barrasa, M.I., Ambros, V.R., and Walhout, A.J. (2008). Genome-scale spatiotemporal analysis of Caenorhabditis elegans microRNA promoter activity. Genome Res *18*, 2005-2015.

Martinez-Jimenez, C.P., Kyrmizi, I., Cardot, P., Gonzalez, F.J., and Talianidis, I. (2010). Hepatocyte nuclear factor 4alpha coordinates a transcription factor network regulating hepatic fatty acid metabolism. Molecular and cellular biology *30*, 565-577.

McCormick, M., Chen, K., Ramaswamy, P., and Kenyon, C. (2011). New Genes that Extend C. elegans' Lifespan in Response to Reproductive Signals. Aging cell.

Mello, C., and Fire, A. (1995). DNA transformation. Methods Cell Biol *48*, 451-482.

Mello, C.C., Kramer, J.M., Stinchcomb, D., and Ambros, V. (1991). Efficient gene transfer in C.elegans: extrachromosomal maintenance and integration of transforming sequences. Embo J *10*, 3959-3970.

Menzel, R., Rodel, M., Kulas, J., and Steinberg, C.E. (2005). CYP35: xenobiotically induced gene expression in the nematode Caenorhabditis elegans. Arch Biochem Biophys *438*, 93-102.

Miska, E.A., Alvarez-Saavedra, E., Abbott, A.L., Lau, N.C., Hellman, A.B., McGonagle, S.M., Bartel, D.P., Ambros, V.R., and Horvitz, H.R. (2007). Most Caenorhabditis elegans microRNAs are individually not essential for development or viability. PLoS genetics *3*, e215.

Motola, D.L., Cummins, C.L., Rottiers, V., Sharma, K.K., Li, T., Li, Y., Suino-Powell, K., Xu, H.E., Auchus, R.J., Antebi, A.*, et al.* (2006). Identification of ligands for DAF-12 that govern dauer formation and reproduction in C. elegans. Cell *124*, 1209-1223.

Murray, R.L. (2009). The evolution of *Caenorhabditis elegans* sperm traits involved in reproductive success by self-fertilizing hermaphrodites and in male-male post-mating contests. In Graduate Department of Ecology and Evolutionary Biology (Toronto, University of Toronto).

Naiki, T., Nagaki, M., Shidoji, Y., Kojima, H., Imose, M., Kato, T., Ohishi, N., Yagi, K., and Moriwaki, H. (2002). Analysis of gene expression profile induced by hepatocyte nuclear factor 4alpha in hepatoma cells using an oligonucleotide microarray. J Biol Chem *277*, 14011-14019.

Ng, V.Y., Huang, Y., Reddy, L.M., Falck, J.R., Lin, E.T., and Kroetz, D.L. (2007). Cytochrome P450 eicosanoids are activators of peroxisome proliferator-activated receptor alpha. Drug Metab Dispos *35*, 1126-1134.

O'Sullivan, S.E. (2007). Cannabinoids go nuclear: evidence for activation of peroxisome proliferator-activated receptors. Br J Pharmacol *152*, 576-582.

Oxombre, B., Kouach, M., Moerman, E., Formstecher, P., and Laine, B. (2004). The G115S mutation associated with maturity-onset diabetes of the young impairs hepatocyte nuclear factor 4alpha activities and introduces a PKA phosphorylation site in its DNA-binding domain. Biochem J *383*, 573-580.

Palanker, L., Tennessen, J.M., Lam, G., and Thummel, C.S. (2009). Drosophila HNF4 regulates lipid mobilization and beta-oxidation. Cell Metab *9*, 228-239.

Partridge, L., Gems, D., and Withers, D.J. (2005). Sex and death: what is the connection? Cell *120*, 461-472.

Parviz, F., Matullo, C., Garrison, W.D., Savatski, L., Adamson, J.W., Ning, G., Kaestner, K.H., Rossi, J.M., Zaret, K.S., and Duncan, S.A. (2003). Hepatocyte nuclear factor 4alpha controls the development of a hepatic epithelium and liver morphogenesis. Nat Genet *34*, 292-296.

Pathare, P. (submitted). Coordinate regulation of lipid metabolism by novel nuclear receptor partnerships. Genetics.

Peitsch, M.C. (1995). Protein modeling by E-mail. Nature Biotechnology *13*, 658-660.

Perez, C.L., and Van Gilst, M.R. (2008). A 13C isotope labeling strategy reveals the influence of insulin signaling on lipogenesis in C. elegans. Cell Metab *8*, 266-274.

Praitis, V., Casey, E., Collar, D., and Austin, J. (2001). Creation of low-copy integrated transgenic lines in Caenorhabditis elegans. Genetics *157*, 1217-1226.

Rajagopal, A., Rao, A.U., Amigo, J., Tian, M., Upadhyay, S.K., Hall, C., Uhm, S., Mathew, M.K., Fleming, M.D., Paw, B.H.*, et al.* (2008). Haem homeostasis is regulated by the conserved and concerted functions of HRG-1 proteins. Nature *453*, 1127-1131.

Reddien, P.W., and Horvitz, H.R. (2000). CED-2/CrkII and CED-10/Rac control phagocytosis and cell migration in Caenorhabditis elegans. Nat Cell Biol *2*, 131-136.

Resnick, T.D., McCulloch, K.A., and Rougvie, A.E. (2010). miRNAs give worms the time of their lives: small RNAs and temporal control in Caenorhabditis elegans. Dev Dyn *239*, 1477-1489.

Rowley, C.W., Staloch, L.J., Divine, J.K., McCaul, S.P., and Simon, T.C. (2006). Mechanisms of mutual functional interactions between HNF-4alpha and HNF-1alpha revealed by mutations that cause maturity onset diabetes of the young. Am J Physiol Gastrointest Liver Physiol *290*, G466-475.

Rozen, S., and Skaletsky, H. (2000). Primer3 on the WWW for general users and for biologist programmers. Methods Mol Biol *132*, 365-386.

Ryffel, G.U. (2001). Mutations in the human genes encoding the transcription factors of the hepatocyte nuclear factor (HNF)1 and HNF4 families: functional and pathological consequences. J Mol Endocrinol *27*, 11-29.

Savkur, R.S., and Burris, T.P. (2004). The coactivator LXXLL nuclear receptor recognition motif. J Pept Res *63*, 207-212.

Schwede, T., Kopp, J., Guex, N., and Peitsch, M.C. (2003). SWISS-MODEL: An automated protein homology-modeling server. Nucleic Acids Res *31*, 3381-3385.

Sel, S., Ebert, T., Ryffel, G.U., and Drewes, T. (1996). Human renal cell carcinogenesis is accompanied by a coordinate loss of the tissue specific transcription factors HNF4 alpha and HNF1 alpha. Cancer Lett *101*, 205-210.

Shaham, S. (2006). WormBook: Methods in Cell Biology. In WormBook, T.C.e.R. Community, ed.

Shih, D.Q., Dansky, H.M., Fleisher, M., Assmann, G., Fajans, S.S., and Stoffel, M. (2000). Genotype/phenotype relationships in HNF-4alpha/MODY1: haploinsufficiency is associated with reduced apolipoprotein (AII), apolipoprotein (CIII), lipoprotein(a), and triglyceride levels. Diabetes *49*, 832-837.

Shmookler Reis, R.J., Xu, L., Lee, H., Chae, M., Thaden, J.J., Bharill, P., Tazearslan, C., Siegel, E., Alla, R., Zimniak, P.*, et al.* (2011). Modulation of lipid biosynthesis contributes to stress resistance and longevity of C. elegans mutants. Aging (Albany NY) *3*, 125-147.

Singson, A. (2001). Every sperm is sacred: fertilization in Caenorhabditis elegans. Dev Biol *230*, 101-109.

Sladek, F.M. (2011). What are nuclear receptor ligands? Mol Cell Endocrinol *334*, 3-13.

Snider, N.T., Walker, V.J., and Hollenberg, P.F. (2010). Oxidation of the endogenous cannabinoid arachidonoyl ethanolamide by the cytochrome P450 monooxygenases: physiological and pharmacological implications. Pharmacol Rev *62*, 136-154.

Stewart, A.D., and Phillips, P.C. (2002). Selection and maintenance of androdioecy in Caenorhabditis elegans. Genetics *160*, 975-982.

Suaud, L., Hemimou, Y., Formstecher, P., and Laine, B. (1999). Functional study of the E276Q mutant hepatocyte nuclear factor-4alpha found in type 1 maturity-onset diabetes of the young:

impaired synergy with chicken ovalbumin upstream promoter transcription factor II on the hepatocyte nuclear factor-1 promoter. Diabetes *48*, 1162-1167.

Takagi, S., Nakajima, M., Kida, K., Yamaura, Y., Fukami, T., and Yokoi, T. (2010). MicroRNAs regulate human hepatocyte nuclear factor 4alpha, modulating the expression of metabolic enzymes and cell cycle. The Journal of biological chemistry *285*, 4415-4422.

Taubert, S., Ward, J.D., and Yamamoto, K.R. (2011). Nuclear hormone receptors in nematodes: evolution and function. Mol Cell Endocrinol *334*, 49-55.

Updike, D., and Strome, S. (2010). P granule assembly and function in Caenorhabditis elegans germ cells. J Androl *31*, 53-60.

Van Gilst, M.R., Hadjivassiliou, H., Jolly, A., and Yamamoto, K.R. (2005a). Nuclear hormone receptor NHR-49 controls fat consumption and fatty acid composition in C. elegans. PLoS Biol *3*, e53.

Van Gilst, M.R., Hadjivassiliou, H., and Yamamoto, K.R. (2005b). A Caenorhabditis elegans nutrient response system partially dependent on nuclear receptor NHR-49. PNAS *102*, 13496-13501.

Vasudevan, S., Tong, Y., and Steitz, J.A. (2007). Switching from repression to activation: microRNAs can up-regulate translation. Science *318*, 1931-1934.

Viollet, B., Kahn, A., and Raymondjean, M. (1997). Protein kinase A-dependent phosphorylation modulates DNA-binding activity of hepatocyte nuclear factor 4. Molecular and cellular biology *17*, 4208-4219.

Wang, J., and Kim, S.K. (2003). Global analysis of dauer gene expression in Caenorhabditis elegans. Development *130*, 1621-1634.

Wang, M.C., O'Rourke, E.J., and Ruvkun, G. (2008). Fat metabolism links germline stem cells and longevity in C. elegans. Science *322*, 957-960.

Ward, S., and Carrel, J.S. (1979). Fertilization and sperm competition in the nematode Caenorhabditis elegans. Dev Biol *73*, 304-321.

Watts, J.L., and Browse, J. (2002). Genetic dissection of polyunsaturated fatty acid synthesis in Caenorhabditis elegans. Proc Natl Acad Sci U S A *99*, 5854-5859.

Watts, J.L., and Browse, J. (2006). Dietary manipulation implicates lipid signaling in the regulation of germ cell maintenance in C. elegans. Dev Biol *292*, 381-392.

Watts, J.L., Phillips, E., Griffing, K.R., and Browse, J. (2003). Deficiencies in C20 polyunsaturated fatty acids cause behavioral and developmental defects in Caenorhabditis elegans fat-3 mutants. Genetics *163*, 581-589.

Wisely, G.B., Miller, A.B., Davis, R.G., Thornquest, A.D., Jr., Johnson, R., Spitzer, T., Sefler, A., Shearer, B., Moore, J.T., Miller, A.B.*, et al.* (2002). Hepatocyte nuclear factor 4 is a transcription factor that constitutively binds fatty acids. Structure *10*, 1225-1234.

Yang, Z., and Wang, L. (2011). Regulation of microRNA expression and function by nuclear receptor signaling. Cell Biosci *1*, 31.

Yuan, X., Ta, T.C., Lin, M., Evans, J.R., Dong, Y., Bolotin, E., Sherman, M.A., Forman, B.M., and Sladek, F.M. (2009). Identification of an endogenous ligand bound to a native orphan nuclear receptor. PLoS One *4*, e5609.

Zhu, Q., Yamagata, K., Miura, A., Shihara, N., Horikawa, Y., Takeda, J., Miyagawa, J., and Matsuzawa, Y. (2003). T130I mutation in HNF-4alpha gene is a loss-of-function mutation in hepatocytes and is associated with late-onset Type 2 diabetes mellitus in Japanese subjects. Diabetologia *46*, 567-573.

Appendix I: Structure-function analysis of NHR-49

One of my initial aims was to interrogate the relationship between structure and function in NHR-49, with the goal of learning more about how this nuclear receptor is able to selectively modulate so many different groups of target genes. I planned to introduce these constructs into the *nhr-49(nr2041)* deletion line and assay for rescue of mutant phenotypes with the goal of defining the role of each domain in the transcription of NHR-49 targets. While technical difficulties (described in Chapter II) prevented me from conducting this series of experiments, I describe below the experimental design I had intended.

Site-directed mutagenesis of NHR-49

To interrogate the role of NHR-49 subdomains, I constructed a panel of 8 plasmids, each containing a point mutation designed to selectively disrupt the function of a single structural domain of the nuclear receptor (Figure S1.1 and Table S1.1). Another 9 plasmids contained point mutants associated with maturity onset diabetes of the young (MODY). A small percentage of cases of this disease are due to heterozygous mutation of HNF4α, the mammalian homolog of NHR-49 (Gupta and Kaestner, 2004). Whereas the domain-specific mutations will allow me to determine if sets of target genes are differentially regulated, the MODY mutations correspond to known phenotypes, making it possible for me to associate changes in transcription with human disease outcomes.

The parent plasmid contained the *nhr-49* cDNA downstream of 2100 base pairs of the *nhr-49* promoter and the sequence for a 2x FLAG tag (Figure S1.1A). I chose to introduce a FLAG tag to take advantage of commercially available anti-FLAG antibodies. Following introduction of this mutant plasmid panel into *nhr-49(nr2041)* mutants, I planned to investigate their transcriptional and regulatory effects by qRT-PCR on an already-established panel of NHR-49-activated and –repressed genes. I also planned to assay fat content and longevity to determine if the mutant proteins were able to restore fat storage and desaturation to wild-type levels or rescue the shortened lifespan. Results from these experiments would help to differentiate the transcriptional targets of the various domains, as well as set the stage for biochemical assays to investigate the ability to bind to protein, DNA, or lipids of any mutants with a biological effect. However, introduction of even the native cDNA as a high-copy array was unable to rescue *nhr-49* mutant lifespans or transcriptional profiles. Because I was unable to establish a baseline

degree of rescue to which I could compare effects of the site-directed mutants, I chose to focus instead on the toxicity of the NHR-49-overexpressing construct (see Chapter II). However, now that I have determined that inclusion of genomic sequences and low copy number of the transgenic array permit some rescue, these constructs could be remade, incorporating introns and the 3'UTR in a vector backbone that is compatible with low-copy insertion technologies such as bombardment or MosSCI. With the new set of constructs, it might then be possible to address the original questions of structure-function relationship.

Experimental Procedures

Cloning and plasmids

All plasmids were constructed using standard molecular techniques. Rescue constructs contained 2100 base pairs of the *nhr-49* promoter driving expression of the *nhr-49* cDNA tagged with 2-4 copies of the FLAG epitope sequence subcloned into the L3691 backbone. Site-directed mutagenesis was conducted using the Finnzymes Phusion Site-Directed Mutagenesis kit (New England BioLabs, Ipswich, MA), following included protocols.

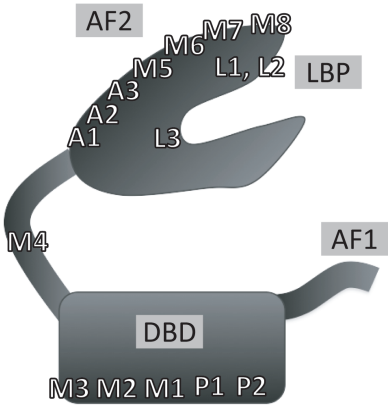

Figure S1.1. Structure-function analysis of NHR-49. Schematic of NHR-49 protein structure, including resides targeted by site-directed mutagenesis (see Table S1.1 for explanation of mutations). AF: activation function domain; DBD: DNA-binding domain; LBP: ligand-binding pocket.

Table S1.1. Residues targeted by site-directed mutagenesis.

Category	Mutant	Residue	Desired result of mutation
DBD-targeting	P1	R60A	Disrupt DNA binding by mutating conserved residues within the P-box (Lu et al., 2008)
	P2	R61A	
LBD-targeting	L1	R272A	Destabilize ligand binding by interrupting hydrogen bonding to fatty acid head group
	L2	R272K	
	L3	I306M	Alter binding capability of longer-chain fatty acids by adding a bulky side-chain midway down the ligand-binding pocket
AF2 targeting	A1	L233F	Prevent co-activator binding by mutating residues at the interface (Duda et al., 2004)
	A2	K240A	
	A3	F245A	
MODY-associated	M1	G99S	Introduce a PKA phosphorylation site, decreasing transactivation potential (Oxombre et al., 2004)
	M2	P111W	Disrupt cooperative gene activation with HNF1α (Rowley et al., 2006)
	M3	V155I	Disrupt DNA binding to reduce transactivation potential (Zhu et al., 2003)
	M4	R171X	Mimic MODY-associated truncation mutant deficient in DNA binding (Lausen et al., 2000)
	M5	E327Q	Reduce transactivation potential by decreasing cofactor affinity (Suaud et al., 1999)
	M6	R378H	Destabilize homodimers to reduce transactivation (Aggelidou et al., 2006)
	M7	G380R	Unknown (predicted to affect cofactor binding based on location of mutation)
	M8	T393I	Decrease transactivation potential (Suaud et al., 1999)

Appendix II: Additional characterization of the *cyp-35a5;fhc10* mutant

Initial characterization of the *cyp-35a5;fhc10* strain included epistasis analysis with *nhr-49(nr2041)*. However, once it became apparent that phenotypes caused by misregulation of the desaturase genes in the *nhr-49* mutant background made it difficult to define any other interactions, I stopped working with these strains. These early experiments also included lifespan and bagging frequency analysis on desaturase RNAi plates. Preliminary results are shown below.

Genetic interaction of nhr-49(nr2041)*,* cyp-35a5(ok1985) *and* fhc10 *alleles*

Once I had generated the a putative triple mutant by crossing the RB1613 (*cyp-35a5;fhc10*) strain to the *nhr-49* mutant, I performed standard phenotypic analyses to determine whether the interaction of these alleles was able to rescue any *nhr-49* mutant phenotypes. A caveat to this set of experiments is that, while I was able to confirm the presence of the *cyp-35a5* deletion by PCR, I did not know about the secondary *fhc10* allele at the time. However, the outcrossed *nhr-49;cyp-35a5* double mutant has a different phenotypic profile than the *nhr-49* x RB1613 strain, indicating that this latter strain is probably a *nhr-49;cyp-35a5;fhc10* triple mutant (Figure S2.1A, B, C).

Brood size and lifespan experiments suggested that *nhr-49* is not affecting these phenotypes through the same pathway as *cyp-35a5* and *fhc10*. While the differences between *nhr-49* and *nhr-49;cyp-35a5;fhc10* are not significantly different, it seems that the effects of *nhr-49* and the *cyp-35a5;fhc10* mutations are additive (Figure S2.1A, B). For example, the *cyp-35a5;fhc10* mutant shows a 17% increase in mean lifespan in an *nhr*-49(+) background and a 19% increase when the *nhr-49* deletion is present (Figure S2.1A). Similarly, the *nhr-49* and *cyp-35a5;fhc10* allele combinations both decrease brood size by about 75%, while the *nhr-49;cyp-35a5;fhc10* line demonstrates a 63% reduction in progeny production (Figure S2.1B). Although I would expect a more dramatic reduction if the combination of alleles were completely additive, the additional decrease in the *nhr-49;cyp-35a5;fhc10* is nevertheless indicative of alleles affecting brood size through distinct pathways.

In contrast to the longevity and fecundity phenotypes, desaturation and fat storage phenotypes do seem to show interactions between *nhr-49* and the *cyp-35a5* and *fhc10* alleles. Increased desaturation of lipids within the neutral lipid fraction of *nhr-49* mutants trends

downward with the addition of the *cyp-35a5* and *fhc10* alleles (Figure S2.1D). Interestingly, in the phospholipid fraction the *cyp-35a5;fhc10* strain has higher saturation levels on its own, comparable to those of the *nhr-49* single mutant (Figure S2.1E). The saturation ratio discrepancy between the fractions might represent preferential regulation of the saturation of neutral lipids in the mutant or a role for *cyp-35a5*/*fhc10(+)* in membrane composition. Finally, although the *cyp-35a5;fhc10* mutant has decreased fat storage, these alleles have no effect on the increased storage of the *nhr-49* mutant (Figure S2.1F).

Desaturase activity affects lifespan, brood size, and bagging phenotypes

Because many *nhr-49* mutant phenotypes result from misregulation of desaturase genes, I was interested to determine the effect of knocking down these genes in my other mutants. My initial experiments focused on knocking down the Δ9 desaturase *fat-7*, which is dependent on *nhr-49* for normal expression (Van Gilst et al., 2005a). Loss of *fat-7* significantly reduced brood size of all mutants, but made any strain containing the *nhr-49(nr2041)* allele essentially sterile (Figure S2.2A). Since the interaction between *nhr-49* and *fat-7* masked any relationship *nhr-49* might have with the other alleles, I focused on *nhr-88, cyp-35a5*, and *fhc10* for the rest of the experiments. Just as these alleles increase progeny production only in the triple mutant assayed on control RNAi bacteria, the *nhr-88;cyp-35a5;fhc10* brood size is significantly larger than that of N2 on *fat-7* RNAi, despite a significant reduction in the fecundity of both the *nhr-88* and *cyp-3a5;fhc10* strains (Figure S2.2A).

Knockdown of *fat-7* also affects lifespan. Although the decrease is not significant in N2, *nhr-88* and *nhr-88;cyp-35a5;fhc10* are reduced from 14.7 ± 3.6 days to 9.5 ± 3.3 days and 16.6 ± 5.0 days to 12.9 ± 5.1 days, respectively (Figure S2.2B). The *cyp-35a5;fhc10* strain also experiences a major decrease in longevity on *fat-7* RNAi; while long-lived on control plates, the *cyp-35a5; fhc10* line is shorter-lived than N2 when *fat-7* is knocked down (Figure S2.2B). I also did experiments knocking down other desaturases with the goal of dissecting which polyunsaturated fatty acids (PUFAs) might be important for the increased brood and lifespan of the mutants. RNAi against the Δ12 desaturase *fat-2* should prevent the formation of any PUFAs, while knocking down the Δ5 desaturase *fat-4* will disrupt the ratio of C20 PUFAs. I found that *fat-2* RNAi reduced the lifespan of all mutants tested, but that *fat-4* RNAi had opposite effects depending on the genotype (Figure S2.2B). As has since been reported for the wild-type strain

(Shmookler Reis et al., 2011), *fat-4* RNAi increased lifespan of N2 and *nhr-88* mutants (Figure S2.2B). However, knocking down this desaturase decreased longevity of the *cyp-35a5;fhc10* and *nhr-88;cyp-35a5;fhc10* strains (Figure S2.2B), indicating the CYP-35A5 and *fhc10(+)* might be involved in the signaling that links decreased C20 PUFAs to increased lifespan. Based on my findings linking lifespan and the number of proliferating cells within the mitotic region (MR) of the germline, described in Chapter III, I would be very curious to characterize any germline phenotypes of these treated animals. However, RNAi studies are not currently compatible with quantification of the mitotic region, since food source seems to also dictate the size of the MR. Preliminary experiments comparing the mitotic region length of N2 and *cyp-35a5;fhc10* worms grown on HT115 do not detect a difference in size, despite a significant decrease in worms fed OP50. While conducting the lifespan experiments, I also noticed a marked increase in the number of worms that had to be censored from the *fat-7* data set due to bagging. Over 60% of N2 and *nhr-88* animals bagged when *fat-7* was knocked down, whereas *cyp-35a5;fhc10* and *nhr-88;cyp-35a5;fhc10* mutants seemed to be slightly protected from this fate (Figure S2.C). The bagging phenotype was limited to the *fat-7* RNAi plates, as the percent of animals that bagged remained low on *fat-2* and *fat-4* RNAi plates (Figure S2.C). Again, the involvement of fatty acids and a cytochrome P450 that is predicted to metabolize these lipids into ligands suggests that the differences in propensity to bag are caused by altered levels of some signal molecule.

cyp-35a5;fhc10 *and the dauer diapause*

Finally, there is anecdotal evidence that *cyp-35a5* and *fhc10(+)* may also play a role in the dauer diapause, as there is an increased number of dauer animals on naturally starved *nhr-88;cyp-35a5;fhc10*, *nhr-88;cyp-35a5*, *nhr-88;fhc10*, and *cyp-35a5* plates. I have noted this tendency to dauer multiple times in these mutants, but do not ever see it in the *nhr-88* or *fhc10* single mutants; dauer frequency seems to be highest in strains containing the *nhr-88* deletion. Although I need to repeat and quantify these experiments, possibly using a sensitized dauer-entry strain, this observation lays the groundwork for investigation of the role of NHR-88 and possibly CYP-35A5 in the dauer diapause. If NHR-88 is found to be involved in dauer as well as ARD, the mutant could prove a valuable tool in investigating the potential regulatory similarities between these two physiologically similar diapause states.

Experimental Procedures

Strains and maintenance

The wild-type N2 (Bristol) strain and RB1613 *cyp-35a5(ok1985)V;(fhc10)X* were provided by the Caenorhabditis Genome Center, which is funded by the NIH National Center for Research Resources (NCRR). *nhr-88(tm1033)II* was provided by the Mitani lab and *nhr-49(nr2041)I* was a gift from Carl Johnson at Axys Pharmaceuticals. All mutants were outcrossed to N2 a minimum of 5 times. Worm maintenance was carried out at 20˚C using standard methods.

Lifespan assays

Lifespans were determined by counting the number of days individual worms survived after the L4 molt. Experiments were conducted at 20˚C on *Escherichia coli* strain HT115 transformed with empty vector or RNAi construct indicated. RNAi plasmids are from the Ahringer RNAi library (Fraser et al., 2000; Kamath et al., 2003). Live animals were moved to fresh plates daily during the reproductive period, after which they were moved every two to three days. Worms were considered dead when they no longer responded to gently prodding. Bagged animals were censored. Lifespan curves and statistical data, including *P*-values from a one-way ANOVA followed by a Bonferroni multiple comparison test of relevant strains, were produced and analyzed using GraphPad Prism 5 (GraphPad Software, San Diego, CA). Bagging data was analyzed by two-way ANOVA using GraphPad Prism 5.

Brood size assays

L4 animals were picked to individual OP50 plates on day 0. Adults were moved to new plates daily as long as they were laying embryos. Progeny plates were maintained at 20˚C until worms were L3-L4, at which point the number of larvae were counted and recorded. Individuals that bagged while other worms in the group were still laying were censored. Statistical analyses, including *P*-values from a one-way ANOVA followed by a Bonferroni multiple comparison test of relevant strains, used GraphPad Prism 5 (GraphPad Software, San Diego, CA).

Lipid purification and analysis

To collect worms for lipid analysis, approximately 30,000 L1s synchronized by an overnight hatch on unseeded NGM plates were plated to NGM plates seeded with *Escherichia coli* strain OP50 and grown at room temperature. Once the population reached mid-L4, the worms were collected and washed 5 times with M9. Excess buffer was aspirated from the worm pellet, the sample was frozen in an ethanol-dry ice bath, and transferred to -80˚C until processing.

For fatty acid profiles and desaturation ratios, total lipids were extracted and converted to fatty acid methyl esters (FAMEs) as described (Watts and Browse, 2002). The resultant FAMEs were analyzed by gas chromatography/mass spectrometry (GC/MS) (Agilent 5975GC, 6920MS). Data were presented as relative abundance (profiles) or the ratio of abundance of C18:0 to that of C18:1n9 (desaturation ratio). To measure fat storage, total lipids were extracted and separated into neutral lipid, glycolipid, and phospholipid fractions as described (Perez and Van Gilst, 2008).

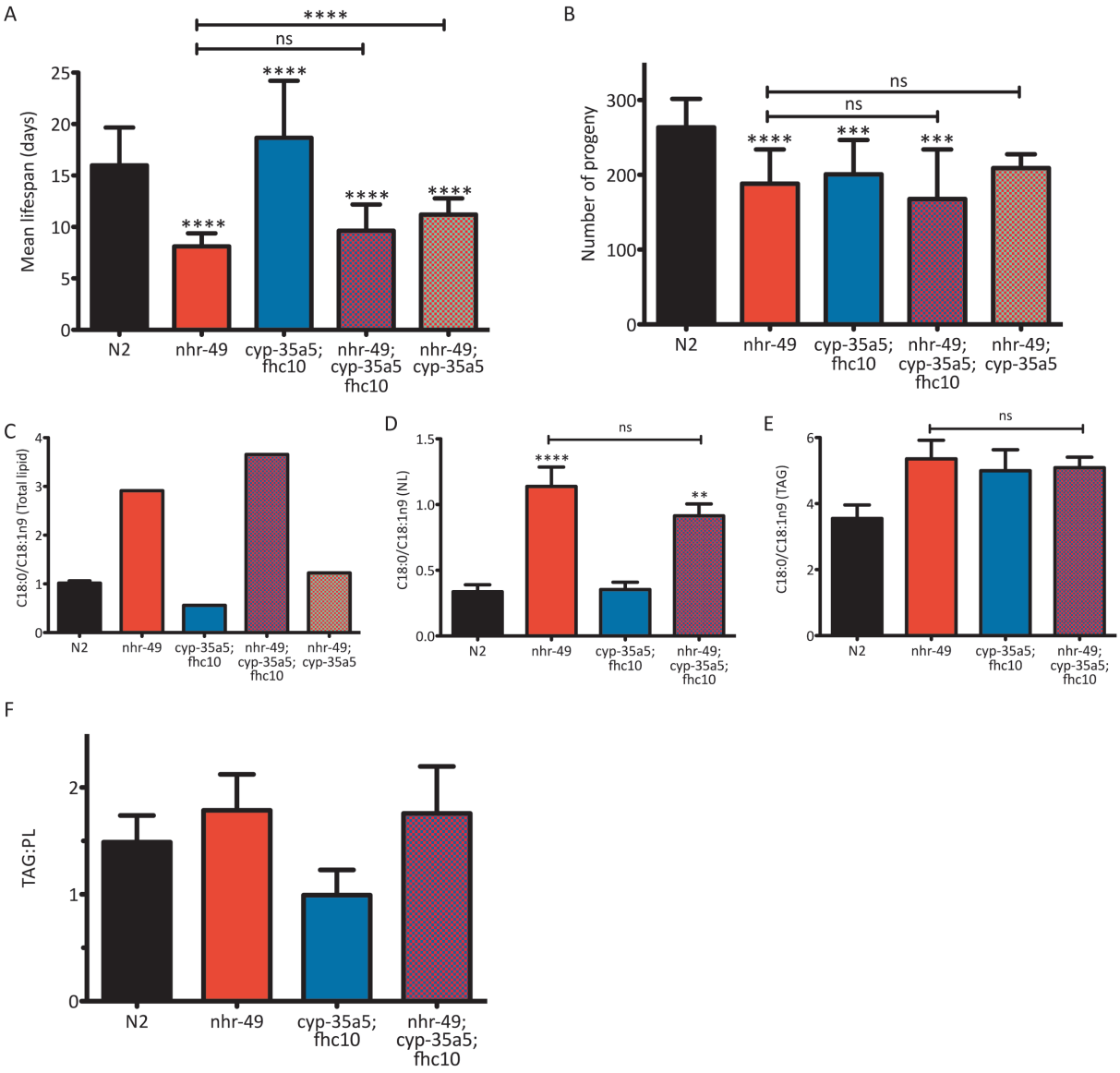

Figure S2.1. *nhr-49* interactions with the *cyp-35a5* and *fhc10* alleles are limited to fat phenotypes. (A) Lifespans of *nhr-49* and *cyp-35a5;fhc10* mutants alone and in combination. Data shown are mean lifespans ± SD from at least 57 individuals assayed in 1 experiment. (B) Total progeny produced by *nhr-49* and *cyp-35a5;fhc10* mutants. Shown are means from at least 17 individuals in at least 4 separate experiments, except for *nhr-49;cyp-35a5,* for which the mean is from 4 animals from a single experiment. Error bars represent SD. (C-E) Desaturation ratios measured in total lipid (C), neutral lipid (D), and phospholipid (E) fractions. Shown are means ± SEM from at least 4 experiments, except in C, which has only one replicate. (F) Ratio of triglyceride to phospholipid as a measure of fat storage. Mean from at least 3 experiments is shown ± SEM. $^{**}P < 0.01$, $^{***}P < 0.001$, $^{****}P < 0.0001$.

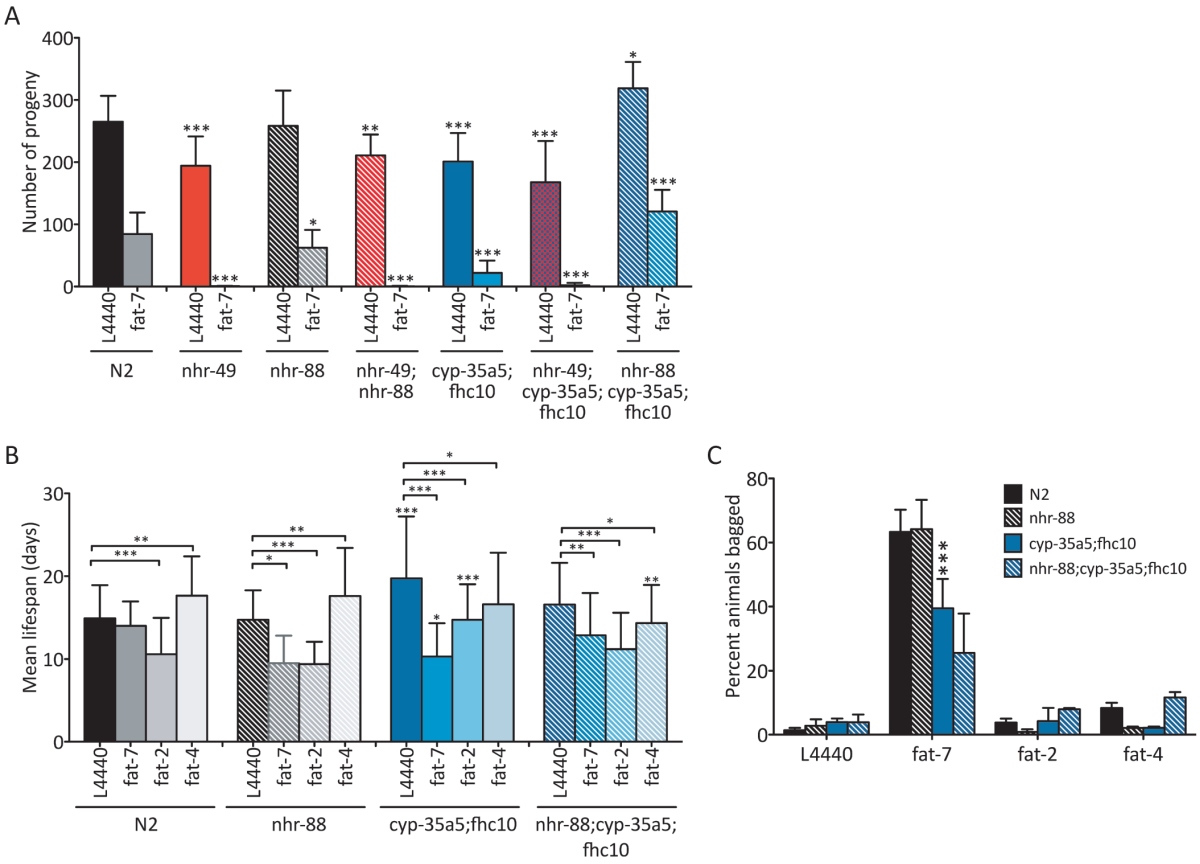

Figure S2.2. Knockdown of Δ9, Δ12, and Δ5 desaturases affects lifespan, brood size, and bagging phenotypes. (A) Brood sizes for mutants grown on HT115 bacteria transformed with empty vector (L4440) or the RNAi plasmid targeting the Δ9 desaturase *fat-7*. Means are shown ± SD and result from at least 9 individual worms tested in three different experiments. Statistics shown compare mutant strains to N2 controls on the same food source; the brood reduction caused by *fat-7* RNAi is significant for all strains. (B) Longevity of mutants grown on HT115 bacteria transformed with empty vector (L4440) or RNAi plasmids targeting *fat-7*, the Δ12 desaturase *fat-2*, or the Δ5 desaturase *fat-4*. Data are the mean ± SD of at least 17 individuals assayed in 1 experiment, with the exception of *nhr-88* on *fat-7* RNAi. This mean is from only 4 individuals due to a high number of animals being censored due to bagging. Asterisks directly above a bar represent statistical significance when compared to N2 animals grown on the same food source, while asterisks associated with lines compare the same strain grown on different RNAi plates. (C) Percent of animals censored due to bagging during lifespan experiments described above. $^{*}P < 0.05$, $^{**}P < 0.01$, $^{***}P < 0.001$, $^{****}P < 0.0001$.

Vita

Born in Boston, Massachusetts, Alison Brooks spent the bulk of her formative years in San Diego, California. After becoming enamored with genetics in her high school biology classes, Alison went on to earn a Bachelor of Sciences in Biological Sciences and a minor in Chemistry from Stanford University. In 2011 she earned a Doctor of Philosophy in Molecular and Cellular Biology from the University of Washington.